Design Analysis of a Dual-Cylinder Electrohydraulic Load Simulator for Motion Tracking by Individual Metering under Feedforward-PI Control

A thesis submitted in partial fulfilment of the requirement for the degree of

Master of Mechanical Engineering

By

Mithun Mondal

Exam Roll No - M4MEC23008

Registration No - 160292 of 2021-22

Under the guidance of

Prof. Saikat Mookherjee

&

Prof. Dipanakar Sanyal

DEPARTMENT OF MECHANICAL ENGINEERING

FACULTY OF ENGINEERING AND TECHNOLOGY

JADAVPUR UNIVERSITY

KOLKATA-700032

2023

FACULTY OF ENGINEERING & TECHNOLOGY

DEPARTMENT OF MECHANICAL ENGINEERING

JADAVPUR UNIVERSITY, KOLKATA

CERTIFICATE OF RECOMMENDATION

*This is to certify that the thesis entitled "**Design Analysis of a Dual-Cylinder Electrohydraulic Load Simulator for Motion Tracking by Individual Metering under Feedforward-PI Control**", which is being submitted by **Mithun Mondal** in partial fulfilment for the award of the degree of **Master of Mechanical Engineering** to Jadavpur University, Kolkata 700032, during the academic year 2022-2023, is the record of the student's own work carried out by him under our supervision.*

.....

Prof. Saikat Mookherjee
Thesis Advisor
Department of Mechanical Engineering
Jadavpur University
Kolkata-700032

.....

Prof. Dipankar Sanyal
Thesis Advisor
Department of Mechanical Engineering
Jadavpur University
Kolkata-700032

.....

Prof. Amit Karmakar
Head
Department of Mechanical Engineering
Jadavpur University
Kolkata-700032

.....

Prof. Ardhendu Ghoshal
Dean
Faculty of Engineering and Technology
Jadavpur University
Kolkata-700032

FACULTY OF ENGINEERING & TECHNOLOGY

DEPARTMENT OF MECHANICAL ENGINEERING

JADAVPUR UNIVERSITY, KOLKATA

DECLARATION OF ORIGINALITY

AND

COMPLIANCE OF ACADEMIC ETHICS

I hereby declare that this thesis contains literature survey and original research work, by the undersigned, as part of his ***Master of Mechanical Engineering*** *studies.*

All information in this document have been obtained and presented in accordance with academic rules and ethical conduct.

I also declare that, as required by these rules and conduct, I have fully cited and referenced all material and results that are not original to this work.

NAME: **MITHUN MONDAL**

Examination Roll Number: **M4MEC23008**

Thesis Title: ***Design Analysis of a Dual-Cylinder Electrohydraulic Load Simulator for Motion Tracking by Individual Metering under Feedforward-PI Control***

Signature:

Date:

FACULTY OF ENGINEERING & TECHNOLOGY

DEPARTMENT OF MECHANICAL ENGINEERING

JADAVPUR UNIVERSITY, KOLKATA

CERTIFICATE OF APPROVAL*

The foregoing thesis is hereby approved as a creditable study of an engineering subject carried out and presented in a manner satisfactory to warrant its acceptance as a prerequisite to the degree for which it has been submitted. It is understood that by this approval the undersigned do not necessarily endorse or approve any statement made opinion expressed or conclusion drawn therein but approve the thesis only for the purpose for which it is submitted.

Committee on Final Examination

For Evaluation of the Thesis

\- -

\- -

\- -

Signature of Examiners

*Only in case the recommendation is concurred in

ACKNOWLEDGEMENT

I would like to express my deepest gratitude and appreciation to the following individuals of Jadavpur University who have played a significant role in the completion of my thesis:

First and foremost, I would like to thank my academic advisors, **Prof. Saikat Mookherjee and Professor Dipankar Sanyal**, for their unwavering guidance, support, and expertise throughout this research journey. Their valuable insights and constructive feedback have been instrumental in shaping the direction of my thesis.

I would like to extend my sincere thanks to **Prof. Amit Karmakar**, Head, Department of Mechanical Engineering, Jadavpur University.

I extend my sincere appreciation to the research scholars Mr. Aniruddha Sarkar and Mr. Niladri Naskar who generously shared their time, knowledge, and experiences.

Furthermore, I am grateful to my family and friends for their unwavering support, encouragement, and understanding throughout this challenging journey. Their love, patience, and belief in my abilities have been a constant source of motivation.

Lastly, I would like to express my gratitude to all the faculty members, staff, and fellow students at Project Neptune who have created a conducive learning environment and provided valuable resources for my academic growth.

In conclusion, I am deeply thankful to all those who have contributed directly or indirectly to the completion of this thesis. Your support and encouragement have been invaluable, and I am truly grateful for your presence in my academic journey.

Table of Contents

LIST OF FIGURES

LIST OF TABLES

LIST OF ABBREVIATIONS

Abbreviation	Description
BDC	: **B**ottom **D**ead **C**entre
CIMV	: **C**oupled **I**ndividual **M**etering **V**alve
CV	: **C**heck **V**alve
EHAS	: **E**lectro-**H**ydraulic **A**ctuation **S**ystem
EHFS	: **E**lectro-**H**ydraulic **F**orce **S**ystem
EHLS	: **E**lectro-**H**ydraulic **L**oad **S**imulator
FDP	: **F**ixed **D**isplacement **P**ump
FF	: **F**eed-**F**orward
FFPI	: **F**eed-**F**orward with **P**roportional-**I**ntegral
GUI	: **G**raphical **U**ser **I**nterface
HIL	: **H**ardware **I**n **L**oop
IAE	: **I**ntegral **A**bsolute **E**rror
IMV	: **I**ndividual **M**etering **V**alve
ISCE	: **I**ntegral **S**quare **C**ontrol **E**ffort
LVDT	: **L**inear **V**ariable **D**ifferential **T**ransformer
MRAC	: **M**odel-**R**eference **A**daptive **C**ontrol
PI	: **P**roportional-**I**ntegral
PV	: **P**roportional **V**alve
RV	: **R**elief **V**alve
SMC	: **S**liding **M**ode **C**ontrol
TDC	: **T**op **D**ead **C**entre
VDP	: **V**ariable **D**isplacement **P**ump

NOMENCLATURE

Symbol	Unit	Description
a_x	m	Amplitude of sinusoid position demand
a_F	N	Amplitude of sinusoid force demand
A_c	m^2	Cap end area of cylinder
A_r	m^2	Rod end area of cylinder
c_d	Ns/m	Damping coefficient of damper
c_{lc}	-	Cap end leakage co-efficient
c_{lp}	-	Leakage co-efficient in hydraulic cylinder
c_{lr}	-	Rod end leakage co-efficient
c_{vci}	-	Cap end valve co-efficient for *i*=1,2
c_{vri}	-	Rod end valve co-efficient for *i*=1,2
d_b	m	Diameter of bore of the cylinders
d_r	m	Diameter of rod of the cylinders
e_x	m	Position error
e_F	N	Force error
f	N	Friction experienced opposite to piston motion
f_c	N	Coulomb friction
f_f	N	Friction in feedforward control
f_0	N	Maximum force considered in trapezoidal wave form
f_s	N	Static friction
F	N	Force generated in EHLS
F_d	N	Demanded force
k_s	N/m	Spring stiffness
K_{Ix}	V/ms	Integral gain for position control
K_{IF}	V/Ns	Integral gain for force control
K_{Px}	V/m	Proportional gain for position control
K_{PF}	V/N	Proportional gain for force control
m	kg	Mass of the piston
n	-	Number of cycles
p_{RV}	Pa	Relief valve pressure
p_{ci}	Pa	Cap end pressure perturbation due to leakage and compressibility, for *i*=1,2
p_p	Pa	Pump pressure perturbation due to leakage and compressibility
p_{ri}	Pa	Rod end pressure perturbation due to leakage and compressibility, for *i*=1,2
P_c	Pa	Scaling pressure of pump
P_{ci}	Pa	Cap end pressure in feedforward control of plant for *i*=1,2
P_{cif}	Pa	Cap end pressure in feedforward model for *i* =1-8
P_{co}	Pa	Cut-off pressure of the Pump in Pa
P_{ciB}	Pa	Motion induced component of cap end pressure in feedforward control for *i*=1,2
P_P	Pa	Pump pressure
P_{Pf}	Pa	Pump pressure in feedforward control

Symbol	Unit	Description
P_{PB}	Pa	Motion induced component of pump pressure in feedforward control
P_{ri}	Pa	Rod end pressure of plant for *i*=1,2
P_{riB}	Pa	Motion induced component of rod end pressure for *i*=1,2
q_p	m^3/s	Pump flow perturbation due to leakage and compressibility
Q_c	m^3/s	Flow scaling factor
Q_{ciB}	m^3/s	Motion induced component of cap end flow in feedforward control for *i*=1,2
Q_{cif}	m^3/s	Cap end flow in feedforward control for *i*=1,2
Q_o	m^3/s	Maximum flow of the pump
Q_P	m^3/s	Pump flow
Q_{Pf}	m^3/s	Pump flow in feedforward control
T	s	Time period of a cycle
v_{il}	V	Leakage compensating voltage in i^{th} valve for *i*=1-8
$v_{i\beta}$	V	Compressibility compensating voltage in i^{th} valve for *i*=1-8
v_F	V	Feedback voltage of metering valves for force cylinder
v_{kb}	V	Feedback voltage of metering valve for *k* = 1-8
v_x	V	Feedback voltage of motion cylinder
V_{iB}	V	Motion induced component of feedforward voltage i^{th} valve for *i*=1-8
V_{kf}	V	Feedforward voltage for k^{th} valve for *k* =1-8
V_k	V	Total FFPI voltage for k^{th} valve for *k* =1-8
x	m	Position of the piston
$\dot{x}$	m/s	Velocity of the piston
$\ddot{x}$	m/s^2	Acceleration of the piston
x_d	m	Demanded Position of the piston
$\dot{x}_d$	m/s	Demanded velocity of the piston
$\ddot{x}_d$	m/s^2	Demanded acceleration of the piston
$\dot{x}_s$	m/s	Stribeck velocity in friction
x_0	m	Bias in position demand
α	N/s	Slope of linearly varying load demand
α_v	Ns/m	Viscous coefficient in friction
ϕ_x	Radian	Phase in sinusoid position demand
ϕ_F	Radian	Phase in sinusoid force demand
κ	Pa	Bulk modulus of oil
ε	Radian	Phase difference of demanded velocity and force
Ω_{ci}	m^3/s	Initial volume of cap end of cylinder for *i*=1,2
Ω_{ri}	m^3/s	Initial volume of rod end of cylinder for *i*=1,2
$\overline{\Pi}_{mvl}$	kW	Exit power loss in the metering valves
$\overline{\Pi}_p$	kW	Power input from the variable displacement
$\overline{\Pi}_{ps}$	kW	Power saved
ω_x	rad/s	Frequency of sinusoid position demand
ω_F	rad/s	Frequency of sinusoid force demand

ABSTRACT

This thesis presents a comprehensive analysis of the design and performance of a dual-cylinder electrohydraulic load simulator (EHLS) for motion tracking applications. The EHLS serves as a crucial component in hardware-in-loop (HIL) experiments, particularly in the aerospace and automotive industries. The objective of the EHLS is to generate desired force profiles using a hydraulic cylinder, while simultaneously achieving precise motion tracking despite varying external loads.

The study focuses on the challenges posed by nonlinearities in electrohydraulic systems, including the pressure-discharge relationship in variable openings of metering valve ports, friction effects, and oil compressibility. These challenges require advanced control strategies beyond simple PID feedback. Moreover, low-cost systems utilizing proportional valves and high-friction cylinder pairs exhibit additional nonlinear features, necessitating careful controller design to achieve comparable tracking performance to more expensive servo systems.

Furthermore, the thesis investigates the energy efficiency and tracking accuracy of electrohydraulic systems. The use of variable-displacement pumps, proportional valves, individual metering valve (IMV) and combined individual metering valve (CIMV) arrangements are examined to reduce power losses and improve system efficiency. A composite feedforward position-force controller coupled with a feedback controller is designed. in developing the feedforward control, order-separation technique is used to estimate motion inducing terms, compressibility, and leakage related terms. Comparison of position and force response, FFPI control voltages of metering valves and chamber pressures for CIMV & IMV configurations is explored. Different combinations of position and load demands are explored to study the position and force tracking performances.

Additionally, the thesis also cited the area to be explored in future. Different control strategies, valve and cylinder arrangements, are referred in the last chapter. As this thesis is entirely a simulation-based studies, hence a real-time experiment of the configurations should be carried out in future.

The research findings provide insights into the design and control of electrohydraulic systems for motion tracking applications. The analysis contributes to the development of improved control strategies, energy-efficient designs, and enhanced tracking accuracy in EHLS and electrohydraulic force systems. The results have implications for industries such as aerospace, automotive, robotics, and fault-tolerant fields, where precise motion control and force tracking are crucial.

CHAPTER 1

INTRODUCTION

1.1 Introduction

Two broad classes of electrohydraulic, or EH, applications pertain to actuation systems and force systems, which in short are referred respectively as EHAS and EHFS (Dai et. al., 2022). Representative use of EHAS are found in air-born (Cochoy et. al., 2007; Yan et. al., 2021), off-road (Park et. al., 2020) and on-road (Horn et. al., 2003; Plummer, 2007) vehicles as well as in manufacturing (Cho et. al., 2009) and material handling, say by excavators (Feng et. al., 2019). In each case, the objective is to achieve control of motion against application-specific precision levels and wide variations of the external load. The nonlinear pressure-discharge relation in orifice-like variable openings of the metering valve ports and the nonlinear effects of friction and oil compressibility on the actuation dynamics led to the use of controllers more advanced than simple PID feedback (Truong & Ahn, 2009; O'Brien & Carruthers, 2013). In comparison to these effects arising in EH systems with servovalve-servocylinder pairs, low-cost systems with proportional valve and high-friction cylinder pairs exhibit additional nonlinear features (Sarkar et. al., 2013).

Proportional valves have deadband nonlinearity in the form of insignificant actuation flow against excitation signal up to 10 to 20% of the maximum magnitudes in typical excitation ranges of –10 to +10V or 4 to 20mA. In contrast, overlap or underlap of only 2 to 3% is achieved within the tolerance band of costly and sophisticated machining employed in case of servovalves. A consequence of the cheaper machining is much higher leakage flow bypassing the actuator through relatively larger radial clearance between the spool-sleeve pair of a proportional valve. In comparison to servoactuators, low-cost actuators give rise to significantly higher static friction and nonlinearities in dynamic friction in the low-speed actuation range. These features make the controller design for the low-cost systems quite challenging for achieving tracking performance comparable to the corresponding servosystems.

The pressure transients in the actuator chambers get moderated by the system inertia in the eventual manifestation as the response against motion-tracking demands in EHAS. In EHFS, the response against variable load demands could have amplitudes higher than the pressure transients, since the poles of the load in the linearized model form the zeros in the closed loop (Alleyne & Liu, 2000). EHFS are employed typically in car brakes (Yuan et. al., 2018; Han et. al., 2020; Xiong et. al, 2020), vibration isolators for seismic structures and car suspension (Zhang et. al., 2005; Bongain & Jamett, 2018), forging machines (Yan & Chen, 2021), hydraulic press (Komsta et. al., 2013; Li et. al., 2016) and load simulators (Karpenko & Sepehri, 2010; Luo et. al., 2017; Jing et. al., 2019, 2020).

1.2 Electrohydraulic Load Simulator

A common application for the simultaneous deployment of the EHAS and EHFS is an electrohydraulic load simulator or EHLS which is an important component in hardware-in-loop (HIL) experiments in the aerospace industry (Chengwen et. al., 2013; Jacazio & Balossini, 2007; Nam & Hong, 2002), automotive industry (Plummer, 2007), robotics and fault tolerant field (Isserman et. al., 1999). The principal objective of the EHLS is to generate prescribed profiles of force (or torque) by a hydraulic cylinder (or motor), acting on a coupled second hydraulic cylinder (or motor) which is to follow a desired linear (or angular) motion profile inspite of the loading. For linear motion, the pair of hydraulic cylinders, usually single-rod type, may be connected end-to-end (Li et. al., 2009) or may be parallel (Huang et. al., 2023). These arrangements are commonly used for simulating and performance monitoring of flight simulators and cold rolling mills (LeQuoc et. al., 1994), rudder systems (Li et. al., 2009), machine tools (Truong & Ahn, 2011) and aircraft actuations systems or AASs (Yang & Yao, 2022).

Because of the direct coupling of the two hydraulic cylinders, the force response of the loading cylinder is severely affected by the motion of the actuating cylinder. This is often termed as surplus force and is viewed as a disturbance to the force control architecture of the loading cylinder (Chengwen et. al., 2013; Huang et. al., 2023). A leading challenge in the design of precise, accurate, and fast EHLS lies in the surplus load compensation or SLC. Several strategies have been adopted over the years for successful SLC. While LeQuoc et. al., 1994 used a bypass adjustable throttle valve across the two flow lines of the loading cylinder to this end, Li et. al., 2009 used a flow-press servo valve along with a flow servo valve. Truong & Ahn, 2011 employed a parallel force and position control strategy using the proportional integral derivative (PID) control method and an online self-tuning fuzzy-neural mechanism on a linear system model. To ensure SLC, Chengwen et. al., 2013 used a linear feedforward compensation for the actuating cylinder, while Yang & Yao, 2022 used a multilayer neuro adaptive controller with a linear plant model. Huang et. al., 2023 used an adaptive sliding mode control strategy on a linear state space model of the system to overcome this difficulty. A combined force-motion simulator was built as a coaxial arrangement of two cylinders with facing piston rods, with one cylinder having controller for emulating the force demand and the other cylinder for the motion demand (Truong & Han, 2009).

1.3 Controller Development

The load transient issue together with highly nonlinear friction variation due to the major involvement of the low-speed range in EHFS leave ample scope of improving controller performance (Xiao et. al., 2015). For handling friction in EHFS, use was made of generalized Maxwell slip model with parameter identification experiment (Kang et. al., 2018) and modified LuGre model executed with fast pressure measurement and a disturbance observer (Dai et. al., 2022). For tackling unmeasured or un-modelled effects in these studies, back-stepping controller and sliding-mode control, or SMC, were respectively used with adaptive schemes in both the cases. Of course, a fast-response pressure sensor is costly. Moreover, an SMC is known for its robustness as well as inducing chattering in the control excitation (Jerouane et. al., 2004; Xu, et. al., 2019; Cheng et al., 2020). Another issue that confronts its real-time use for fast actuation is the nonlinear relation between the signal and the linearized input (Komsta et. al., 2013). In many cases, the nonlinear relation could make the extraction of the excitation signal iterative and time consuming. A back-stepping controller involves a large number of tuneable parameters that was also implemented for force control with a PI observer for estimating the system states of a single-rod cylinder (Nakkarat & Kuntanapreeda, 2009). When a back-stepping scheme combines dynamic surface control, the explosion of parameters is prevented to some extent (Kang et. al., 2018).

Implementing a feedforward model also involves several parameters and a procedure for their identification. Irrespective of formulating the model for control of motion (Horn et. al., 2003) or force (Kemmetmuller et. al., 2010), an accompanying linear dynamic of error arises that could be compensated by combining a simple feedback strategy with the feedforward estimation. In the above force-control study, a variable-displacement pump with passive hydromechanical compensator, was used. The compensator endowed the pump the ability of quick variation of flow from the high rate of the mould-filling phase to the slow rate of the cooling-induced volume shrinkage phase arising from solidification of the material at a constant pressure.

Of course, the variable rate of the pump flow conforming to the process requirement gives significant energy saving with respect to what would have occurred in case of a fixed-displacement pump letting most of its discharge to wasteful return through a relief valve to the tank during the solidification stage. Energy saving in force control were also accomplished by using variable-displacement pumps either with only an active electrohydraulic compensator (Park et. al., 2009) or with an additional valve control (Yu

el. al., 2020). While SMC was used in the earlier study, the latter study employed a combined feedforward-feedback strategy.

A bump-less switching between a stable robust H_∞ control and less stable but more precise model-reference adaptive control, MRAC, was employed in a force-control study (Zhang et. al., 2005). In order to have smooth switching, two pre-set limits were regularly compared with sampled errors, each taken as the maximum within a set sampling interval executed by keeping the controller unchanged. For the high sensitivity of the MRAC to un-modelled dynamics, it was invoked only if the robust operation reduced the sampled error below the lower limit. If the sampled MRAC error went above the higher limit, the H_∞ control was invoked. During dwelling of the error between the limits, the controller was not changed. Of course, successful implementation of MRAC is very sensitive to the choice of the reference plant that is emulated by the controller. Such a choice could be tricky, if the system involves strong nonlinear features.

In certain EHFS (Sekhavat et al., 2006), switching also arises between motion and force control regimes during engagement and disengagement of the actuated end point with a soft or hard contact surface. Tustin friction model with pressure measurement of both the chambers across a double-rod double-acting cylinder were used along with a feedback control formulated on the basis of direct Lyapunov function. In the face of sharp transients during such a switching, the controller kept the system stable. Switching between free travel and force tracking modes arises in friction-stir welding machines (Gain et. al., 2022) and certain robotic operations (Asokan & Singaperumal, 1997).

1.4 Energy Efficiency and Tracking Accuracy

Valve-controlled electrohydraulic motion actuation is widely deployed in land-based large systems and for aircraft navigation [1-7] for their higher power-to-weight ratio, payload capacity and fault resistance than the more easily controllable and dominantly linear electrical systems. The nonlinear flow behaviour and oil compressibility pose greater challenge in force tracking applications [8]. A major drawback of these systems is low energy efficiency noted as about only 9.3% in a hydraulic press [1] and 14% in an earlier survey for mobile hydraulic systems in US [9]. A relief valve maintains a constant system pressure at the delivery of a fixed-displacement pump (FDP). Variable-displacement pumps (VDP) used mostly for mobile systems removes the relief-valve loss. A double-acting cylinder is mostly paired with a 4-port metering-in-metering-out valve controlled by a single command. Independent-metering of flow in each

cylinder chamber by a pair of 3-port valves controlled by separate commands reduces the metering-out power loss.

1.5 Scope of Work

The research status summarized above has motivated a study involving a low-cost EHLS with combined force-motion simulator, built as a coaxial arrangement of two cylinders with facing piston rods, with one cylinder having controller for emulating the force demand and the other cylinder for the motion demand. While in almost all the previous studies, the compensation of the surplus force was addressed through suitable compensation in the individual control loops, in the present work a novel unified feedforward nonlinear was used to provide feedforward signals simultaneously to both the cylinders to compensate the surplus force.

The above survey further motivates a detail study to demonstrate improved energy efficiency of energy-saving systems through separate valve control for each cylinder chamber coupled with a variable displacement pump (VDP). Some of these will be variable-excitation proportional valves while the remaining will be fixed-excitation proportional valves behaving as ON-OFF valves. Such a configuration will be henceforth termed as individual metering valve, or IMV, arrangement. If all the valves are operated in variable-excitation mode with identical signals for the supply and return flow metering valves in a cylinder, then such a configuration will be henceforth termed as coupled individual metering valve, or CIMV, arrangement. For a fixed installation on land, the benefit of high energy saving is longer oil life due to its slower degradation caused by lower heating from the power-loss reduction in metering orifices that are higher in faster valve-controlled systems with variable excitation. The consequent less frequent disposal of degraded oil reduces the environmental impact [1/10]. Much lower power is expended in moving or flying a mobile hydraulic system by equipping it with an oil tank of much lower size that keeps the temperature rise in check due to the lower orifice loss.

In Section 2, the EHLS and the relevant modelling are described. Instead of two 4×3 proportional valves for the two cylinders, the setup has four pairs of 2×2 proportional valves – a pair being connected to one of the four chambers of the two cylinders. One of the valves of this pair provide high pressure fluid to the respective cylinder chamber, while the other can drain low pressure fluid form the chamber – depending on the situation. This gives the capability of individual metering of each of the four cylinders chambers which can be suitably explored to achieve an energy efficient hydraulic system. The two double-acting-

single-rod cylinders are connected end-to-end coaxially with a load cell and LVDT lying in between to assess the force generated of the EHFS and the displacement of the EHAS respectively. Of course, use of a load cell and a single-acting cylinder renders greater compactness than having two pressure transducers and a double-acting cylinder in an earlier set up (Sekhavat et al., 2006).

Sections 3 detail the contributing unified order-separated feedforward control formulation coupled with the dual PI feedback schemes or FFPI.

Results are arranged in Section 4 to ascertain if the robustness of the proposed unified order-separated feedforward control formulation coupled with the dual PI feedback could avert triggering of instability by each mode-switching transient (Sekhavat et al., 2006). Also, the wide-range compensation capability of the order-separated formulation should ensure high-precision tracking.

Conclusions and future scope of work are summarized in Section 5.

CHAPTER 2

SYSTEM DESCRIPTION AND MATHEMATICAL MODELING

2.1 Introduction

The present work involves simulation of an EHLS consisting of two coaxial double-acting, single-rod cylinders with facing piston rods, through separate valve control for each cylinder chamber coupled with a variable displacement pump (VDP). One of the cylinders, called the motion cylinder is coupled with a controller for emulating the motion demand while the other having controller for emulating the force demand.

Mathematical modelling of the EHLS involves using a suitable model for the variable displacement pump whereby depending on the flow to the system, the pump delivery port pressure is adjusted. The eight solenoid-operated metering valves are modelled as flow orifices where the flow through each valve is related to the square root of the pressure drop across the metered ports. This is augmented with the leakage flow through the spool-bush clearances in the valves. The pressure dynamics in the valve cylinder chambers modelled based on the bulk modulus of the fluid. The dynamics of the coupled piston of the two cylinders of the EHLS depends on the chamber pressures as well as the friction between the piston and inner surface of the cylinders. A suitable friction model has been proposed.

The nonlinear model of the EHLS depends on several system parameters whose values have been used from a previous work where a single actuator test bench has been developed. The model provides the capability to study the performance of the piston – in terms of position achieved and force developed – for suitable excitations of any four of the solenoid-operated metering valves - either in CIMV or IMV mode.

2.2 System Description of the EHLS

2.2.1 Metering Valves

The proposed EHLS consists of two co-axial single-rod, double-acting hydraulic cylinders connected end-to-end. Conventionally double acting hydraulic cylinders are driven by 4×3 proportional valves (PV) as shown in Fig,2.1(a). The ports P and T are connected to the pump and tank respectively. The control ports A and B are connected the cap-end chamber C1 and rod-end chamber C2 of the hydraulic cylinder. The sliding spool inside the valve body/bush are connected to two solenoid motors. In absence of any electrical signal to the solenoid motors, no net force acts on the spool and it remains in the neutral position –

completely covering ports A and B. Hence there is no flow to or from the cylinder and the piston remains stationery. To connect C1 to the high-pressure pump line and C2 to low pressure tank line, a positive voltage V is given to solenoid motor 1. This causes the spool to slide to the left, indicated by the red lines. Thus, port A gets connected to P and B to T. The respective flows are indicated by red arrows. To connect C2 to the high-pressure pump line and C1 to low pressure tank line, a negative voltage V is given to solenoid motor 2, causing the spool to slide to the right. Thus, port A gets connected to T and B to P. This way the cylinder piston can be moved to the right or left, as required. The symbolic representation of the valve is also shown, where the 3 adjacent boxes indicate the connectivity among the 4 ports. The 2 parallel lines above and below the adjacent boxes indicate that it can be operated in a fashion such that for a constant pressure drop across the metered ports, the flow through the valve is proportional to the impressed voltage in the respective solenoid motor.

The coupled individual metering valve (CIMV) or individual metering valve (IMV) configurations are shown in Fig. 2.1(b) for C1 connected to high pressure pump line and C2 to low pressure tank line. Here instead of a single 4×3 PV, four 2×2 PVs are used. In Fig. 2.1(b) only 2 such valves are shown for C1 connected to high pressure pump line and C2 to low pressure tank line. The port A of valve 1 is connected to the pump line while that of valve 2 is connected to the tank line. If the voltage signals to valves 1 and 2 are zero, the ports B of the 2 valves remain blocked and no flow occurs to or from the cylinder. To connect C1 to high pressure pump line and C2 to low pressure tank line, positive voltages are given to both the valves and the corresponding flows are indicated in the figure by red arrows.

To connect C1 to low pressure tank line and C2 to high pressure pump line, another pair of 2×2 PVs are used. The valve connected to pump line will then be connected to C2 and the one connected to tank line will be connected to C1. Positive voltages in both these valves will ensure that C1 is connected to high pressure pump line and C2 to low pressure tank line. The symbol of a 2×2 PV is also given in Fig. 21(b).

The purpose of this arrangement is to explore whether any power saving is achieved if the return side valve is excited by a constant voltage and opened by a fixed amount, as a simple on-off valve; while the supply side valve is excited by a variable voltage as in any conventional PV. Such a configuration is termed as individual metering valve or IMV configuration.

If both the supply and return valves are excited by identical variable voltage, then such an arrangement is termed as coupled individual metering valve or CIMV arrangement. Independent-metering of flow in each

cylinder chamber by a pair of 2×2 PVs, controlled by separate commands reduces the metering-out power loss.

For the 2×2 PVs a case drain will be essential at the cap end for free movement of the spool. This is not shown in the figure to avoid clutter.

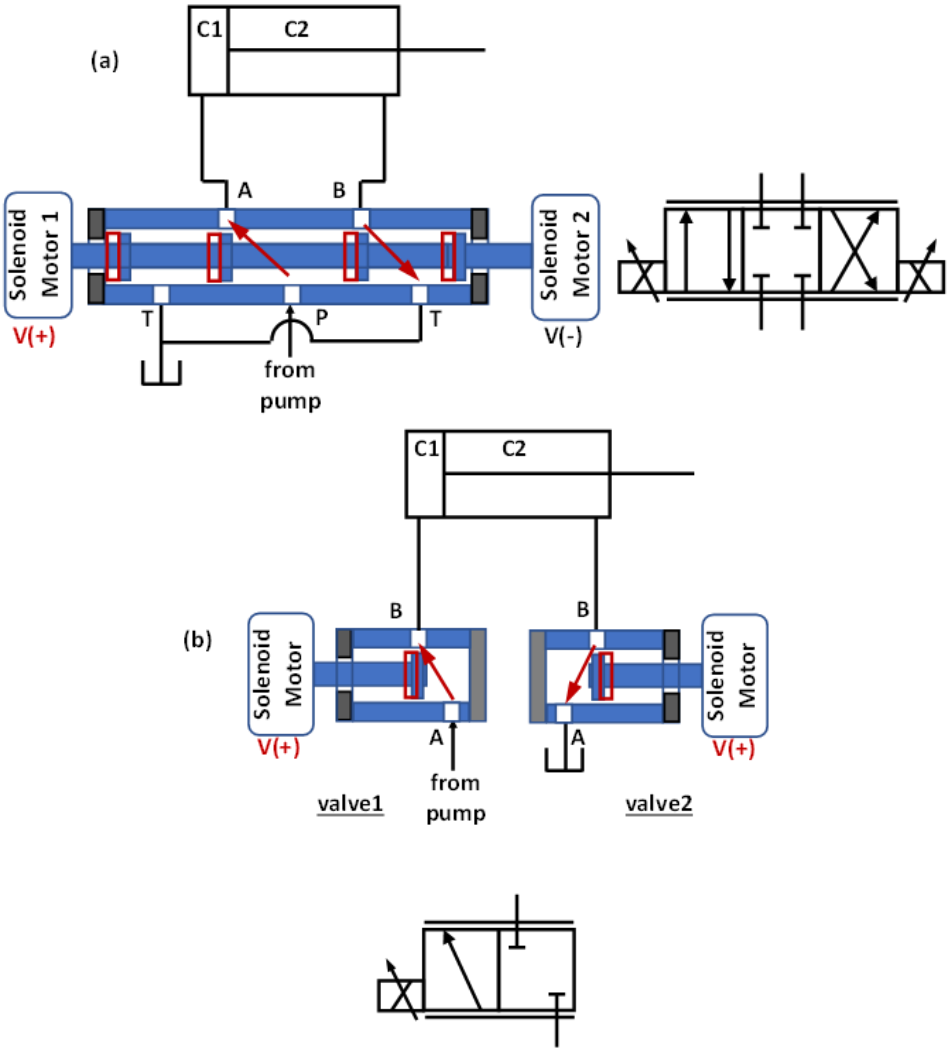

Fig.2.1: Double-acting, Single-rod Hydraulic Cylinder in (a) Conventional PV Configuration, (b) CIMV/IMV Configuration

In the present work each of the two hydraulic cylinders is provided with 2 pairs of 2×2 PVs – one pair for C1 connected to high pressure and C2 to low pressure and another pair for the reverse connection.

2.2.2 Hydraulic Actuators

Hydraulic actuators are devices that use the power from pressurized fluid and converts it mechanical work. Depending on the type of motions generated, they are classified as linear actuators or rotary actuators.

The linear actuator, also often called as a hydraulic cylinder, consists of a piston cylinder arrangement. The piston divides the cylinder into two different compartments. If the one the compartments is connected to high pressure (or low pressure) line while the other connected to low pressure (or high pressure) line, through a pair of ports, then such a linear actuator is called double-actin type. In contrast, if flow lines are connected to only one chamber, while the other is open to atmosphere, such a cylinder is called single-acting type. Single-acting type cylinders can also have a spring attached to the piston to assist the return stroke. If the rod extends from either side of the piston, the cylinder is termed as double-rod or symmetric type. If the rod extends from only one side of the piston, it is called single-rod or asymmetric type. Doubler-rod cylinders have identical pressure bearing areas on either side of the piston; while for the single-rod type, these areas are unequal on either side of the piston. This has a bearing in the symmetry of the mathematical model of the system. It goes without saying that single-rod cylinders are more compact than their double-rod counterparts.

Rotary actuators can be continuous rotation type (often called hydraulic motors) or limited rotation type. Furthermore, they can be unidirectional or bi-directional.

Symbols of some of the hydraulic actuators are shown in Fig. 2.2 below.

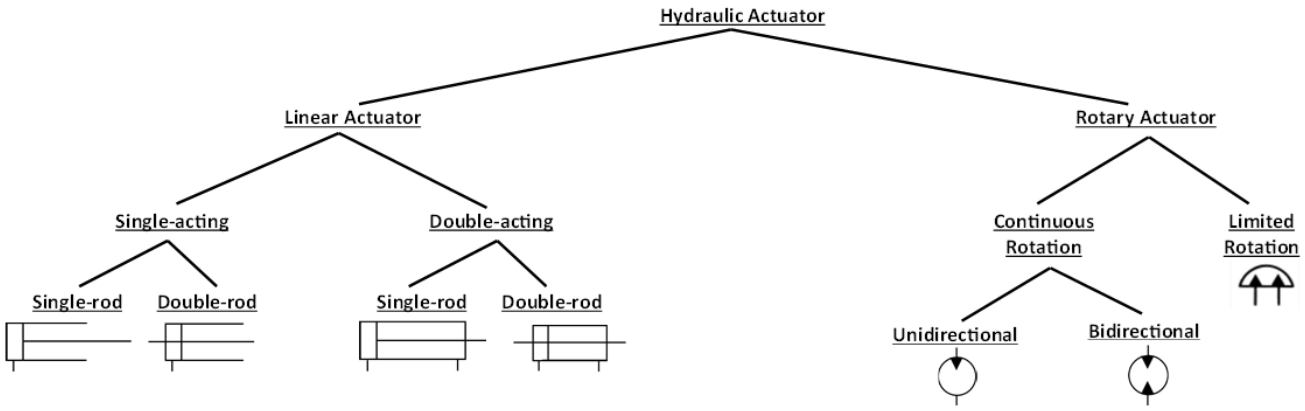

Fig.2.2: Classification of hydraulic actuators

In the present work a pair of coaxial single-rod, double acting hydraulic cylinders – one for motion tracking and another for force generation – are used with their rod ends connected end-to-end.

2.2.3 Hydraulic Powerpack

Any hydraulic powerpack consists of a tank containing hydraulic fluid, a pump driven by a motor, a pressure relief valve, RV, a check valve, CV, gauges, heat exchangers and filters. Pumps used can be

fixed-displacement pump (FDP) or variable displacement pump (VDP). A relief valve maintains a constant system pressure at the delivery of a fixed-displacement pump (FDP). Variable-displacement pumps (VDP) used mostly for mobile systems removes the relief-valve loss. However, a RV is still required in the VDP circuit to prevent any accidental over-pressurization leading to failures and accidents. The symbols for FDP and VDP are shown in Fig. 2.3 below.

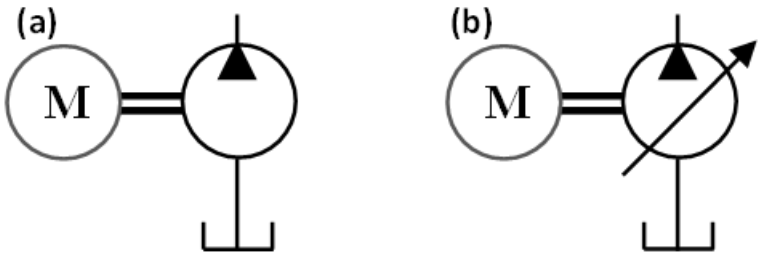

Fig.2.3: Symbols for (a) fixed displacement pump (FDP), (b) variable displacement pump (VDP)

In the present work, a pressure compensated swash plate type axial piston pump has been considered as the VDP. The schematic of such a pump is shown in Fig.2.4 below.

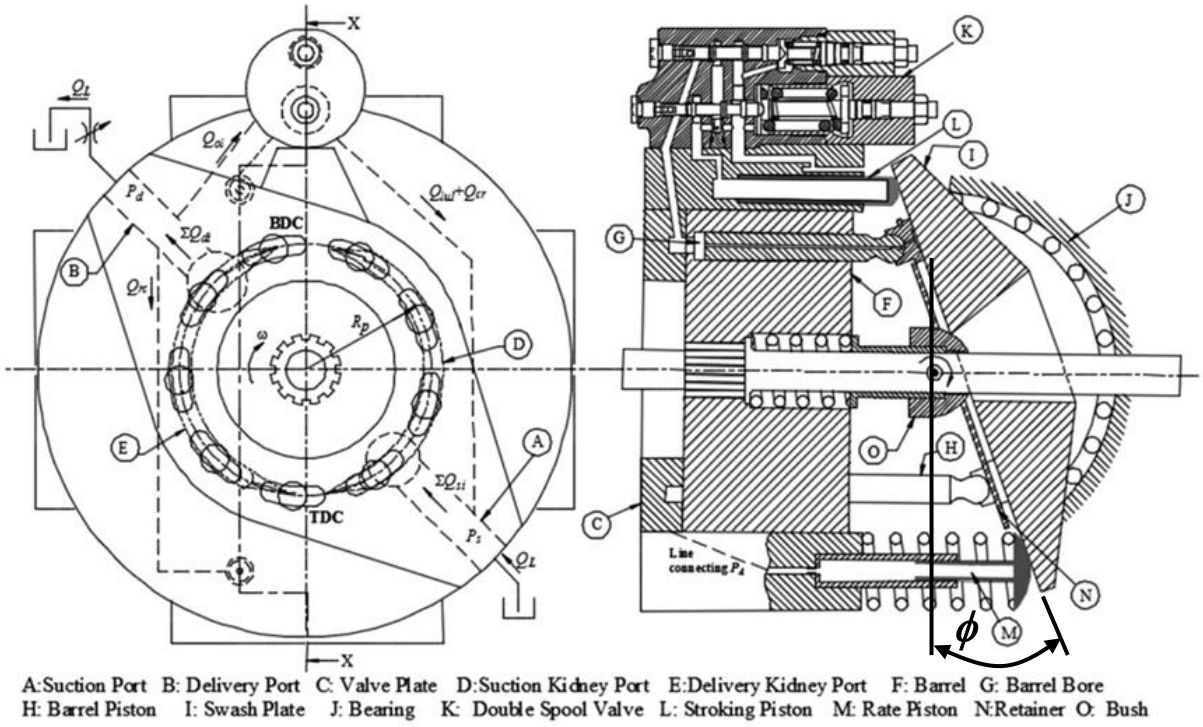

Fig.2.4: Schematic of a swash plate axial piston pump with pressure compensator (Mondal et. al. 2019)

The schematic of a variable displacement swash plate type axial piston pump with pressure compensator as illustrated by Mondal et. al. 2019, is shown above. The barrel pistons **H** (usually 9,11 or 13 in number) slide inside the barrel **F**. This reciprocation is achieved due to the angle ϕ that the swash plate **I** makes

with the vertical direction. For this, as the barrel **F** rotates, the pistons execute a suction stroke as they move in a clockwise sense from the bottom dead centre (BDC) to top dead centre (TDC), and sucks in fluid from the tank through the suction port **A** into each piston chamber across the respective suction kidney ports **D**. For the motion of the pistons from TDC to BDC, they execute delivery stroke whereby high-pressure fluid is directed to the system through the delivery ports **B**. If the system flow demand reduces, pressure in the delivery line increases. This causes the spools of the double spool valve **K** moves, thereby directing pressurized fluid to the stroking cylinder the piston of which moves out pushing the swash plate on the bearing support and against the rate piston. This reduces the swash angle ϕ and the flow is reduced till the delivery pressure is in the acceptable range implying the flow is consistent with the demanded flow of the system. The check valve, **CV** is provided to prevent reverse flow of fluid from the system. In the present work a variable displacement swash plate type axial piston pump is considered to ensure energy efficiency of the system.

2.2.4 The Electrohydraulic Loading System

The proposed EHLS depicted in Fig.2.5 involves a set of 2×2 proportional valves V1 to V4 for actuating one-cylinder Cyl_1. Another cylinder Cyl_2 is equipped with another set of 2×2 proportional valves V5 to V8. These eight metering valves can be operated in variable-excitation mode or simple ON-OFF mode. In the simulation study one can imagine that there is a force feedback F from an S-type load cell mounted between the in-line coaxial pistons and an LVDT inbuilt with Cyl_1. While the displacement feedback x of the LVDT is used for motion control, the load cell feedback F is used for force control with friction compensation. The set up has a VDP driven by a fixed speed motor along with an RV and CV – for reasons mentioned earlier.

All of V1 to V8 remain off, when the system is unexcited. For Cyl_1, excitation of V3-V4 or V1-V2 pair could cause extension or retraction strokes respectively. Similarly, paired excitation of V5-V6 or V7-V8 could be set for actuating Cyl_2 either in IMV mode or CIMV mode by using equal excitation in a pair. For the motion actuation of Cyl_1, the opposite cylinder Cyl_2 is excited for providing the external load.

The voltage signals in the metering valves – 4 at any particular time – is generated by a controller based on the demanded force F_d and motion x_d of the piston and the actual F and x. The controller proposed in the present work consists of a feedforward part and a feedback part. The feedback controllers for the 2

cylinders are Proportional-Integral or PI-controllers. Collectively the controller is termed as Feedforward-PI or FFPI controller.

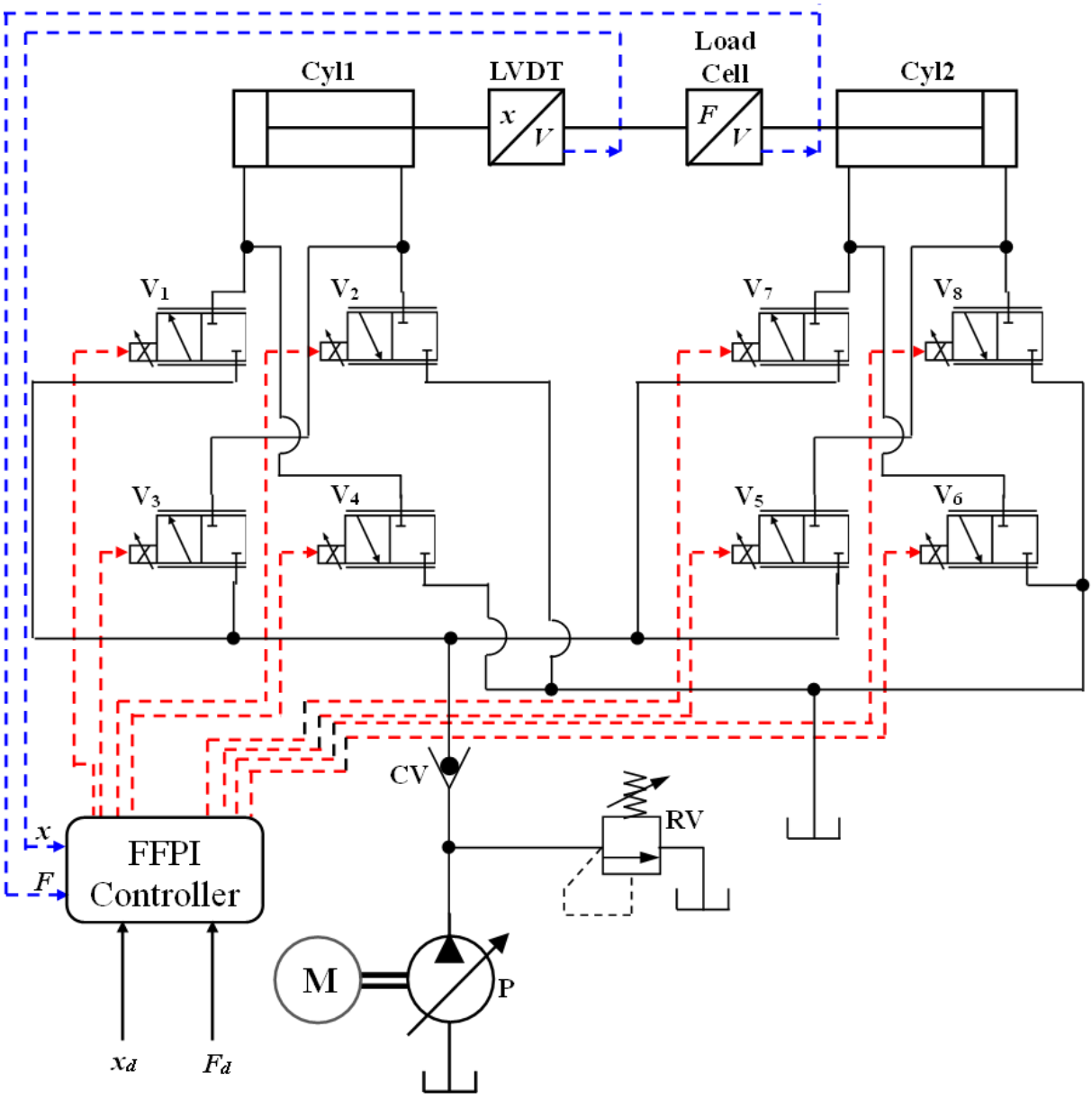

Fig.2.5: Schematic of Electrohydraulic Loading System, EHLS

2.3 Mathematical modeling of the EHLS

A mathematical model of the EHLS is essential on two counts. First, to develop a simulation model of the plant which is essential for studying the closed loop performance of the system. Second, the mathematical model is the basis for developing a suitable feedforward controller. The plant model or the feedforward model – both consists of several parameters; whose values need to be known. The different system

parameters, as used in the feedforward controller and the system model in the simulation has been obtained from the results of Sarkar et.al., 2013 and Naskar et. al.,2022 – where these have been obtained by a Genetic Algorithm based parameter identification scheme.

The mathematical modeling of the system is based on several considerations, which are,

- the hydraulic oil is considered as compressible;
- a variable displacement pump is used;
- leakage flow in the spool-bush clearance of the metering valves and through the piston-cylinder gap in the 2 cylinders are considered;
- dead-band of the metering valves have been ignored;
- friction between the piston O-rings and hydraulic cylinder inner surface is considered;
- the dynamics of spool of the metering valves is considered to be much faster than the piston dynamics;
- transmission losses have been ignored.

The modeling of the present EHLS given in Fig.2.5, involves modeling of the friction in the cylinders, the dynamics of the piston motion, the chamber pressure dynamics in the cylinders considering compressibility and piston leakage, the metered flows in the valves considering leakage, and compressibility and static modelling of the variable mode of pump operations.

2.3.1 Friction in Cylinders

The friction *f* can be considered to exist between the piston O-rings and the cylinder inner surfaces during motion of the piston. A popular nonlinear friction model (Sarkar, et. al., 2013) due to Tustin is given as

$$f = \{f_s + (f_c - f_s)\exp(-\dot{x}^2/\dot{x}_S^2)\}\,\mathrm{sgn}(\dot{x}) + \alpha_v\dot{x} \tag{2.1}$$

where the parameters f_s is static friction, f_c Coulomb friction, $\dot{x}_S$ Stribeck velocity, α_v viscous coefficient and $\mathrm{sgn}(\dot{x})$ =1, 0 and -1 for $\dot{x}$ positive, zero and negative respectively.

2.3.2 Dynamics of the Piston Motion

In the present configuration as shown in Fig. 2.5, the motion of the piston from right to left is considered as positive while it is considered negative when the piston moves towards right. The free body diagrams

of the two cylinders are shown in Fig.2.6 below, where F is the force generated, $x, \dot{x}$ and $\ddot{x}$ are the displacement, velocity and acceleration of the piston respectively, P_{ci} and P_{ri} are the pressures at the cap and rod ends of Cyl$_i$ (i = 1,2) – each of bore diameter d_b and piston-rod diameter d_r.

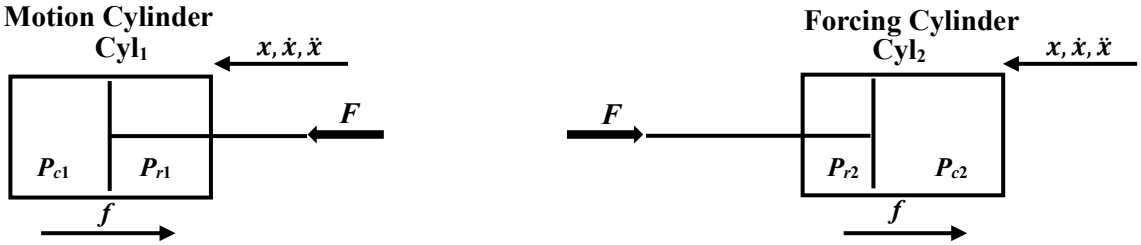

Fig.2.6: Free body diagrams of the 2 cylinders

Cyl$_1$ is called 'motion cylinder' while Cyl$_2$ is termed as the 'forcing cylinder'. This implies that the feedback voltages of the metering valves of the former are estimated from position errors while that of the latter are estimated from force errors. Considering the total mass of the connected piston assembly as m, the acceleration of each piston of mass $m/2$ in Cyl$_1$ and Cyl$_2$ are expressed as

$$(m/2)\ddot{x} = F - P_{c1}A_c + P_{r1}A_r - f \tag{2.2a}$$

$$(m/2)\ddot{x} = -F + P_{c2}A_c - P_{r2}\,A_r - f \tag{2.2b}$$

where the cap end and rod end areas are given as

$$A_c = \pi d_b^2/4 \tag{2.2c}$$

$$A_r = \pi(d_b^2 - d_r^2)/4 \tag{2.2d}$$

Subtracting eq. (2.2a) from (2.2b), the expression of the force generated can be obtained as

$$F = \{(P_{c2} + P_{c1})A_c - (P_{r2} + P_{r1})A_r\}/2 \tag{2.3}$$

Similarly, adding equations (2.2a) and (2.2b), the piston acceleration can be expressed as

$$\ddot{x} = \{(P_{c2} - P_{c1})A_c - (P_{r2} - P_{r1})A_r - 2f\}/m \tag{2.4}$$

2.3.3 Metered Flows in the Valves, Flow from Pump and Chamber Pressure Dynamics

2.3.3.1 V3-V4 in Cyl$_1$ and V5-V6 in Cyl$_2$ activated

With reference to Fig.2.5, for activation of V3-V4 in Cyl$_1$ and V5-V6 in Cyl$_2$, supply flow enters rod-end of Cyl$_1$ through V3 and cap-end of Cyl$_2$ through V5. The return flow goes to the tank from cap-end of

Cyl_1 through V4 and rod-end of Cyl_2 through V6. A flow in each of the cap and rod ends of the i^{th} cylinder respectively of initial volume Ω_{ci} and Ω_{ri} leads to oil pressurization due to its bulk modulus κ. A flow model is proposed here in terms of the difference of the orifice flows through V3-V4 and V5-V6, connected to the respective chamber. The discharge is customarily taken as proportional to square root of the pressure drop across each valve orifice. The metering-in flow between the pump and a cylinder chamber or the metered-out return flow from a chamber to the tank varies linearly with the excitation voltage V_j (j = 3,4,5 and 6) involving a valve coefficient c_{vci} or c_{vri} for the cap or rode end respectively. Each of these flows is in addition to the leakage flow proportional to the leakage coefficients c_{lc} and c_{lr} at the cap and rod sides respectively and c_{lp} across cylinder piston. In the unexcited state, the valve flow involves only the leakage. Taking the pump and tank pressures as P_p and zero respectively, this description of flow in each cylinder chamber is expressed by the set

$$Q_{c1} = A_c\dot{x} - c_{lp}(P_{c1} - P_{r1}) - \dot{P}_{c1}\{\Omega_{c1} - A_c x\}/\kappa \tag{2.5a}$$

$$= (c_{vc1}V_4 + c_{lc})\sqrt{P_{c1}} - c_{lc}\sqrt{P_P - P_{c1}} \tag{2.5b}$$

$$Q_{c2} = A_c\dot{x} - c_{lp}(P_{r2} - P_{c2}) + \dot{P}_{c2}\{\Omega_{c2} + A_c x\}/\kappa \tag{2.5c}$$

$$= (c_{vc2}V_5 + c_{lc})\sqrt{P_P - P_{c2}} - c_{lc}\sqrt{P_{c2}} \tag{2.5d}$$

$$Q_{r1} = A_r\dot{x} - c_{lp}(P_{c1} - P_{r1}) + \dot{P}_{r1}\{\Omega_{r1} + A_r x\}/\kappa \tag{2.5e}$$

$$= (c_{vr1}V_3 + c_{lr})\sqrt{P_P - P_{r1}} - c_{lr}\sqrt{P_{r1}} \tag{2.5f}$$

$$Q_{r2} = A_r\dot{x} - c_{lp}(P_{r2} - P_{c2}) - \dot{P}_{r2}\{\Omega_{r2} - A_r x\}/\kappa \tag{2.5g}$$

$$= (c_{vr2}V_6 + c_{lr})\sqrt{P_{r2}} - c_{lr}\sqrt{P_P - P_{r2}} \tag{2.5h}$$

2.3.3.2 V1-V2 in Cyl_1 and V7-V8 in Cyl_2 activated

Following similar logic as the previous section the flow in each cylinder chamber is expressed by the set

$$Q_{c1} = A_c\dot{x} + c_{lp}(P_{c1} - P_{r1}) + \dot{P}_{c1}\{\Omega_{c1} + A_c x\}/\kappa \tag{2.6a}$$

$$= (c_{vc1}V_1 + c_{lc})\sqrt{P_P - P_{c1}} - c_{lc}\sqrt{P_{c1}} \quad (2.6b)$$

$$Q_{c2} = A_c\dot{x} + c_{lp}(P_{r2} - P_{c2}) - \dot{P}_{c2}\{\Omega_{c2} - A_c x\}/\kappa \quad (2.6c)$$

$$= (c_{vc2}V_8 + c_{lc})\sqrt{P_{c2}} - c_{lc}\sqrt{P_P - P_{c2}} \quad (2.6d)$$

$$Q_{r1} = A_r\dot{x} + c_{lp}(P_{c1} - P_{r1}) - \dot{P}_{r1}\{\Omega_{r1} - A_r x\}/\kappa \quad (2.6e)$$

$$= (c_{vr1}V_2 + c_{lr})\sqrt{P_{r1}} - c_{lr}\sqrt{P_P - P_{r1}} \quad (2.6f)$$

$$Q_{r2} = A_r\dot{x} + c_{lp}(P_{r2} - P_{c2}) + \dot{P}_{r2}\{\Omega_{r2} + A_r x\}/\kappa \quad (2.6g)$$

$$= (c_{vr2}V_7 + c_{lr})\sqrt{P_P - P_{r2}} - c_{lr}\sqrt{P_{r2}} \quad (2.6h)$$

2.3.4 Pump Flow

The pump flow has been estimated as follow.

2.3.4.1 V3-V4 in Cyl_1 and V5-V6 in Cyl_2 activated

$$Q_P = (c_{vr1}V_3 + c_{lr})\sqrt{P_P - P_{r1}} + (c_{vc2}V_5 + c_{lc})\sqrt{P_P - P_{c2}} + c_{lr}\sqrt{P_P - P_{r2}} + c_{lc}\sqrt{P_P - P_{c1}} \quad (2.7)$$

2.3.4.2 V1-V2 in Cyl1 and V7-V8 in Cyl2 activated

$$Q_P = (c_{vc1}V_1 + c_{lc})\sqrt{P_P - P_{c1}} + (c_{vr2}V_7 + c_{lr})\sqrt{P_P - P_{r2}} + c_{lc}\sqrt{P_P - P_{c2}} + c_{lr}\sqrt{P_P - P_{r1}} \quad (2.8)$$

2.3.5 Static Modelling of the Variable Displacement Pump

A pressure compensated swash plate type axial piston pump is endowed with such a feature (Mondal N, et al., 2019). Below the cut-in pressure, its discharge remains close to the maximum discharge Q_0. Above this pressure, the discharge decreases steeply and becomes zero at the cut-off pressure, P_{co}. Based on the discussion above model for such characteristics of pump is proposed here as per Naskar and Pal, 2022 as

$$P_P = P_c + (P_{co} - P_c)\tanh\{(Q_0 - Q_P)/Q_c\} \quad (2.9)$$

where Q_c and P_c are characteristic flow and pressures and Q_P is the total pump discharge. The cut-off pressure P_{co}, the characteristic pressure P_c and the characteristic flow Q_c are unknown parameters of the pump whose optimized value can be found from system identification explained in the subsequent chapter. Such a static characteristic curve has been used in the feedforward estimate by considering the swivelling mass of the pump to be quite smaller than the actuated mass together with the load piston. Moreover, any sluggishness of the pump is expected to get compensated by the much faster valve dynamics by the corrective feedback voltage. The pump characteristics curve based on the above equation (2.8) and the discussions can be visually represented by the Fig.2.7 as shown below.

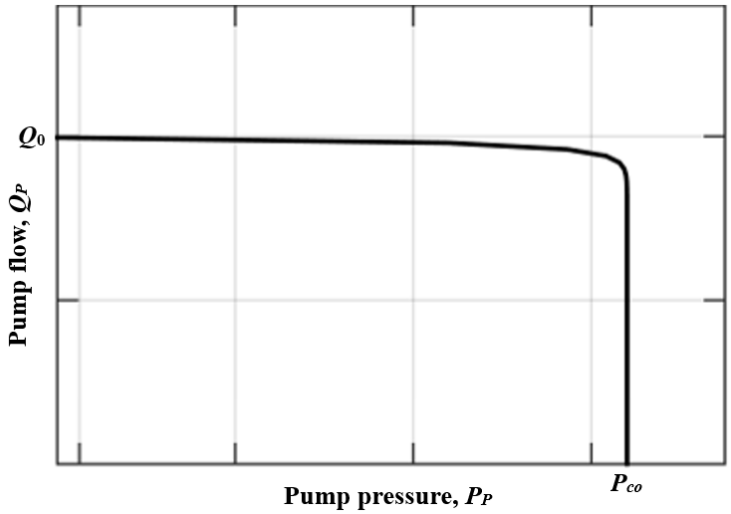

Fig.2.7: Pressure compensated swash plate type variable displacement pump characteristic curve

2.4 System Parameters

The different system parameters of these components as used in the feedforward controller and the system model in the simulation has been obtained from the results of Sarkar et.al., 2013 and Naskar et. al.,2022 – where some of these have been obtained from the manufacturer's specifications of the components while others have been identified by a Real-Coded Genetic Algorithm (RCGA) based optimization technique. These parameters have been listed in Table 2.1 below.

Table 2.1: List of System Parameters
(Sarkar et.al., 2013 and Naskar et. al.,2022)

Symbol	Unit	Value
c_{vc1}	$m^{3.5}V^{-1}kg^{-1/2}$	3.46×10^{-8}
c_{vr1}	$m^{3.5}V^{-1}kg^{-1/2}$	1.73×10^{-8}
c_{vc2}	$m^{3.5}V^{-1}kg^{-1/2}$	3.46×10^{-8}
c_{vr2}	$m^{3.5}V^{-1}kg^{-1/2}$	1.73×10^{-8}
c_{lc}	$m^{3.5}kg^{-1/2}$	3.8×10^{-9}
c_{lr}	$m^{3.5}kg^{-1/2}$	1.9×10^{-9}
c_{lp}	$m^{4}kg^{-1}s$	4.96×10^{-13}
f_s	N	85.0
f_c	N	55.0
α_v	Nsm^{-1}	482.0
$\dot{x}_s$	ms^{-1}	5.2×10^{-3}
d_c	m	0.04
d_r	m	0.02
κ	Nm^{-2}	1.3×10^{9}
Ω_{c1}	m^3	3.4×10^{-3}
Ω_{r1}	m^3	3.1×10^{-3}
Ω_{c2}	m^3	3.4×10^{-3}
Ω_{r2}	m^3	3.1×10^{-3}
m	kg	5.0
P_{co}	Nm^{-2}	52.55×10^{6}
P_c	Nm^{-2}	20.16×10^{6}
Q_o	m^3s^{-1}	1.36×10^{-3}
Q_c	m^3s^{-1}	4.83×10^{-5}

2.5 Summary

The detailed physical description of the electrohydraulic loading system is narrated in this chapter. The functioning of the hydraulic circuit has been elaborated. Also, several alternate configurations for metering valves, actuators and pumps have been discussed and the justifications for choosing the present configurations have been placed.

The mathematical model of friction, metered flows through metering valves considering leakage, piston motion dynamics, chamber pressure dynamics and the static model of the pressure-compensated swash plate type variable displacement pump are proposed. The several considerations at the backdrop of this mathematical formulation have also been clearly stated.

The discussion in this chapter forms the basis of the simulation model for the plant. They also constitute the core of the feedforward controller model developed in the next chapter.

CHAPTER 3

DESIGN OF FEEDFORWARD-FEEDBACK CONTROLLER

3.1 Introduction

The present chapter deals with design of a composite feedforward position-force controller along with PI feedbacks of position and force for an electrohydraulic load simulator system shown in Fig. 2.5. The order-separated approach of Sarkar et. al., 2023 in developing a feedforward controller for position control has been extended to develop the composite feedforward position-force controller in the present work. The mathematical models developed in the last chapter have been utilized in developing this controller. The gains for the PI-controllers – both for position and force control have been decided upon by trial and error.

The combined feedforward-PI control architecture is shown in Fig. 3.1 below, where, the combined control voltage in the k^{th} metering valve is expressed as

$V_k = V_{kf} + v_{kb}$, for k = 1 to 8. (3.1a)

Where V_{kf} is the combined feedforward position-force controller and v_{kb} is the PI feedback voltage. For a reasonably good feedforward model, except where V_{kf} is near to zero, it is expected that

$v_{kb} \ll V_{kf}$ (3.1b)

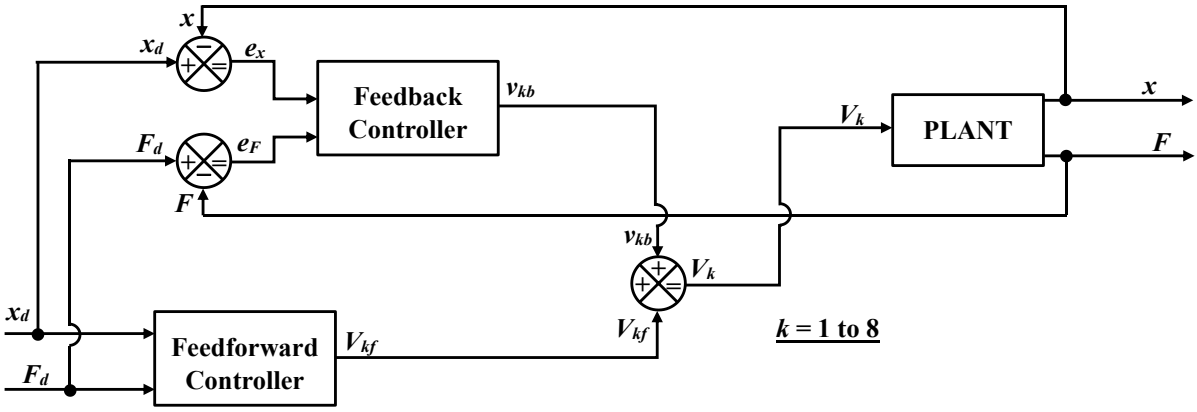

Fig.3.1: Combined Feedforward-PI controller for the EHLS

3.2 The Feedback Controller

The feedback controller implemented consists of two proportional-integral (PI) controllers – one for the metering valves of the motion cylinder, Cyl_1, and the other for the metering valves of the forcing cylinder, Cyl_2. Based on the position error e_x the feedback voltage can be expressed as,

$$v_x = K_{Px} e_x + K_{Ix} \int e_x \, dt \tag{3.2a}$$

where, $e_x = x_d - x$. (3.2b)

In equation (3.2a), K_{Px} and K_{Ix} are the proportional and integral gains and v_x is the feedback voltage for the position controller.

Similarly, based on the force error e_F the feedback voltage can be expressed as,

$$v_F = K_{PF} e_F + K_{IF} \int e_F \, dt \tag{3.2c}$$

where, $e_F = F_d - F$. (3.2d)

In equation (3.2c), K_{PF} and K_{IF} are the proportional and integral gains and v_F is the feedback voltage for the force controller.

Then the feedback voltages for the 8 metering valves can be expressed as,

$v_{kb} = v_x$, where, k = 3 and 4, for $\dot{x}_d \geq 0$, and k = 1 and 2, for $\dot{x}_d < 0$ – for CIMV (3.2e)

where, k = 3 and $v_{4b} = 0$, for $\dot{x}_d \geq 0$, and k = 1 and $v_{2b} = 0$, for $\dot{x}_d < 0$ – for IMV

$= v_F$, where, k = 5 and 6, for $\dot{x}_d \geq 0$, and k = 7 and 8, for $\dot{x}_d < 0$ – for CIMV. (3.2f)

where, k = 5 and $v_{6b} = 0$,, for $\dot{x}_d \geq 0$, and k = 7 and $v_{8b} = 0$, for $\dot{x}_d < 0$ – for IMV.

3.3 Order-separated Composite Feedforward Position-Force Controller

A feedforward modelling for the proposed study is detailed next corresponding to exciting Cyl_1 for motion tracking and Cyl_2 for force control in CIMV or IMV mode. During retraction of Cyl_1, For CIMV mode, the excited pair of valves V3-V4, controlling the flow in Cyl_1 remains under identical variable excitation

mode. For IMV mode, the valve V4 metering the return flow, remains under fixed excitation V_m. During the corresponding piston extension in Cyl_2, V5-V6 remains in identical variable excitation for CIMV mode, while the valve V6 metering the return flow, remains under fixed excitation V_m for IMV mode.

Similarly, during extension of Cyl_1, For CIMV mode, the excited pair of valves V1-V2, controlling the flow in Cyl_1 remains under identical variable excitation mode. For IMV mode, the valve V2 metering the return flow, remains under fixed excitation V_m. During the corresponding piston retraction in Cyl_2, V7-V8 remains in identical variable excitation for CIMV mode, while the valve V8 metering the return flow, remains under fixed excitation V_m for IMV mode.

Following the order-separated approach, considering that the effects of the valve and cylinder leakages and oil compressibility is of lower-order compared to the effect of piston motion, the feedforward voltages in the metering valves can be represented as

$V_{kf} = V_{kB} + v_{kl} + v_{k\beta}$, for k = 1, 3,5,7 (3.3a)

and $V_{(k+1)f} = V_{kf}$, for k = 1, 3,5,7, for CIMV mode (3.3b)

$= V_m =$ a fixed value, for IMV mode. (3.3c)

It goes without saying that

$v_{kl}, v_{k\beta} \ll V_{kB}$, for k = 1, 3,5,7 (3.3d)

where the subscript B indicates the basic feedforward component corresponding to the piston motion under constant-density flow and v_{kl} and $v_{k\beta}$ are the lower-order compensations for the valve leakage and oil compressibility respectively. In the feedforward formulation, the displacement, velocity, and acceleration of the piston are as per the demanded profile of motion and can be presented as $x_d, \dot{x}_d$ and $\ddot{x}_d$ respectively, while the force can be expressed as F_d – where the suffix 'd' stands for the demand. All other variables in equations (2.1) to (2.9) are followed by a suffix 'f' to indicate feedforward formulation. Furthermore, all the chamber pressures, pump pressure and pump flow can be represented as summation of two order-separated components – one as the basic feedforward component corresponding to the piston motion, represented by an uppercase alphabet with suffix 'B', and another lower-order compensation for the combined leakage and oil compressibility, represented by the corresponding lowercase alphabet. Hence,

$P_{cif} = P_{ciB} + p_{ci}$, for i = 1,2 (3.4a)

where, $p_{ci} \ll P_{ciB}$ (3.4b)

$P_{rif} = P_{riB} + p_{ri}$, for i = 1,2 (3.4c)

where, $p_{ri} \ll P_{riB}$ (3.4d)

$P_{Pf} = P_{PB} + p_P$ (3.4e)

where, $p_P \ll P_{PB}$ (3.4f)

and $Q_{Pf} = Q_{PB} + q_P$ (3.4g)

where, $q_P \ll Q_{PB}$ (3.4h)

Also $\dot{p}_{ci}$ and $\dot{p}_{ri}$ (for i = 1,2) are neglected.

Correspondingly using eq. (2.1), the feedforward model of friction can be expressed as,

$$f_f = \{f_s + (f_c - f_s)\exp(-\dot{x}_d^2/\dot{x}_s^2)\}\,\mathrm{sgn}(\dot{x}_d) + \alpha_v \dot{x}_d \quad (3.4i)$$

From eq. (2.9) and considering eq. (3.4e) and using first order Taylor Series expansion, one can write,

$$P_{Pf} = P_{PB} + p_P$$

$$= P_c + (P_{co} - P_c)\tanh\left\{\frac{Q_0 - Q_{Pf}}{Q_c}\right\}$$

$$= P_{PB} + \left.\frac{\partial P_{Pf}}{\partial Q_{Pf}}\right|_B (Q_{Pf} - Q_{PB}) \quad (3.4j)$$

Hence,

$$p_P = P_{Pf} - P_{PB} = \left.\frac{\partial P_{Pf}}{\partial Q_{Pf}}\right|_B (Q_{Pf} - Q_{PB}) = \left.\frac{\partial P_{Pf}}{\partial Q_{Pf}}\right|_B q_P$$

$$= \left(\frac{P_{c0} - P_c}{Q_c}\right)\left\{\tanh^2\left(\frac{Q_0 - Q_{PB}}{Q_c}\right) - 1\right\} q_P \quad (3.4k)$$

The force balance equations given by eqs. (2.2a) and (2.2b) can be expressed as

$$(m/2)\ddot{x}_d = F_d - P_{c1f}A_c + P_{r1f}A_r - f_f$$

$$= F_d - P_{c1B}A_c + P_{r1B}A_r - f_f - (p_{c1}A_c - p_{r1}A_r) \quad (3.4l)$$

$$(m/2)\ddot{x}_d = -F_d + P_{c2f}A_c - P_{r2f}\,A_r - f_f$$

$$= -F_d + P_{c2B}A_c - P_{r2B}\,A_r - f_f + (p_{c2}A_c - p_{r2}\,A_r) \quad (3.4m)$$

3.3.1 V3-V4 in Cyl_1 and V5-V6 in Cyl_2 activated

Based on the above discussion, equations (2.5a) to (2.5h) can now be expressed as,

$$Q_{c1f} = A_c\dot{x}_d - c_{lp}\{(P_{c1B} - P_{r1B}) + (p_{c1} - p_{r1})\} - \dot{P}_{c1B}\{\Omega_{c1} - A_c x_d\}/\kappa$$

$$= A_c\dot{x}_d - c_{lp}(P_{c1B} - P_{r1B})\left\{1 + \frac{(p_{c1}-p_{r1})}{(P_{c1B}-P_{r1B})}\right\} - \dot{P}_{c1B}\{\Omega_{c1} - A_c x_d\}/\kappa \quad (3.5a)$$

$$[\because (p_{c1} - p_{r1}) \ll (P_{c1B} - P_{r1B})]$$

$$= (c_{vc1}V_4 + c_{lc})\sqrt{(P_{c1B} + p_{c1})} - c_{lc}\sqrt{\{(P_{PB} - P_{c1B}) + (p_P - p_{c1})\}}$$

$$= \{c_{vc1}\left(V_{4B} + v_{4l} + v_{4\beta}\right) + c_{lc}\}P_{c1B}\left\{1 + 0.5\frac{p_{c1}}{P_{c1B}}\right\} - c_{lc}(P_{PB} - P_{c1B})\left\{1 + 0.5\frac{(p_P-p_{c1})}{(P_{PB}-P_{c1B})}\right\} \quad (3.5b)$$

$$[\because (p_P - p_{c1}) \ll (P_{PB} - P_{c1B}) \text{ and } p_{c1} \ll P_{c1B}]$$

Similarly,

$$Q_{c2f} = A_c\dot{x}_d - c_{lp}(P_{r2B} - P_{c2B})\left\{1 + \frac{(p_{r2}-p_{c2})}{(P_{r2B}-P_{c2B})}\right\} + \dot{P}_{c2B}\{\Omega_{c2} + A_c x_d\}/\kappa \quad (3.5c)$$

$$= \left\{c_{vc2}\left(V_{5B} + v_{5l} + v_{5\beta}\right) + c_{lc}\right\}(P_{PB} - P_{c2B})\left\{1 + 0.5\frac{(p_P-p_{c2})}{(P_{PB}-P_{c2B})}\right\} - c_{lc}P_{c2B}\left\{1 + 0.5\frac{p_{c2}}{P_{c2B}}\right\} \quad (3.5d)$$

$$Q_{r1f} = A_r\dot{x}_d - c_{lp}(P_{c1B} - P_{r1B})\left\{1 + \frac{(p_{c1}-p_{r1})}{(P_{c1B}-P_{r1B})}\right\} + \dot{P}_{r1B}\{\Omega_{r1} + A_r x_d\}/\kappa \quad (3.5e)$$

$$= \left\{c_{vr1}\left(V_{3B} + v_{3l} + v_{3\beta}\right) + c_{lr}\right\}(P_{PB} - P_{r1B})\left\{1 + 0.5\frac{(p_P-p_{r1})}{(P_{PB}-P_{r1B})}\right\} - c_{lr}P_{r1B}\left\{1 + 0.5\frac{p_{r1}}{P_{r1B}}\right\} \quad (3.5f)$$

$$Q_{r2f} = A_r\dot{x}_d - c_{lp}(P_{r2B} - P_{c2B})\left\{1 + \frac{(p_{r2}-p_{c2})}{(P_{r2B}-P_{c2B})}\right\} - \dot{P}_{r2B}\{\Omega_{r2} - A_r x_d\}/\kappa \quad (3.5g)$$

$$= \{c_{vr2}(V_{6B} + v_{6l} + v_{6\beta}) + c_{lr}\}P_{r2B}\left\{1 + 0.5\frac{p_{r2}}{P_{r2B}}\right\} - c_{lr}(P_{PB} - P_{r2B})\left\{1 + 0.5\frac{(p_P-p_{r2})}{(P_{PB}-P_{r2B})}\right\} \quad (3.5h)$$

From the expression of pump flow in eq. (2.7)

$$Q_{Pf} = Q_{PB} + q_P \quad (3.6)$$

$$= \{c_{vr1}(V_{3B} + v_{3l} + v_{3\beta}) + c_{lr}\}(P_{PB} - P_{r1B})\left\{1 + 0.5\frac{(p_P-p_{r1})}{(P_{PB}-P_{r1B})}\right\} +$$

$$+\{c_{vc2}(V_{5B} + v_{5l} + v_{5\beta}) + c_{lc}\}(P_{PB} - P_{c2B})\left\{1 + 0.5\frac{(p_P - p_{c2})}{(P_{PB} - P_{c2B})}\right\} +$$

$$+c_{lr}(P_{PB} - P_{r2B})\left\{1 + 0.5\frac{(p_P-p_{r2})}{(P_{PB}-P_{r2B})}\right\} + c_{lc}(P_{PB} - P_{c1B})\left\{1 + 0.5\frac{(p_P-p_{c1})}{(P_{PB}-P_{c1B})}\right\} \quad (3.7)$$

3.3.1.1 Estimation of Motion-Inducing Terms

After separation of the higher order terms from eq. (3.5a) – (3.5h), 3.6 and 3.4(j) the valve flows pump flow and pump pressure equations are reduced to

$$Q_{c1B} = A_c\dot{x}_d = (c_{vc1}V_{4B})\sqrt{P_{c1B}} \quad (3.8a)$$

$$Q_{c2B} = A_c\dot{x}_d = (c_{vc2}V_{5B})\sqrt{P_{PB} - P_{c2B}} \quad (3.8b)$$

$$Q_{r1B} = A_r\dot{x}_d = (c_{vr1}V_{3B})\sqrt{P_{PB} - P_{r1B}} \quad (3.8c)$$

$$Q_{r2B} = A_r\dot{x}_d = (c_{vr2}V_{6B})\sqrt{P_{r2B}} \quad (3.8d)$$

$$Q_{PB} = (A_c + A_r)\dot{x_d} \quad (3.8e)$$

$$P_{PB} = P_c + (P_{co} - P_c)\tanh\{(Q_0 - Q_{PB})/Q_c\} \quad (3.8f)$$

Similarly, collecting the higher order terms from eq. (3.4l) and (3.4m)

$$(m/2)\ddot{x}_d = F_d - P_{c1B}A_c + P_{r1B}A_r - f_f \quad (3.8g)$$

$$(m/2)\ddot{x}_d = -F_d + P_{c2B}A_c - P_{r2B}\,A_r - f_f \quad (3.8h)$$

From eq. (3.8a) and (3.8d) P_{c1B}, P_{r2B} can be expressed as

$$P_{c1B} = \{(A_c\dot{x}_d)/(c_{vc1}V_{4B})\}^2 \quad (3.9a)$$

Differentiating the above equation with respect to time, one obtains

$$\dot{P}_{c1B} = 2\dot{x}_d\ddot{x}_d\{(A_c)/(c_{vc1}V_{4B})\}^2 \quad (3.9b)$$

Similarly, $P_{r2B} = \{(A_r\dot{x}_d)/(c_{vr2}V_{6B})\}^2$ (3.9c)

and, $\dot{P}_{r2B} = 2\dot{x}_d\ddot{x}_d\{(A_r)/(c_{vr2}V_{6B})\}^2$ (3.9d)

From the basic force equation expressed in (3.8g)

$$P_{r1B} = \left\{\left(\frac{m}{2}\right)\ddot{x}_d + P_{c1B}A_c + f_f - F_d\right\}/A_r \quad (3.10a)$$

Differentiating eq. (3.10a)

$$\dot{P}_{r1B} = \left\{\left(\frac{m}{2}\right)\dddot{x}_d + \dot{P}_{c1B}A_c + \dot{f}_f - \dot{F}_d\right\}/A_r \quad (3.10b)$$

From basic motion equation expressed in eq. (3.8h)

$$P_{c2B} = \left\{\left(\frac{m}{2}\right)\ddot{x}_d + P_{r2B}A_r + f_f + F_d\right\}/A_c \quad (3.10c)$$

Differentiating eq. (3.10c), one can get

$$\dot{P}_{c2B} = \left\{\left(\frac{m}{2}\right)\dddot{x}_d + \dot{P}_{r2B}A_r + \dot{f}_f + \dot{F}_d\right\}/A_c \quad (3.10d)$$

As Q_{pB} is known from eq. (3.8e), P_{pB} can also derived from eq. (3.8f).

Hence from equation (3.8b) and (3.8c),

$$V_{5B} = A_c\dot{x}_d/\{c_{vc2}\sqrt{P_{PB} - P_{c2B}}\} \quad (3.10e)$$

$$V_{3B} = A_r\dot{x}_d/\{c_{vr1}\sqrt{P_{PB} - P_{r1B}}\} \quad (3.10f)$$

For CIMV,

$$V_{4B} = V_{3B} \tag{3.10g}$$

$$V_{6B} = V_{5B} \tag{3.10h}$$

For IMV,

$$V_{4B} = V_{6B} = V_m \tag{3.10i}$$

3.3.1.2 Estimation of Compressibility Related Terms

Considering the compressibility related terms from valve flow equations expressed in eq. (3.5a) – (3.5h), one can write,

$$-\frac{\dot{P}_{c1B}\{\Omega_{c1}-A_c x_d\}}{\kappa} = (c_{vc1} v_{4\beta})\sqrt{P_{c1B}} \tag{3.11a}$$

$$\dot{P}_{c2B}\frac{\{\Omega_{c2}+A_c x_d\}}{\kappa} = (c_{vc2} v_{5\beta})\sqrt{P_{PB}-P_{c2B}} \tag{3.11b}$$

$$\dot{P}_{r1B}\frac{\{\Omega_{r1}+A_r x_d\}}{\kappa} = \left(c_{vr1} v_{3\beta}\right)\sqrt{P_{PB}-P_{r1B}} \tag{3.11c}$$

$$-\frac{\dot{P}_{r2B}\{\Omega_{r2}-A_r x_d\}}{\kappa} = \left(c_{vr2} v_{6\beta}\right)\sqrt{P_{r2B}} \tag{3.11d}$$

Considering, $v_{m\beta} + v_{ml} = 0$ for m = 4 and 6. (3.11e)

Using the expressions for $\dot{P}_{r1B}, \dot{P}_{c2B}$ are expressed in eq. (3.10b) and (3.10d), the voltages corresponding to compressibility for supply valves (V3, V5) i.e., $v_{3\beta}, v_{5\beta}$ can be derived from eq. (3.11b) and (3.11c)

$$v_{5\beta} = \dot{P}_{c2B}\frac{\{\Omega_{c2}+A_c x_d\}}{\kappa} / \{c_{vc2}\sqrt{P_{PB}-P_{c2B}\}} \tag{3.11f}$$

$$v_{3\beta} = \dot{P}_{r1B}\frac{\{\Omega_{r1}+A_r x_d\}}{\kappa} / \{c_{vr1}\sqrt{P_{PB}-P_{r1B}\}} \tag{3.11g}$$

For CIMV,

$$v_{4\beta} = v_{3\beta} \tag{3.11h}$$

$$v_{6\beta} = v_{5\beta} \tag{3.11i}$$

For IMV,

For the IMV configuration, voltages corresponding to compressibility for return valves (V4 and V6) i.e., $v_{4\beta}$, $v_{6\beta}$ respectively can be derived from eq. (3.11a) and (3.11d).

$$v_{4\beta} = -\frac{\frac{\dot{P}_{c1B}\{\Omega_{c1} - A_c x_d\}}{\kappa}}{c_{vc1}\sqrt{P_{c1B}}} \tag{3.11j}$$

$$v_{6\beta} = -\frac{\frac{\dot{P}_{r2B}\{\Omega_{r2} - A_r x_d\}}{\kappa}}{c_{vr2}\sqrt{P_{r2B}}} \tag{3.11k}$$

3.3.1.3 Estimation of Leakage Related Terms

Separating the leakage related terms from eq. (3.5a) – (3.5h) one can write,

$$0 = 0.5c_{vc1}V_{4B}\left(\frac{p_{c1}}{\sqrt{P_{c1B}}}\right) + (c_{vc1}v_{4l} + c_{lc})\sqrt{P_{c1B}} - c_{lc}\sqrt{P_{PB} - P_{c1B}} + c_{lp}(P_{r1B} - P_{c1B}) \tag{3.12a}$$

$$0 = 0.5c_{vc2}V_{5B}\left(\frac{p_p - p_{c2}}{\sqrt{P_{PB} - P_{c2B}}}\right) + (c_{vc2}v_{5l} + c_{lc})\sqrt{P_{PB} - P_{c2B}} - c_{lc}\sqrt{P_{c2B}} - c_{lp}(P_{c2B} - P_{r2B}) \tag{3.12b}$$

$$0 = 0.5c_{vr1}V_{3B}\left(\frac{p_p - p_{r1}}{\sqrt{P_{PB} - P_{r1B}}}\right) + (c_{vr1}v_{3l} + c_{lr})\sqrt{P_{PB} - P_{r1B}} - c_{lr}\sqrt{P_{r1B}} - c_{lp}(P_{r1B} - P_{c1B}) \tag{3.12c}$$

$$0 = 0.5c_{vr2}V_{6B}\left(\frac{p_{r2}}{\sqrt{P_{r2B}}}\right) + (c_{vr2}v_{6l} + c_{lr})\sqrt{P_{r2B}} - c_{lr}\sqrt{P_{PB} - P_{r2B}} + c_{lp}(P_{c2B} - P_{r2B}) \tag{3.12d}$$

Collecting the lower order terms from eq. (3.7), the pump flow perturbation q_p can be expressed as

$$q_p = 0.5c_{vr1}V_{3B}(p_p - p_{r1})/(P_{PB} - P_{r1B}) + \left(c_{vr1}\{v_{3l} + v_{3\beta}\} + c_{lr}\right)\sqrt{(P_{PB} - P_{r1B})} + \frac{0.5c_{vc2}V_{5B}(p_p - p_{c2})}{\sqrt{(P_{PB} - P_{c2B})}} + \left(c_{vc2}\{v_{5l} + v_{5\beta}\} + c_{lc}\right)\sqrt{(P_{PB} - P_{c2B})} + c_{lr}\sqrt{(P_{PB} - P_{r2B})} + c_{lc}\sqrt{(P_{PB} - P_{c1B})} \tag{3.12e}$$

Collecting the lower order terms from eqs. (3.4l) and (3.4m),

$$p_{c1}A_c - p_{r1}A_r \tag{3.12f}$$

$$p_{c2}A_c - p_{r2}A_r \tag{3.12g}$$

To derive perturbation pressures for both cap-end and rod-end chambers of both the cylinders, one can use equations (3.12a), (3.12d), (3.12f) and (3.12g) and write,

$$p_{r2} = \frac{\sqrt{P_{r2B}}}{0.5c_{vr2}V_{6B}}[c_{lr}\sqrt{P_{PB} - P_{r2B}} - c_{lp}\sqrt{P_{c2B} - P_{r2B}} - (c_{vr2}v_{6l} + c_{lr})\sqrt{P_{r2B}}] \tag{3.13a}$$

$$p_{c2} = p_{r2}A_r/A_c \tag{3.13b}$$

$$p_{c1} = \frac{\sqrt{P_{c1B}}}{0.5c_{vc1}V_{4B}}[c_{lc}\sqrt{P_{PB} - P_{c1B}} - c_{lp}\sqrt{P_{r1B} - P_{c1B}} - (c_{vc1}v_{4l} + c_{lc})\sqrt{P_{c1B}}] \tag{3.13c}$$

$$p_{r1} = p_{c1}A_c/A_r \tag{3.13d}$$

From eq. (3.12b) and (3.12c), one can get v_{3l}, v_{5l} using all the variables derived earlier.

$$v_{3l} = \frac{1}{c_{vr1}}[\frac{c_{lr}\sqrt{P_{r1B}}}{\sqrt{P_{PB}-P_{r1B}}} + \frac{c_{lp}(P_{r1B}-P_{c1B})}{\sqrt{P_{PB}-P_{r1B}}} - 0.5c_{vr1}V_{3B}\left(\frac{p_p-p_{r1}}{P_{pB}-P_{r1B}}\right) - c_{lr}] \tag{3.13e}$$

$$v_{5l} = \frac{1}{c_{vc2}}[\frac{c_{lc}\sqrt{P_{c2B}}}{\sqrt{P_{PB}-P_{c2B}}} + \frac{c_{lp}(P_{c2B}-P_{r2B})}{\sqrt{P_{PB}-P_{c2B}}} - 0.5c_{vc2}V_{5B}\left(\frac{p_p-p_{c2}}{P_{pB}-P_{c2B}}\right) - c_{lc}] \tag{3.13f}$$

For CIMV,

$$v_{4l} = v_{3l} \tag{3.13g}$$

$$v_{6l} = v_{5l} \tag{3.13h}$$

For IMV,

$$v_{4l} = -v_{4\beta} \tag{3.13i}$$

$$v_{6l} = -v_{6\beta} \tag{3.13j}$$

3.3.2 V1-V2 in Cyl_1 and V7-V8 in Cyl_2 activated

When the pistons have a negative velocity demand, the actuating valves are V1-V2 for Cyl_1 and V7-V8 for Cyl_2. In IMV mode the return path valves (i.e.V2 & V8) are excited with a fixed voltage whereas the supply path valves (i.e., V1 & V7) are excited with varying voltages. Following a similar logic as detailed in the previous section, eqs (2.5a) – (2.5h) can be written for the negative velocity of the piston as,

$$Q_{c1f} = A_c\dot{x}_d + \dot{P}_{c1f}\frac{\{\Omega_{c1}+A_c x_d\}}{\kappa} - c_{lp}(P_{c1f} - P_{r1f}) \tag{3.14a}$$

$$= \left(c_{vc1}\{V_{1B} + v_{1l} + v_{1\beta}\} + c_{lc}\right)\sqrt{P_{Pf} - P_{c1f}} - c_{lc}\sqrt{P_{c1f}} \tag{3.14b}$$

$$Q_{c2f} = A_c\dot{x}_d - \frac{\dot{P}_{c2f}\{\Omega_{c2}-A_c x_d\}}{\kappa} + c_{lp}(P_{r2f} - P_{c2f}) \tag{3.14c}$$

$$= \left(c_{vc2}\{V_{8B} + v_{8l} + v_{8\beta}\} + c_{lc}\right)\sqrt{P_{c2f}} - c_{lc}\sqrt{P_{Pf} - P_{c2f}} \tag{3.14d}$$

$$Q_{r1f} = A_r\dot{x}_d - \frac{\dot{P}_{r1f}\{\Omega_{r1}-A_r x_d\}}{\kappa} - c_{lp}(P_{c1f} - P_{r1f}) \tag{3.14e}$$

$$= \left(c_{vr1}\{V_{2B} + v_{2l} + v_{2\beta}\} + c_{lr}\right)\sqrt{P_{r1f}} - c_{lr}\sqrt{P_{Pf} - P_{r1f}} \tag{3.14f}$$

$$Q_{r2f} = A_r\dot{x}_d + \dot{P}_{r2f}\frac{\{\Omega_{r2}+A_r x_d\}}{\kappa} + c_{lp}(P_{r2f} - P_{c2f}) \tag{3.14g}$$

$$= \left(c_{vr2}\{V_{7B} + v_{7l} + v_{7\beta}\} + c_{lr}\right)\sqrt{P_{Pf} - P_{r2f}} - c_{lr}\sqrt{P_{r2f}} \tag{3.14h}$$

Pump pressure will be expressed by the same eq. (3.4j) and pump flow equation can be expressed as

$$Q_{Pf} = Q_{PB} + q_p = \left(c_{vr2}\{V_{7B} + v_{7l} + v_{7\beta}\} + c_{lr}\right)\sqrt{P_{Pf} - P_{r2f}} + c_{lr}\sqrt{P_{r2f}} +$$

$$\left(c_{vc1}\{V_{1B} + v_{1l} + v_{1\beta}\} + c_{lc}\right)\sqrt{P_{Pf} - P_{c1f}} - c_{lc}\sqrt{P_{c1f}} \tag{3.15a}$$

Applying order separation method, as in the earlier section, feedforward voltages corresponding to higher order basic and lower order compressibility($v_{k\beta}$) and leakage(v_{kl}) for valves V1-V2 in cyl_1 and V7-V8 in cyl_2 using the valve flow, pump flow, pump pressure considering piston motion, force, friction; one can eventually come to

$$V_{1B} = A_c\dot{x}_d/\{c_{vc1}\sqrt{P_{PB} - P_{c1B}}\} \quad (3.15a)$$

$$V_{7B} = A_r\dot{x}_d/\{c_{vr2}\sqrt{P_{PB} - P_{r2B}}\} \quad (3.15b)$$

$$v_{1\beta} = \frac{\dot{P}_{c1B}\{\Omega_{c1} + A_c x_d\}}{\kappa}/\{c_{vc1}\sqrt{P_{PB} - P_{c1B}}\} \quad (3.15c)$$

$$v_{7\beta} = \frac{\dot{P}_{r2B}\{\Omega_{r2} + A_r x_d\}}{\kappa}/\{c_{vr2}\sqrt{P_{PB} - P_{r2B}}\} \quad (3.15d)$$

$$v_{1l} = \frac{1}{c_{vc1}}\left[\frac{c_{lc}\sqrt{P_{c1B}}}{\sqrt{P_{PB} - P_{c1B}}} + \frac{c_{lp}(P_{c1B} - P_{r1B})}{\sqrt{P_{PB} - P_{c1B}}} - 0.5c_{vc1}V_{1B}\left(\frac{p_p - p_{c1}}{P_{PB} - P_{c1B}}\right) - c_{lc}\right] \quad (3.15e)$$

$$v_{7l} = \frac{1}{c_{vr2}}\left[\frac{c_{lr}\sqrt{P_{r2B}}}{\sqrt{P_{PB} - P_{r2B}}} + \frac{c_{lp}(P_{r2B} - P_{c2B})}{\sqrt{P_{PB} - P_{r2B}}} - 0.5c_{vr2}V_{7B}\left(\frac{p_p - p_{r2}}{P_{PB} - P_{r2B}}\right) - c_{lr}\right] \quad (3.15f)$$

For CIMV,

$$V_{2B} = V_{1B} \quad (3.16a)$$

$$V_{8B} = V_{7B} \quad (3.16b)$$

$$v_{2\beta} = v_{1\beta} \quad (3.16c)$$

$$v_{8\beta} = v_{7\beta} \quad (3.16d)$$

$$v_{2l} = v_{1l} \quad (3.16e)$$

$$v_{8l} = v_{7l} \quad (3.16f)$$

For IMV

$$V_{2B} = V_{8B} = V_m \quad (3.16g)$$

$$v_{2\beta} = -\frac{\dot{P}_{r1B}\{\Omega_{r1} - A_r x_d\}}{\kappa}/c_{vr1}\sqrt{P_{r1B}} = -v_{2l} \quad (3.16h)$$

$$v_{8\beta} = -\frac{\dot{P}_{c2B}\{\Omega_{c2} - A_c x_d\}}{\kappa}/c_{vc2}\sqrt{P_{c2B}} = -v_{8l} \quad (3.16i)$$

3.4 Summary

The present chapter deals with design and development of a comprehensive feedforward position-force controller coupled with a pair of proportional-integral (PI) feedback controllers to drive an electrohydraulic load simulator comprising of a pair of double-acting single rod cylinders – connected end-to-end, along with a variable displacement pump and eight solenoid-operated 2×2 proportional valves. The uniqueness of the control scheme is control of a set of valves for individual metering of the cap-end and rod-end chambers of the 2 actuators. The feedforward controller comprehensively uses the motion and force demands to estimate the control voltages of the valves. An order-separated approach has been followed for designing the feedforward controller where the contributions of the valve and cylinder leakage as well as fluid compressibility is considered to be of lower order compared to the effect induced by the piston motion. An explicit method to design the above-mentioned system has been proposed here. The most notable aspect of the latter design is its wide range of applicability for compressible and incompressible flow, for fixed-displacement to pressure-compensated pumps, proportional and servo proportional valves as well as single and double-rod double-acting cylinders. Where the flatness-based controller design is the outcome of conventional technique, the novelty of the approach followed here (Sarkar et.al., 2023) for feedforward design lies in exploiting the natural order-separated form of the oil flow, leading to a non-iterative algebraic sequential estimation algorithm. A pair of PI-feedback controllers has been considered for the motion and force control – which augment the feedforward control signals. The performance of the controller has been tested for different scenarios as discussed in detail in the next chapter.

CHAPTER 4

RESULTS AND DISCUSSIONS

4.1 Introduction

A simulation study in MATLAB-SIMULINK with ODE45 (Dormand-Prince) solver with a variable time step with a maximum of 10^{-5}s and relative tolerance of 10^{-3} has been executed. A schematic of the Simulink GUI is shown in Fig. 4.1 below.

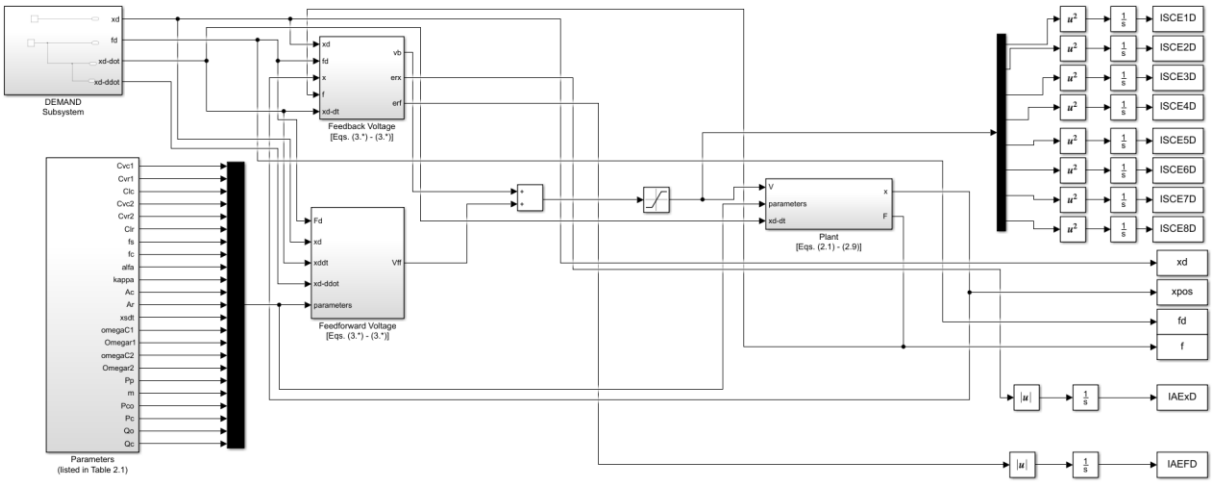

Fig.4.1: Simulink GUI for feedforward-pi control of dual-cylinder electrohydraulic load simulator

The "DEMAND Subsystem" generates the demanded position $x_d(t)$ and force $F_d(t)$ along with demanded velocity $x_{d\text{-dot}}(t)$ and acceleration $x_{d\text{-ddot}}(t)$ profiles – to be used in the feedforward control voltage estimations and error calculations in the feedback voltage estimations. The "Parameters" block provides all the plant parameters as listed in Table 2.1 – to be used in the plant model as well as the controller models. The "Feedback Voltage" block estimates the PI voltages for the 8 metering valves based on the position and force errors. The "Feedforward Voltage" block calculates the feedforward voltages for the 8 metering valves. The "Plant" block estimates the position of the piston and the force generated due the combined control voltages in the metering valves.

Results of the closed loop simulations performed for sinusoidal position and force tracking demand has been compared for both the CIMV and IMV configurations. Several force demands, like sinusoid, fixed, linearly time-varying, spring load, spring-damper load has been explored for sinusoid and fixed position demands. Results of position and force tracking, the control voltages in the 8 metering valves, the chamber pressures have been presented and explained. Several performance parameters have been calculated for quantitatively comparing the performances of the different cases. The first of these is the integral absolute position error given by

$$\text{IAE}_x = (\int_0^{nT} |e_x| dt)/(a_x nT), \tag{4.1a}$$

where, e_x is the position error given by eq. (3.2b).

The second one is the integral absolute force error given by

$$\text{IAE}_F = (\int_0^{nT} |e_F| dt)/(a_F nT), \tag{4.1b}$$

where, e_F is the force error given by eq. (3.2d).

The next one is the integral square control effort

$$\text{ISCE}_i = (\int_0^{nT} V_i^2 dt)/(V_{\max}^2 nT), \text{ for } i = 1 \text{ to } 8 \tag{4.1c}$$

Where V_i is the combined FFPI voltage in the i^{th} metering valve.

Power input from the variable displacement pump is

$$\overline{\Pi}_p = \left(\frac{\int_0^T (Q_p p_p) dt}{T}\right) \tag{4.1d}$$

By operating the pump in the variable-displacement mode in comparison to the fixed displacement mode maintaining the pump delivery at the relief valve pressure p_{RV}. The power saving is calculated as

$$\overline{\Pi}_{ps} = \overline{\Pi}_p - Q_0 p_{RV}. \tag{4.1e}$$

Where Q_0 is the fixed discharge from the fixed displacement pump and p_{RV} is the relief valve pressure setting.

The exit power loss in the metering valves can be estimated as,

$$\overline{\Pi}_{mvl} = \sum_{i=1}^{2} (\int_0^T (Q_{ij} p_{ij}) dt \,/T)\,, j = C \text{ or } R. \tag{4.1f}$$

The variations of IAE_x, IAE_F, ISCE_i, $\overline{\Pi}_{ps}$ and $\overline{\Pi}_{mvl}$ are also presented for quantitative comparison of the performances of the different cases.

The proportional and integral gains in evaluating the feedback voltages as per eqs. (3.2a) and (3.2c) are taken as, K_{Px} = 500 V/m, K_{Ix} = 150 V/(ms), K_{PF} = 0.02 V/N, K_{Ix} = 0.003 V/(Ns). These values have been obtained by several trial and error with the simulation tool developed. The same gain values have been used for the CIMV and IMV configurations.

4.2 Performance Comparison of IMV and CIMV Configurations

In Figures 4.2(a) and 4.2(b), the position response and the force response of the dual-cylinder loading system are presented respectively. The position demand is given by

$$x_d(t) = a_x \sin\{(2\pi t/T) + \phi_x\} + x_0 \qquad (4.2a)$$

where the demand amplitude a_x = 0.1m, the time period T = 2s, the phase $\phi_x = 1.5\pi$ and the bias x_0 = 0.1m. The force demand is expressed as

$$F_d(t) = a_F \sin\{(2\pi t/T) + \phi_F\} \qquad (4.2b)$$

where the demand amplitude a_F = 1500N, the time period T = 2s, the phase $\phi_F = 1.5\pi$. Results are presented for a CIMV arrangement where excitations of the valves metering the return flows from the 2 cylinders are identical to the corresponding valves metering the supply flows in these cylinders. Along with these, results for the IMV arrangements where the metering valves in the return paths of the flows from the 2 cylinders are excited by identical fixed voltages – namely 2V, 4V, 6V, 8V and 10V – are shown in Figures 4.2(a) and 4.2(b).

As can be seen, the best performances have been exhibited by the CIMV configuration compared to the IMV configurations. This is also evident from the non-dimensional performance indices IAE_x and IAE_F – as listed in Table 4.1. This is likely to happen, as, for the IMV configurations, one forfeits the continuous control of the return path metering valves based on the position or force errors. On the other hand, for the CIMV, the control of the return path metering valves is continuously monitored based on the errors – similar to, the supply path metering valves. Hence, the performance on IMV appears inferior to the CIMV. However, further exploration needs to be carried out to see if the IMV performances can be improved by suitable tuning of the PI-controller gains – at values different from those used for CIMV. It is further observed that for higher IMV return path valve voltages, the error is higher for voltages greater than or equal to 4V. However, for the negative piston velocity zone the highest error is seen for 2V IMV

excitation. The best performance of the IMV is seen when the return path voltage is set at 4V. This is evident from Figs. 4.2(a) and 4.2(b), as well as from Table 4.1.

It is further observed in Fig. 4.2(a) that as the demanded piston velocity changes sign at half the cycle time, the position response shows a sudden drop and then follows a track with lesser slope than that of the demand for some duration till it catches up with the demand again. This effect is manifested as spikes – first positive which is soon followed by a negative one – in the force response as shown in Fig. 4.2(b). This is attributed to the nature of the control structure. For positive $\dot{x}_d$, the metering valve combinations which are activated are V3 – V4 for Cyl_1 and V5 – V6 for Cyl_2 – all intending to move the cylinders in the positive *x* – direction.

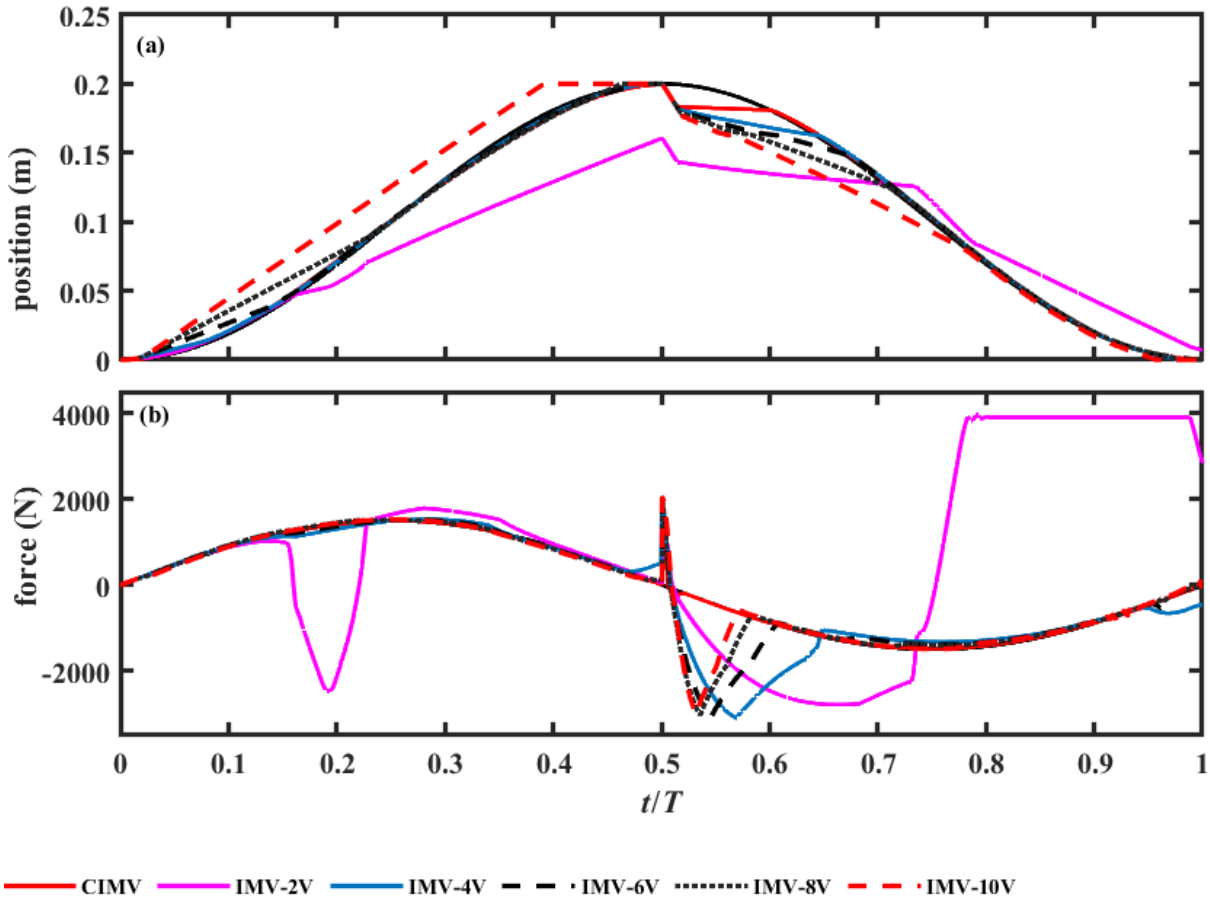

Fig. 4.2: Comparison of (a) position response and (b) force response – for a CIMV and IMV arrangements at different return path valve excitations.

Since the demanded piston velocity changes sign at half the cycle time, the active valve combination also changes to V1 – V2 for Cyl_1 and V7 – V8 for Cyl_2 – all now intending to move the cylinders in the negative *x* – direction. But during this reversal, if the position error is still positive, to minimize this error,

it is essential for the piston to carry on moving in the positive x – direction – which it is unable to do due to switching of the valve combinations. Hence this sudden drop occurs and it regains effective tracking once the demand falls below the actual position i.e.; the position error becomes negative.

Figures 4.3(a) – 4.3(h) presents the FFPI control voltage for the 8 metering valves. For $\dot{x}_d \geq 0$, supply flows to the rod end of Cyl1 and cap end of Cy2 occur through valves V3 and V5, respectively; while return flows from the cap end of Cyl1 and rod end of Cyl2 occur through valves V4 and V6, respectively. For $\dot{x}_d < 0$, the corresponding supply flows to the alternate chambers of the cylinders occur through valves V1 and V7 and return flows through valves V2 and V8. For the positive cycle ($\dot{x}_d \geq 0$) i.e. for half cycle ($t/T \leq 0.5$), V3 – V6 are the active metering valves. The complementary metering valves are activated during the negative cycle (i.e. $\dot{x}_d \leq 0$). Hence, for positive 1st half cycle the metered valves (V3 – V6) have some voltages while the remaining valves have zero voltage input. For the 2nd half of the cycle the metering valves (V1, V2, V7 & V8) have some voltages but voltage for valves V3, V4, V5 and V6 are zero.

A comparison of Figs. 4.3(b), (d), (f) and (h), with Figs. 4.3(a), (c), (e) and (g) reveals that the value 4V (in V4 – V6 for $\dot{x}_d \geq 0$, V2 –V8 for $\dot{x}_d < 0$, for IMV) is close to the maximum voltage in the return path metering valves of the CIMV. So, looking at Figs. 4.2(a) and (b), one may conclude, that for IMV configuration, the best performance is ensured when the fixed voltage in the return path metering valves of IMV is close to the maximum voltage is the return path metering valves of the CIMV. Furthermore, if the IMV return path metering valve fixed voltage is less than this value of 4V (as in IMV-2V in the present study), then to compensate for the loss of continuous control is the return path metering valves, the voltages in the supply paths for IMV-2V shoots up to very high values (in V3, V5, V1 and V7) – often reaching a voltage saturation of 10V leading to a loss of control henceforth. This explains the poor tracking performances for IMV-2V in Figs. 4.2(a) and 4.2(b).

For IMV, if the fixed voltage in return path metering valve is greater than this value of 4V (as in IMV-6V, 8V, in the present study), the voltages in the supply paths are comparable to those of CIMV (in V3, V5, V1 and V7). For IMV-10V, some incidence of voltage saturation is observed in Fig. 4.3(g) and some high overshoots in Fig. 4.3(c). This leads to the degradation in tracking performances for IMV-10V, as seen in Figs. 4.2(a) and 4.2(b).

Since for the IMV cases, the return path metering valves are kept wide open, hence for voltages in the range 4-10V, the average return chamber pressures are lower than the CIMV case. For the first half cycle, when the demanded velocity is positive, the return chambers are the cap end for Cyl_1 and rod end for Cyl_2. From Figs. 4.4(a) and 4.4(d), indeed the average pressures for IMV are lower than those for CIMV. From expressions of the force generated in eq. (2.3), if the cap end (or rod end) pressure reduces, then to maintain the load, the corresponding rod end (or cap end) pressures must also diminish. This is revealed in Fig. 4.4. For IMV-10V, the return path pressures are almost equal to zero which is the tank pressure. So, the supply path pressure needs to be very low also. This is ensured by the low value the control voltage in V3 as shown in Fig. 4.3(a).

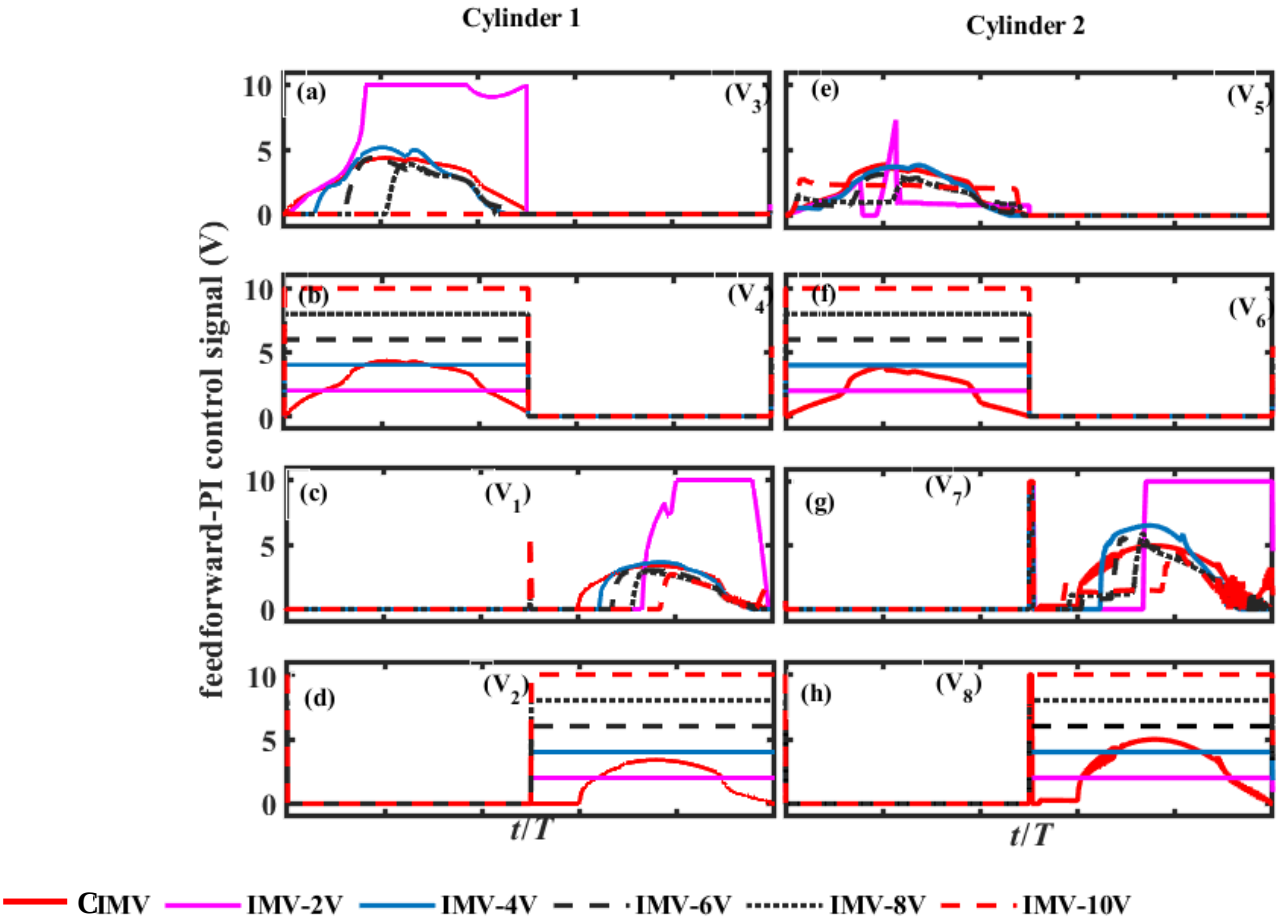

Fig. 4.3: Comparison of FFPI control voltage for metering valves 1 to 8 – for a CIMV and IMV arrangements at different return path valve excitations.

Figures 4.5(a) and 4.5(b) represent the power saved as compared to a fixed displacement pump and the exit loss in the return path metering valves respectively. As can be seen, for almost all the cases the power saving is maximum for the CIMV. This is again due to poor tracking performances by the IMV cases resulting in higher power requirement from the pump. As mentioned earlier, further study by tuning the

PI gains need to be carried out. Also, the exit loss reduces with greater opening of the return path metering valve in the IMV cases for voltages greater than 4V. For the latter, it is comparable with the CIMV for reasons mentioned earlier. The exit loss is sufficiently high for the IMV-2V case due to control saturation.

From the discussion presented earlier and the Table 4.1 below, it can be concluded that for a fixed gain FFPI controller, CIMV exhibits better performance than IMV –on count of tracking error, control effort, power savings and exit loss. Thus, the remaining studies have been carried out for CIMV configuration.

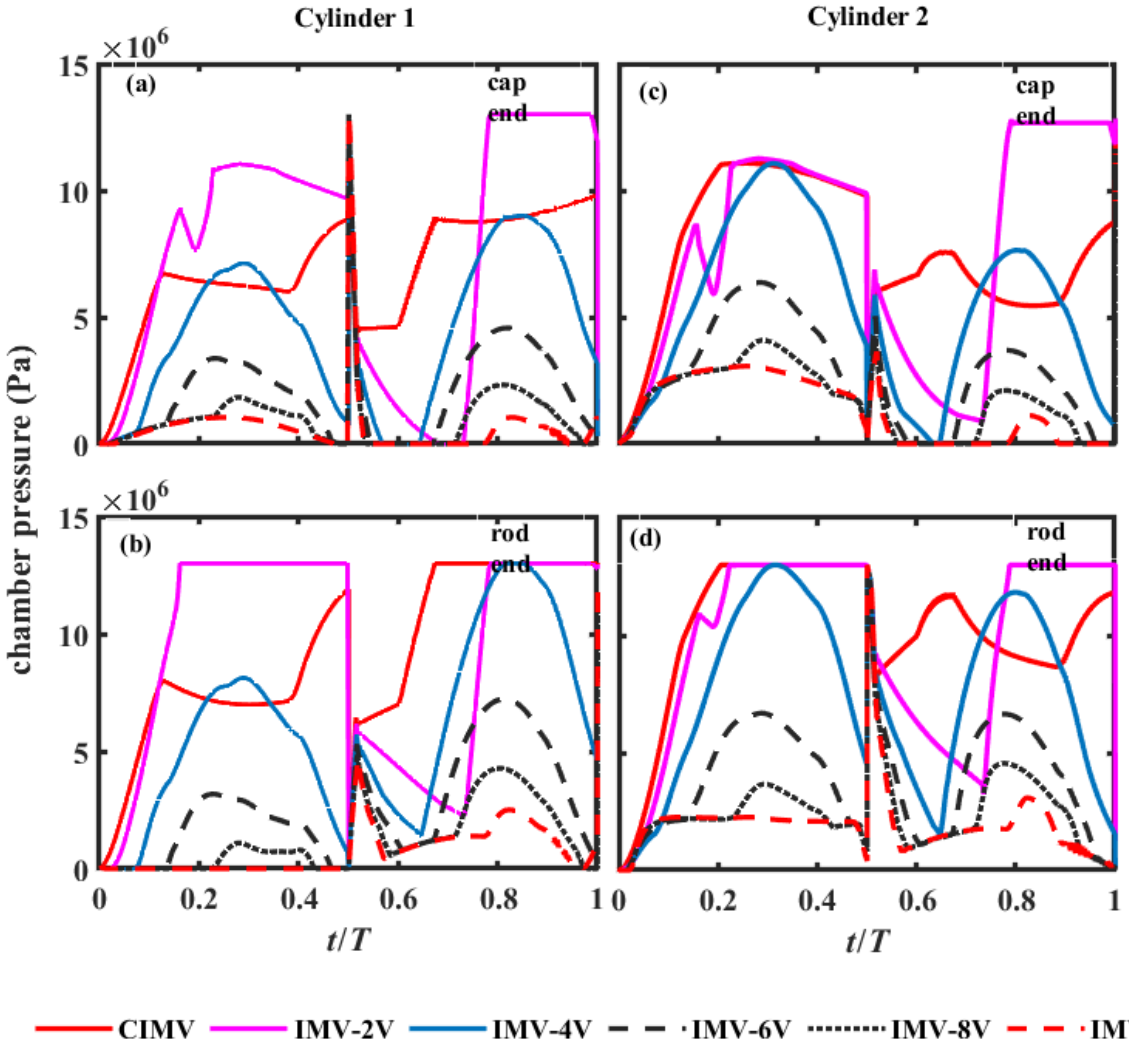

Fig. 4.4: Comparison of cylinder chamber pressures in (a) cap end of cylinder 1, (b) rod end of cylinder 1, (c) cap end of cylinder 2 and (d) rod end of cylinder 2 – for a CIMV and IMV arrangements at different return path valve excitations.

Table 4.1: Controller Performance Indices for a CIMV and IMV arrangements at different return path valve excitations

Configuration	IAE_x	IAE_F	$ISCE_1$	$ISCE_2$	$ISCE_3$	$ISCE_4$	$ISCE_5$	$ISCE_6$	$ISCE_7$	$ISCE_8$
CIMV	0.03	0.10	0.02	0.02	0.05	0.05	0.03	0.03	0.06	0.06
IMV(2V)	0.25	1.25	0.21	0.02	0.33	0.02	0.01	0.02	0.27	0.02
IMV(4V)	0.05	0.22	0.02	0.08	0.05	0.08	0.03	0.08	0.08	0.08
IMV(6V)	0.06	0.15	0.02	0.18	0.03	0.18	0.01	0.18	0.05	0.18
IMV(8V)	0.10	0.12	0.01	0.32	0.01	0.32	0.01	0.32	0.04	0.326
IMV (10V)	0.22	0.14	0.10	0.50	0.00	0.50	0.02	0.50	0.07	0.50

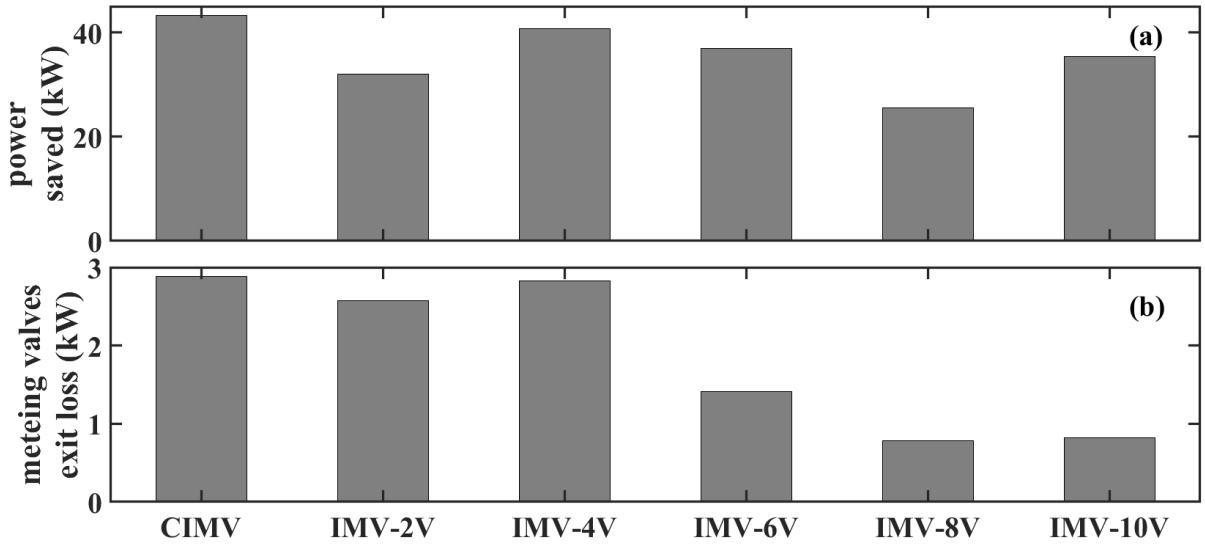

Fig. 4.5: Comparison of (a) pump output power and (b) total exit loss in the metering valves of the 2 cylinders – for a CIMV and IMV arrangements at different return path valve excitations.

4.3 Performance Comparison for Different Constant Load Demands and Sinusoidal Position Demand

Constant load operation is often desirable in case of cutting tools to ensure that the best overall cutting parameters can be used, resulting in substantially lower cycle times. Moreover, this practice enables better utilization of the cutting tool while extending its life in the bargain. At the same time faithful trajectory tracking of the cutter is also required. Hence load simulators are often used to check the controlled position response of the piston in the face of a simulated constant load. For single cylinder arrangements, such constant loads may be generated using a dead weight as shown in Fig. 4.6 below, where a wire is attached at the rod end of a double-acting single-rod hydraulic cylinder. This wire passes over a pulley and a dead weight can be suspended from its end to create the constant force loading scenario.

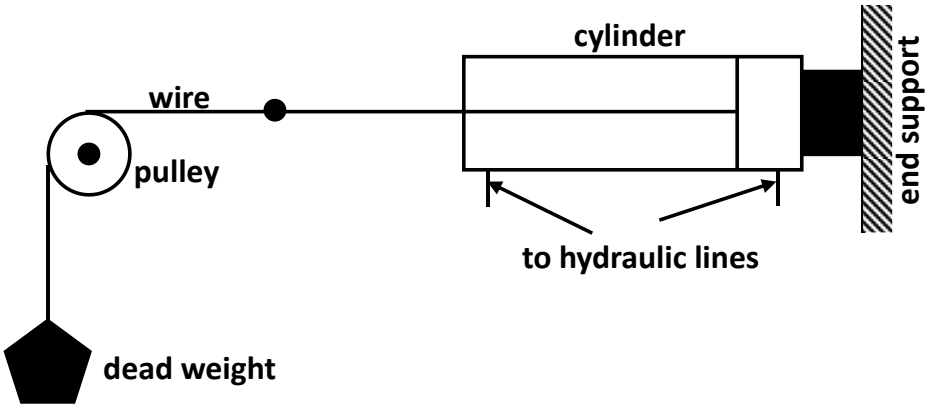

Fig. 4.6: Constant force loading of a hydraulic cylinder.

In the case of the load simulator, this is achieved by a constant load demand to the forcing cylinder and desired position demand to the motion cylinder. Simulation results for four constant load demand of 0N, 1500N, 5000N and 10000N are shown in Figs. 4.7, 4.8 and 4.9 for a sinusoid position demand of 0.1m amplitude at 0.5Hz frequency. From Figs. 4.7(b), (c), (d) and (e), for the entire cycle, the force demand is satisfactorily achieved barring the initial transience at t = 0s for nonzero force demands and at half the cycle time with the sign reversal of the demanded velocity leading to switching from one set of metering valves to another which leads to another transience. For the force demand of 0N, the initial condition of force, set for the dynamics of the piston in the simulation model of the piston matches with the demand. Hence at t = 0s, the force response matches with the demand. However, for the other nonzero demands, there is a transience at t = 0s. This initial error between the force responses and demands for the cases of nonzero demands, leads to large control voltages at t = 0s in V5 and V6 in the force cylinder (Cyl_2) – as seen in Figs. 4.8(e) and (f). These lead to a deviation of the initial position response from the corresponding demand as seen in Fig. 4.7(a). The transience at half the cycle time is larger for larger force demands.

It is evident from the expression of the generated force given by eq. (2.3) that for increasing its magnitude, P_{c1} and P_{c2} should increase and P_{r1} and P_{r2} should decrease. This is manifested in the variation of control voltages in Fig. 4.8 and variation of chamber pressures in Fig. 4.9.

During the first half cycle, the cap end chamber of Cyl_1 is connected to the tank through valve V4, while that of Cyl_2 is connected to the pump line through V5. To increase or decrease the pressures in these cap end chamber, the openings of V4 and V5 should be increased or decreased by respectively increasing or decreasing the control voltages. The predicted variations in Figs. 4.8(b) and 4.8(e) are consistent with these observations and the sinusoidal demand forms. Similar variations of voltages in Figs. 4.8(a) and 4.8(f) respectively for effecting the periodic variations of the openings of V3 and V6 produce corresponding variations of the rod-end chamber pressures. These

valves remain closed during the second half cycle as the other four valves remain closed during the first half cycle. Voltage variations similar to V4 – V5 and V3 – V6 pairs in the first half is apparent for V1 – V8 and V2 – V7 pairs respectively in the second half in view of the corresponding switching of the valve connections with the cylinder chambers. For the entire cycle, consistent variations of the chamber pressures in the cap and rod ends are seen in Figs. 4.9(a) – (d).

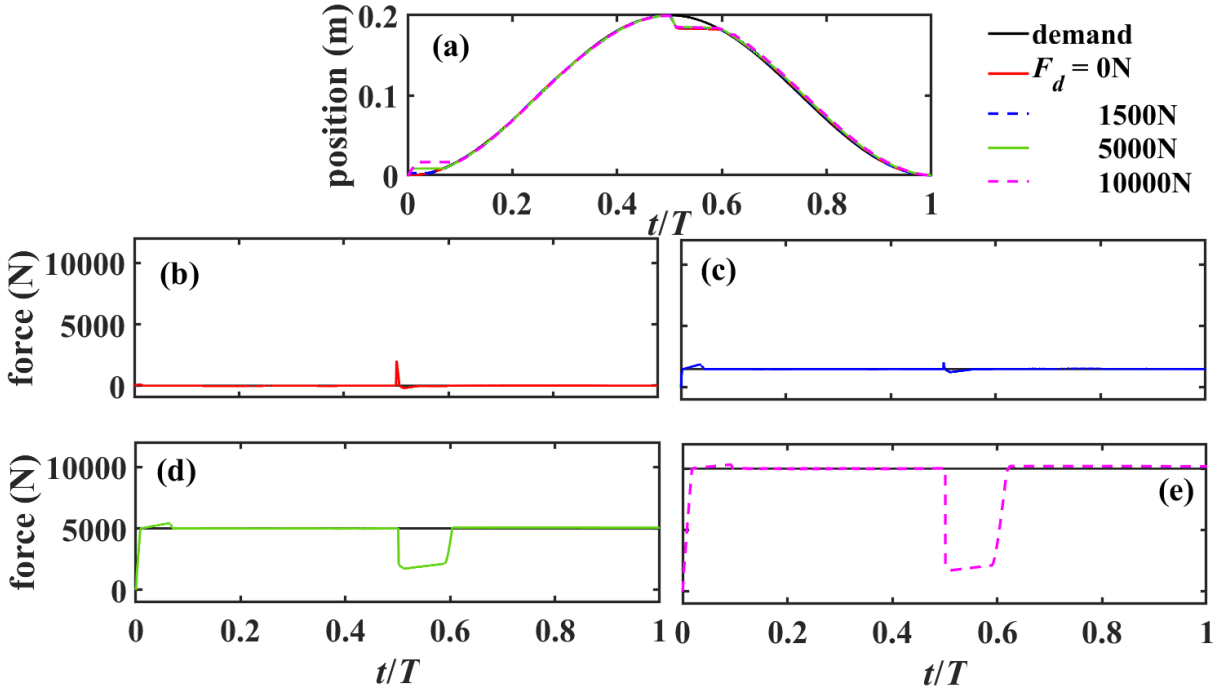

Fig. 4.7: (a) Position response and force responses with CIMV for a sinusoid position demand and constant force demands of magnitude (b) 0N, (c) 1500N, (d) 5000N and (e) 10000N.

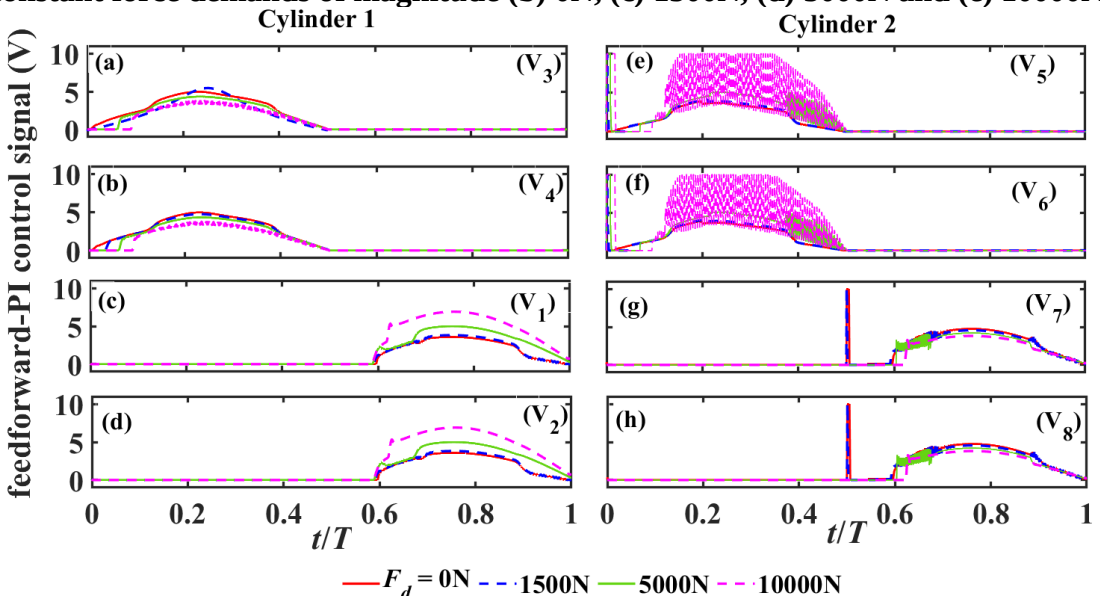

Fig. 4.8: FFPI control voltage for metering valves 1 to 8 – for a CIMV with a sinusoid position demand and constant force demands of magnitude 0N, 1500N, 5000N and 10000N.

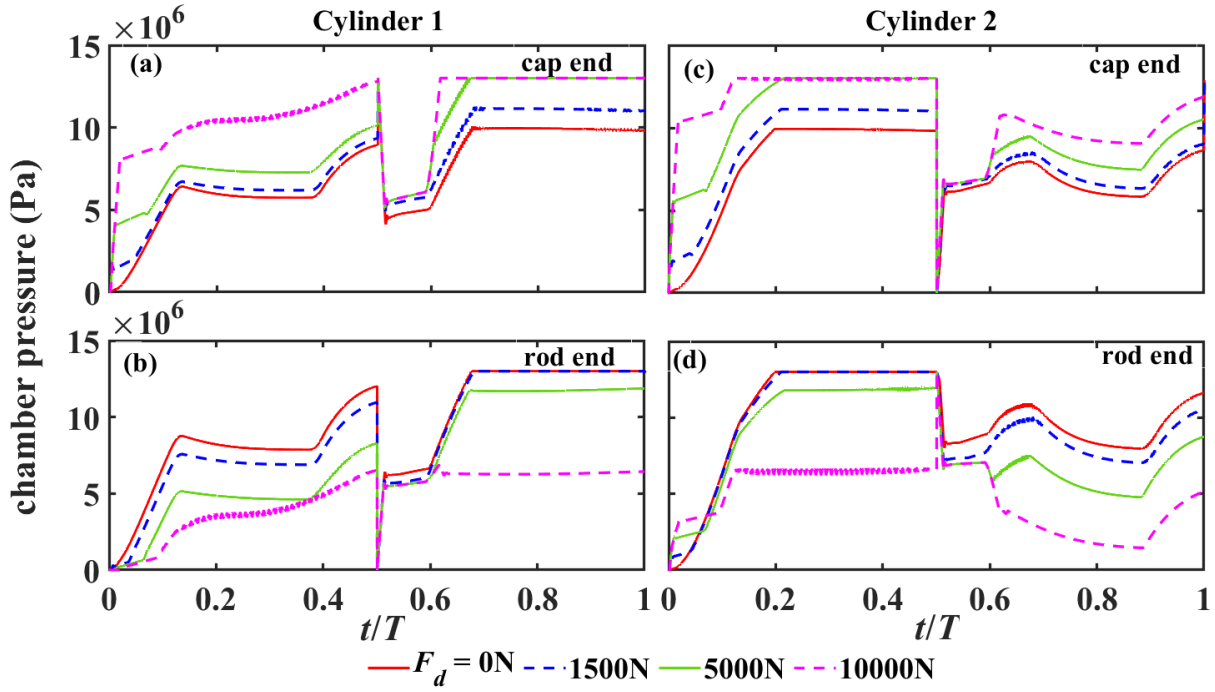

Fig. 4.9: Comparison of cylinder chamber pressures in (a) cap end of Cylinder 1, (b) rod end of Cylinder 1, (c) cap end of Cylinder 2 and (d) rod end of Cylinder 2 – for a CIMV with a sinusoid position demand and constant force demands of magnitude 0N, 1500N, 5000N and 10000N.

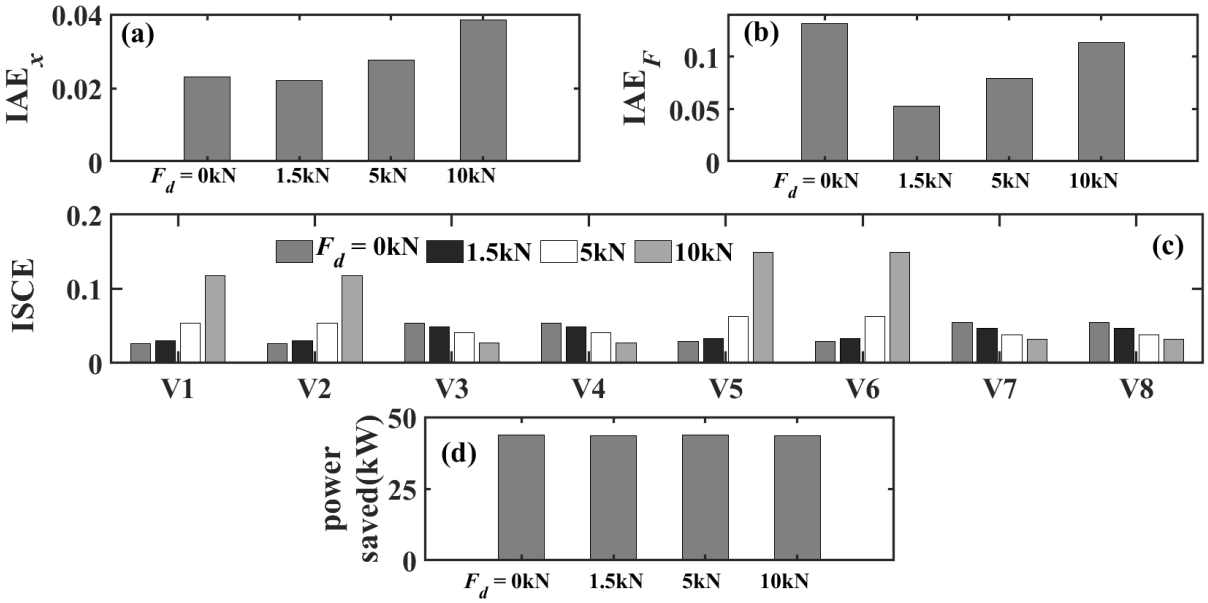

Fig. 4.10: Comparison of (a) IAE_x, (b) IAE_F, (c) ISCE and (d) power saving for variable displacement pump – for a CIMV with a sinusoid position demand and constant force demands of magnitude 0N, 1500N, 5000N and 10000N.

As seen in Fig. 4.10(b), the IAE_F increases progressively with the load value, barring the case of 0N. This is because, for the case of 0N, to calculate the IAE_F, a small force magnitude is used for normalization to avoid division by zero. The IAE_F for the other cases and IAE_x, as evident in Fig. 4.10(a), is consistent with the findings in Fig. 4.7.

To counter the higher force tracking error, the control efforts for the motion cylinder increase for V1, V2, V5 and V6 increases with the load – as is seen in Fig. 4.10(c).

4.4 Performance Comparison for Different Spring Stiffness for a Spring-Loaded Cylinder with Sinusoidal Position Demand

Spring-loaded hydraulic cylinders are quite common in several applications like active car suspension systems, aircraft fin-control, machine tools and earthmoving vehicles. For single cylinder arrangements, such loads may be simulated using a linear spring as shown in Fig. 4.11 below, attached between the rod end of a double-acting single-rod hydraulic cylinder and a rigid end support.

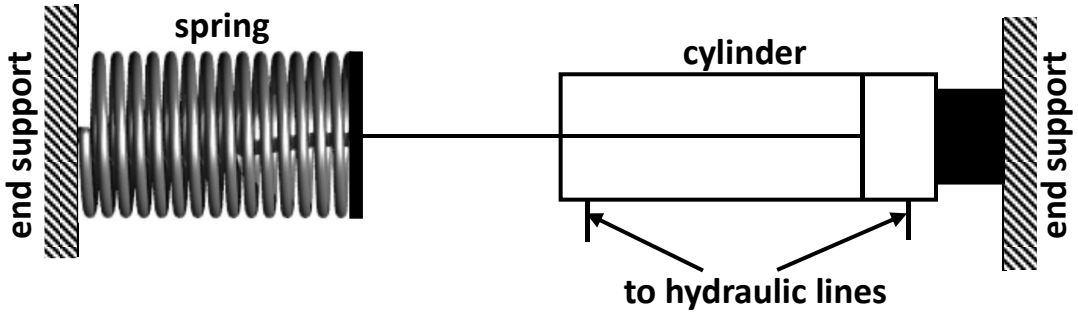

Fig. 4.11: Spring loading of a hydraulic cylinder.

In the case of the load simulator, this is achieved by using a force demand to the forcing cylinder expressed as

$$F_d = k_s x_d, \tag{4.3a}$$

where k_s is the spring stiffness and x_d is the desired position demand to the motion cylinder. Simulation results for four spring stiffness values of 2500N/m, 15000N/m, 50000N/m and 75000N/m are shown in Figs. 4.12, 4.13 and 4.14 for a sinusoid position demand of 0.1m amplitude at 0.5Hz frequency. If one looks into the Fig. 4.12(a) closely, one can say that the position response for CIMV with increasing stiffness of the spring (k_s) does not show any significant change, except at the half the cycle time as the velocity of the piston changes its sign from positive to negative at this point. But from Figs. 4.12(b) – (e), one can say that as the stiffness of spring increases, not only the force error increases, but also the time duration to catch up the recover the deviation from the force demand also increases. Hence, it is evident from these figures that the tracking responses is getting poorer with increasing spring stiffness for a CIMV with sinusoid position demand and spring force demand.

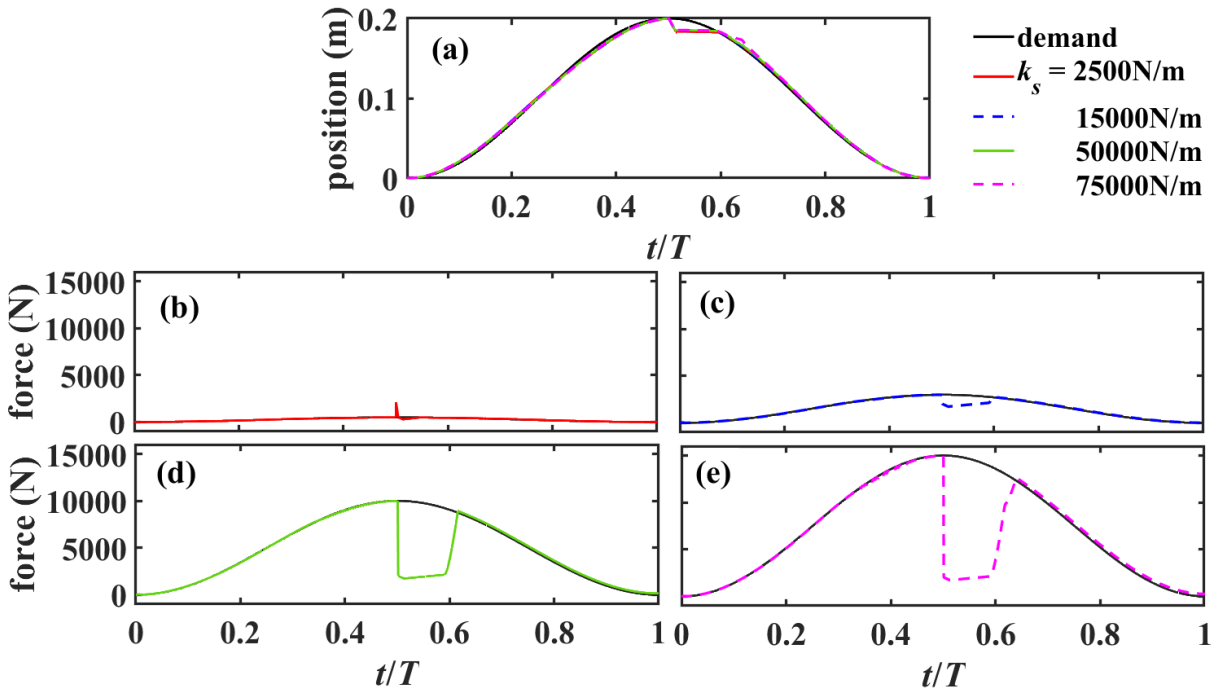

Fig. 4.12: (a) Position response and force responses with CIMV for a sinusoid position demand and spring force demands of spring stiffness of (b) 2500N/m, (c) 15000N/m, (d) 50000N/m and (e) 75000N/m.

From the expression of generated force in equation (2.3), it is evident that it increases with increase in cap-end pressures of both the cylinders together with the decrease in the rod-end pressures. As spring stiffness increases, the generated force also increases. For positive cycle, to increase pressure at cap end of cylinder 1 the valve V4 which is connected to the tank, should have less opening, hence voltage V_4 should decrease as spring stiffness increases. Similarly, to increase pressure at cap end of cylinder 2 the valve V5, connected to supply, should be wide opened. Hence, the voltage V_5 should increase with increasing stiffness of the spring. Again, to reduce pressure at rod end of Cyl_1, voltage in V3 should gradually reduce with increase in k_s and to reduce pressure at rod end of Cyl_2, voltage in V6 should gradually increase with increase in k_s.

This is exactly what one can see from the Figs. 4.13.(a), (b), (e) &(f). The opposite behavior is seen from Figs. 4.13(c), (d), (e) and (g). The initial voltages for the first half cycle in these figures are zero as valves V1, V2, V7, V8 are excited during the negative velocity demand phase. In 2nd half cycle, it is observed that with increasing spring stiffness V_1 and V_2 increase and V_7 and V8 decrease –. This is consistent with the expression of force derived in eq. (2.3).

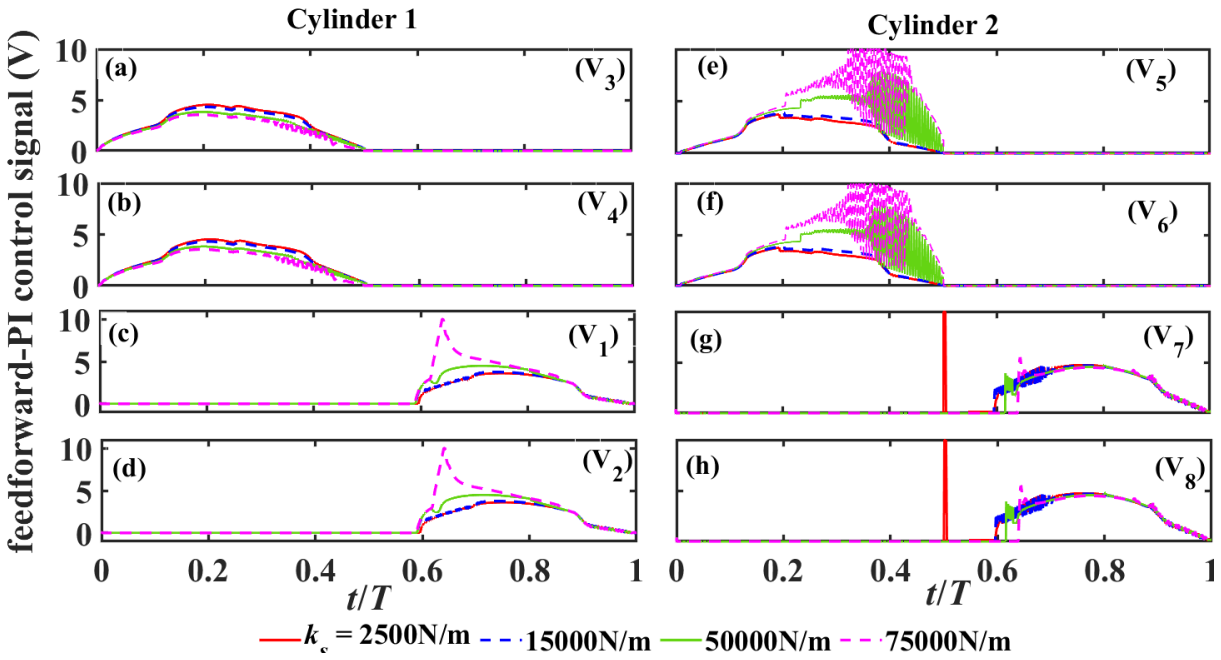

Fig. 4.13: FFPI control voltage for metering valves 1 to 8 – for a CIMV with a sinusoid position demand and spring force demands of spring stiffness of 2500N/m, 15000N/m, 50000N/m and 75000N/m.

Figures 4.14(a) – (d) present the chamber pressures with a non-dimensional time (t/T) for both the cylinders for a CIMV with sinusoid position demand and different spring stiffness k_s. It is evident from Figs. 4.14(a) & (c) that with increase in spring stiffness the cap end pressures increase and at some time even reached the saturation value. It is observed from Figs. 4.14(b) & (d), that the rod end pressure decreases as the spring stiffness increases – opposite to cap end pressures. From the force equation, one can easily relate to these. To increase load or force, cap end chamber pressures need to be increased but the rod end pressures must be decreased.

Fig 4.15(a) – (b) shows the integral absolute error for both motion and force, integral square control effort and power saved for a CIMV with sinusoid motion demand and different force demands. It is noticed that IAE_x is almost insensitive to k_s – in the range explored. Howe IAE_F is nearly close to 0.7 at stiffness 2.5 kN/m. Then it drops suddenly, for the stiffness value of 15kN/m and then it increases with stiffness.

Fig 4.15(c) shows that the integral square control effort (ISCE) for the forcing cylinder, V1, V2, V5 and V6 follow the same pattern. It is increased with increasing k_s for these valves. But for the motion cylinder V3, V4, V7, V8 ISCE shows opposite trend. Again, it is seen that power saved is almost equal in all the cases.

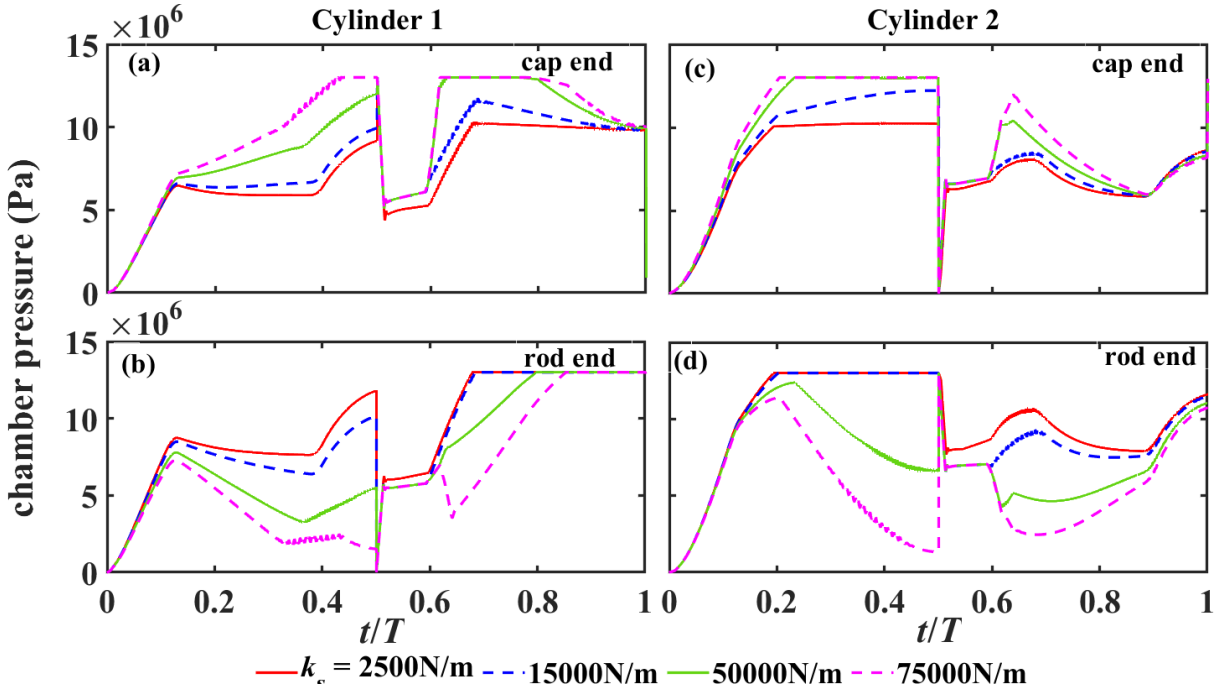

Fig. 4.14: Comparison of cylinder chamber pressures in (a) cap end of Cylinder 1, (b) rod end of Cylinder 1, (c) cap end of Cylinder 2 and (d) rod end of Cylinder 2 – for a CIMV with a sinusoid position demand and spring force demands of spring stiffness of 2500N/m, 15000N/m, 50000N/m and 75000N/m.

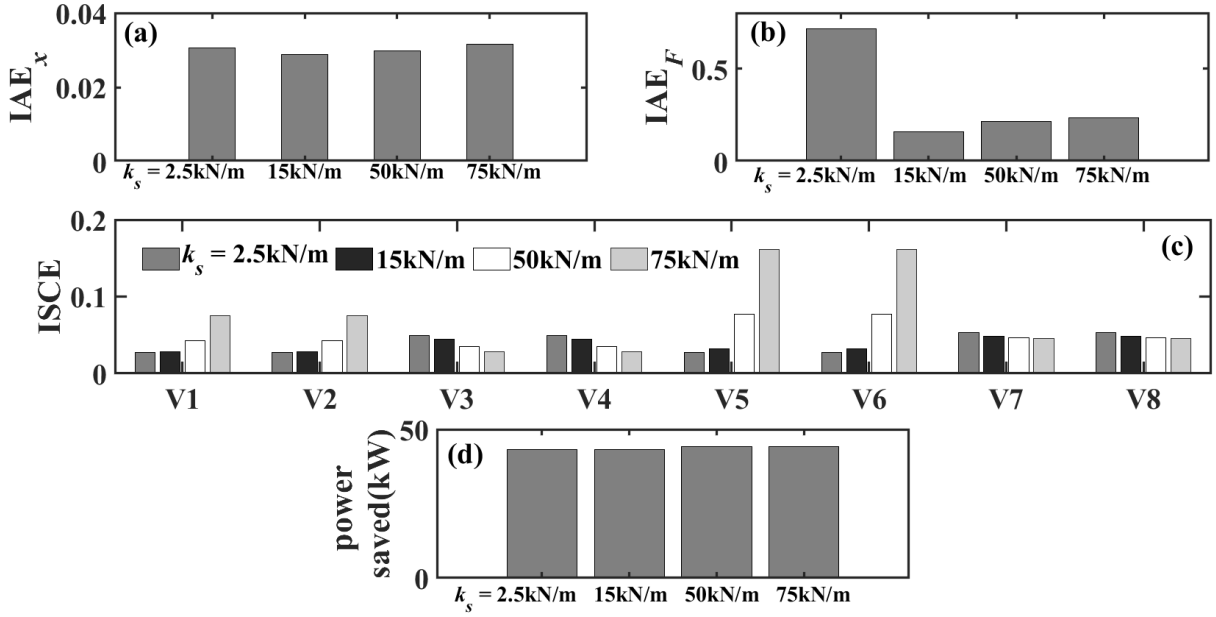

Fig. 4.15: Comparison of cylinder (a) IAE$_x$, (b) IAE$_F$, (c) ISCE and (d) power saved – for a CIMV with a sinusoid position demand and spring force demands of spring stiffness of 2500N/m, 15000N/m, 50000N/m and 75000N/m.

4.5 Performance Comparison for Different Damping Coefficients for a Spring-Damper Loaded Cylinder with Sinusoidal Position Demand

Spring-damper loading of hydraulic cylinder are commonly used in various industrial and automotive applications for example automotive suspension systems, construction equipment, industrial machinery, aerospace industry, material handling equipment, etc. These are just a few examples, but hydraulic cylinders with spring-damper loads can be found in many other applications where controlled motion, vibration damping, and shock absorption are necessary.

A spring- damper loaded single-rod double-acting hydraulic cylinder is shown below in Fig. 4.16. For a constant spring stiffness (k_s) of 15000 N/m and different damping co-efficient (c_d), values of 2.5kNs/m, 15kNs/m, 20kNs/m and 30kN/s, the combined force and position responses for a position demand with 0.1m amplitude and 0.5Hz frequency, are shown in Figs. 4.17(a)-(e) for the force demand

$$F_d = k_s x_d + c_d \dot{x}_d. \tag{4.3b}$$

It is seen from Fig. 4.17(a), that the position responses are nearly same for different values of the damping coefficients. The position response slightly deviates from demand after first half cycle (i.e., after t/T= 0.5). As negative cycle starts at this point, the active metering valve combination suddenly changes from V3-V4-V5-V6 (for positive demanded velocity) to V1-V2-V7-V8 (for negative demanded velocity). This is why the deviation occurs at this point for each case.

It is clearly viewed from Figs. 4.17(b) – (e), the force error decreases with increasing damping co-efficient values. At c_d = 30 kNs/m, the force error is almost negligible, as seen from Fig 4.17(e). So, it is revealed that force tracking improves with increasing damping co-efficient.

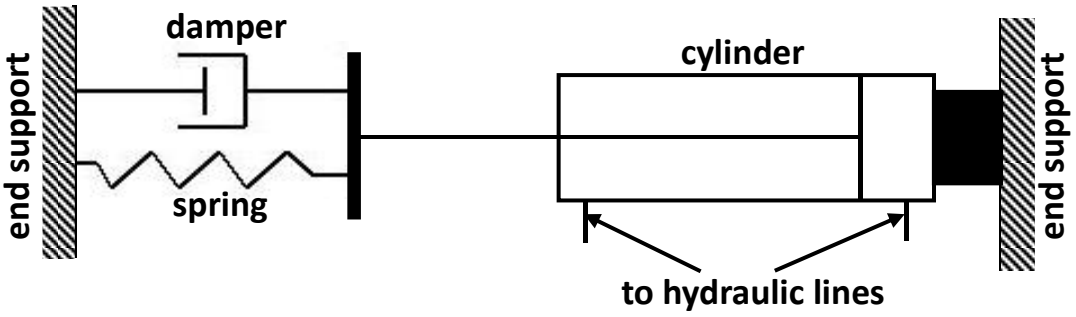

Fig. 4.16: Spring Loading of a Hydraulic Cylinder.

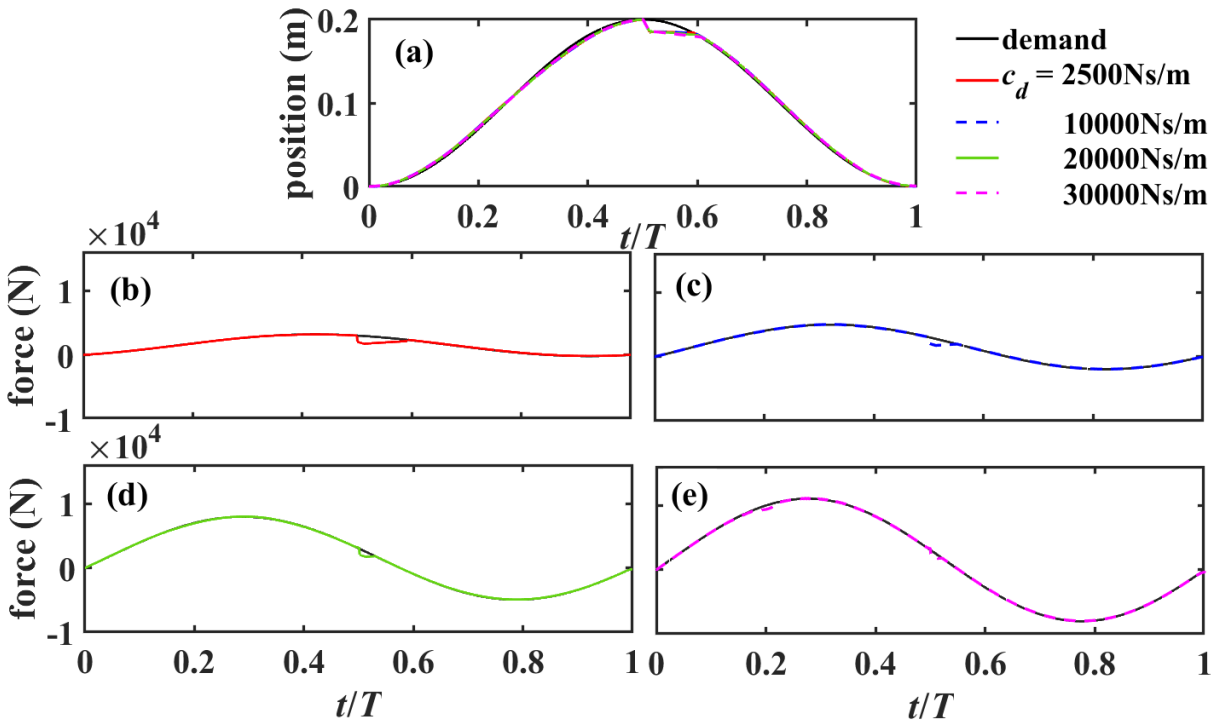

Fig. 4.17: (a) Position response and force responses with CIMV for a sinusoid position demand and combined spring-damper force demands of spring stiffness of 15000n/m and damping coefficient (b)2500Ns/m, (c) 10000Ns/m, (d) 20000Ns/m and (e) 30000Ns/m.

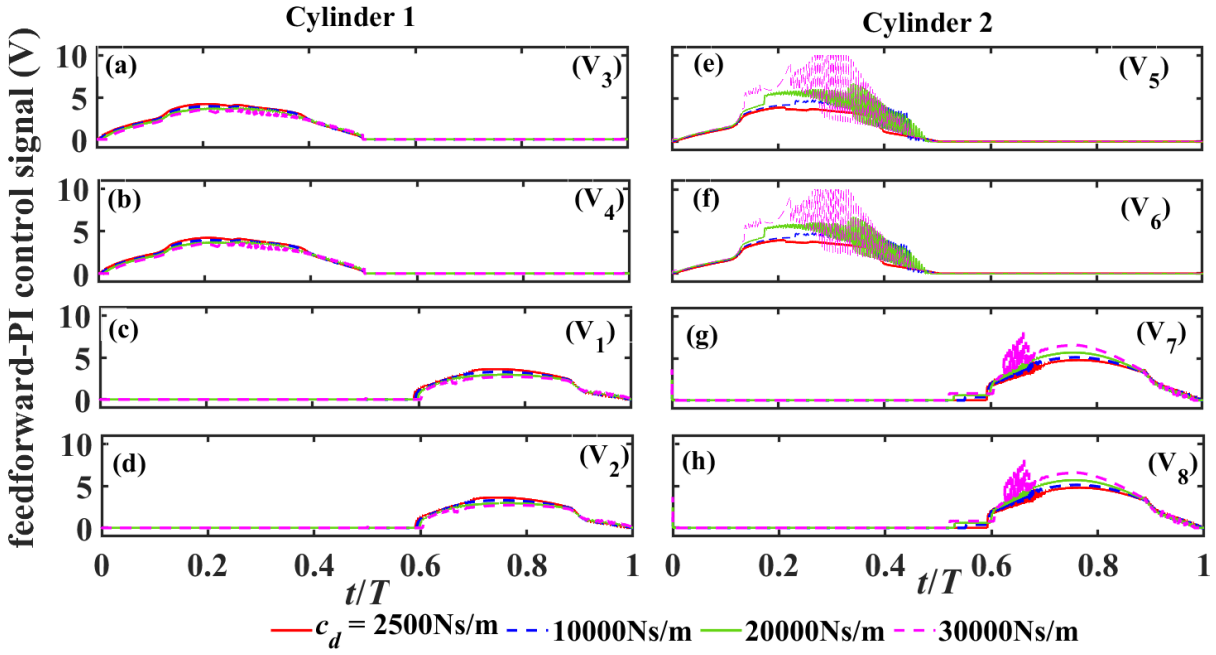

Fig. 4.18: FFPI control voltage for metering valves 1 to 8 – for a CIMV with a sinusoid position demand and combined spring-damper force demands of spring stiffness of 15000N/m and Damping Coefficient of 2500Ns/m, 10000Ns/m, 20000Ns/m 30000Ns/m.

Figures 4.18(a) – (h) show the control voltage variations for the eight valves. It is clear from these figures that with rise in damping coefficient value, there is a drop in the voltages for motion cylinder i.e., Cyl_1. But the opposite behavior is seen for force cylinder i.e., Cyl_2.

Figures 4.19(a) – (d) express the pressure at cap end and rod end for both the cylinder. Here an interesting issue is noted when compared with the spring-loaded system. For the spring-loaded system, as the demanded position is positive throughout the cycle time, the spring force also is always positive. To cope up with this positive force, the cap-end chamber pressures should be higher and rod-end chamber pressures should be lower throughout the cycle, as per eq. (2.3). However, with the damper, the damping force being proportional to the piston velocity is positive in the first half cycle and negative in the second half cycle. Hence the cap-end pressures should increase and rod-end pressures decrease with increase in damping coefficient for the first half cycle. The reverse is expected to happen for the second half cycle. This is consistent with the results in Figures 4.19(a) – (d).

Based on the discussions in the previous section, the control voltages shown in Figs. 4.18(a) – (h) are consistent with the pressure variation mentioned above.

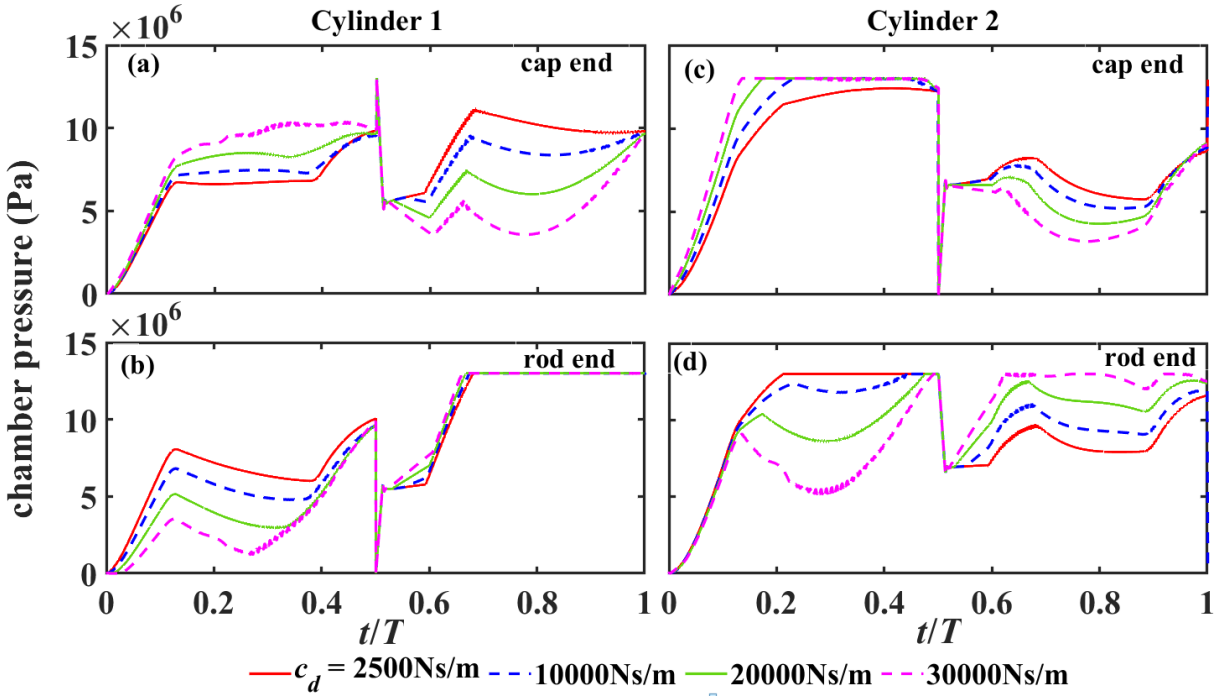

Fig. 4.19: Comparison of cylinder chamber pressures in (a) cap end of Cylinder 1, (b) rod end of Cylinder 1, (c) cap end of Cylinder 2 and (d) rod end of Cylinder 2 – for a CIMV with a sinusoid position demand and combined spring-damper force demands of spring stiffness of 15000n/m and damping coefficient of 2500Ns/m, 10000Ns/m, 20000Ns/m 30000Ns/m.

Fig 4.20(a) indicates that the IAE_x is almost insensitive to the value of the damping coefficient which is consistent with the tracking performances revealed in Fig. 4.17(a). Also, from 4.20(b) it is obvious to say that the IAE_F decreases with the rise in the value of c_d – again something consistent with Figs. 4.17(b) – (e). Fig. 4.20(c) indicates that the ICSE decreases for the valves V1, V2, V3 and V4 associated with the motion cylinder and rises for the valves V5, V6, V7 and V8, associated with the force cylinder – with the increase in damping coefficient. This is consistent with the variations of IAE_x and IAE_F.

Fig 4.20(d) indicates that c_d has no major effect on the power saved.

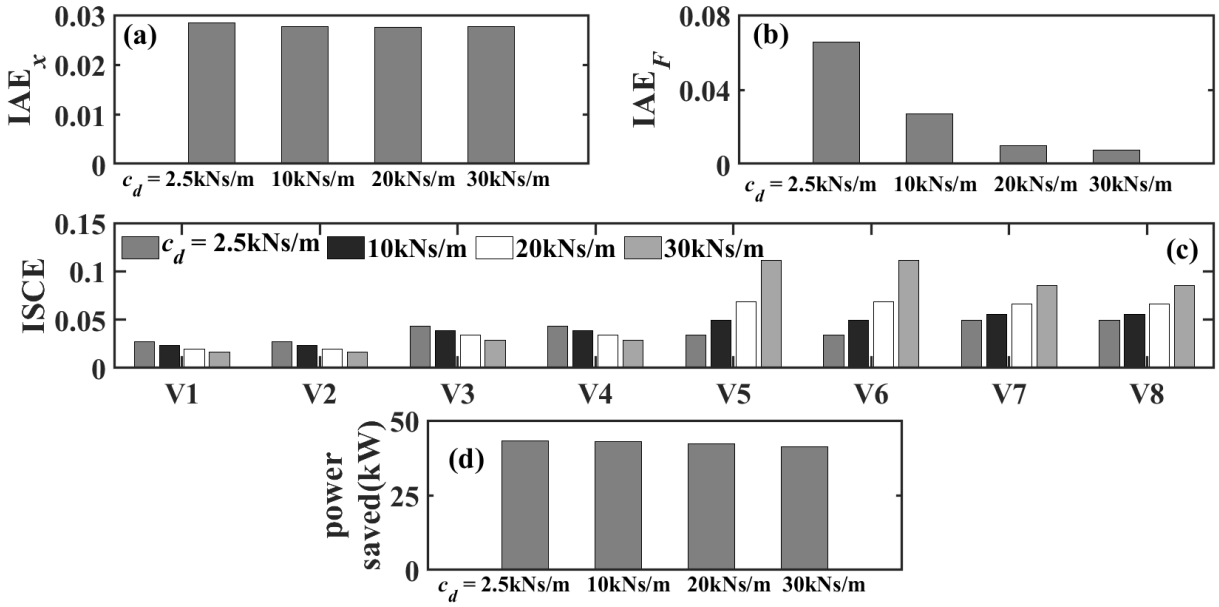

Fig. 4.20: Comparison of cylinder (a) IAE_x, (b) IAE_F, (c) ISCE and (d) power saved – for a CIMV with a sinusoid position demand and combined spring-damper force demands of spring stiffness of 15000n/m and damping coefficient of 2500Ns/m, 10000Ns/m, 20000Ns/m 30000Ns/m.

4.6 Performance Comparison for Linearly Time Varying Load Demands at Different Rates with Sinusoidal Position Demand

For this case the position demand is given by the same sinusoid expression as per eq. (4.2a) with the demand amplitude a_x = 0.1m, the time period T = 2s, the phase $\phi_x = 1.5\pi$ and the bias x_0 = 0.1m. The linearly time varying load demand is generated using a trapezoidal wave form of fixed positive and negative slope $\pm\alpha$ as shown in Fig. 4.21 and equations 4.4(a) – (i) below where T, α and f_0 represents the time period of the cycle, slope and maximum force generated in the trapezoidal wave form respectively.

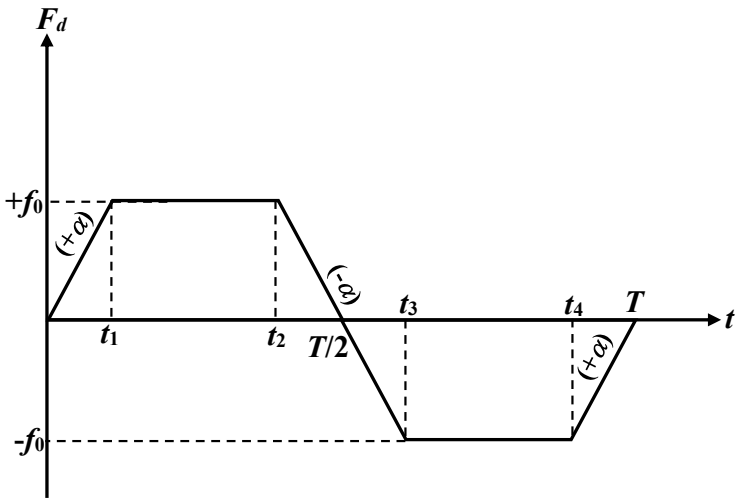

Fig. 4.21: Trapezoidal waveform for linearly time-varying force demand

$$F_d = \alpha t \quad \text{for } 0 \le t \le t_1 \tag{4.4a}$$

$$= f_0 \quad \text{for } t_1 < t \le t_2 \tag{4.4b}$$

$$= f_0 - \alpha(t - t_2) \quad \text{for } t_2 < t \le t_3 \tag{4.4c}$$

$$= -f_0 \quad \text{for } t_3 < t \le t_4 \tag{4.4d}$$

$$= -f_0 + \alpha(t - t_4) \quad \text{for } t_4 < t \le T \tag{4.4e}$$

where $t_1 = {}^{f_0}/_{\alpha}$; (4.4f)

$$t_2 = {}^{T}/_{2} - t_1; \tag{4.4g}$$

$$t_3 = {}^{T}/_{2} + t_1; \tag{4.4h}$$

$$t_4 = T - t_1; \tag{4.4i}$$

Figures 4.22(a) – (e) indicates the position and force responses with CIMV and Figs. 4.23(a) – (h) the control voltages for a sinusoid position demand and the time-varying force demand given by equations (4.4a) – (4.4i). The position tracking performances do not show any major differences for different force demands. This is also revealed in the near constancy of the IAE_x in Fig. 4.25(a). As noted in the earlier cases, there is a deviation between the demanded position and the response during switching of the active valve combinations. Eventually the position response catches up with the demanded track within a short time. In Figs. 4.22(b) – (c), a spike is seen at the beginning of the cycle of the force responses. As the initial condition of force is zero in the simulation model, it attains the maximum force demand (i.e. f_0)

which is 1500N through the spike in response. With decrease in α, the slope becomes gentler and consequently the initial spike also reduces almost vanishes for α values of 3×10^4 N/s and 3×10^3 N/s. The decrease in IAE_F in Fig. 4.25(b) is a manifestation of this. In all the force responses i.e., in Figs. 4.22(b) – (e), at half the cycle time, there is another spike due to the switching of the active valve combination.

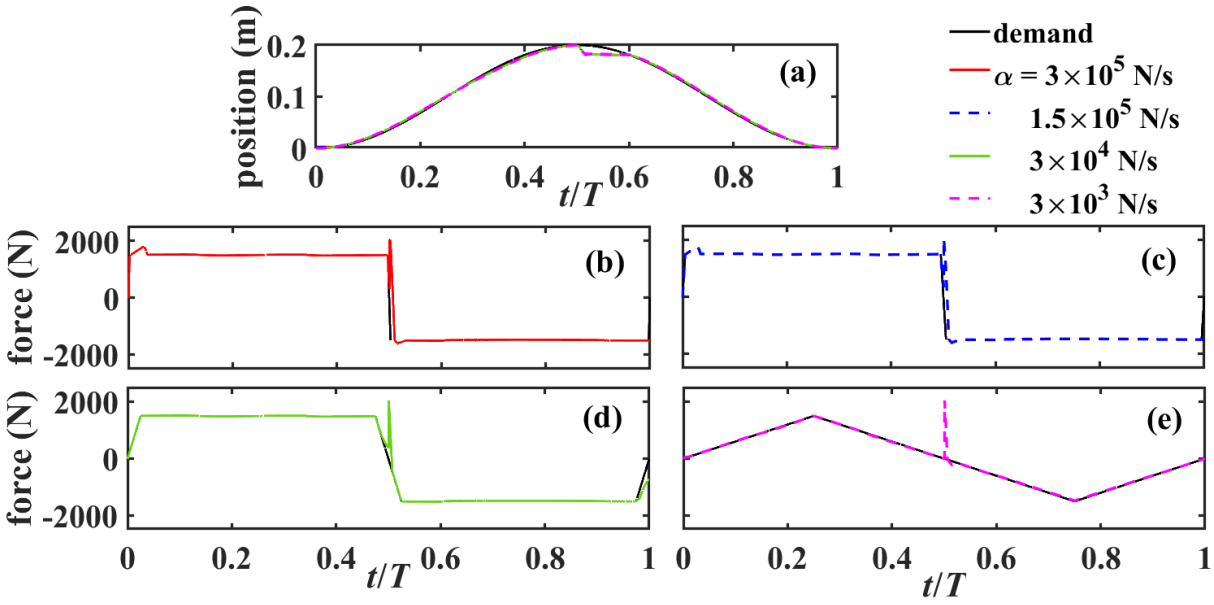

Fig. 4.22: For a sinusoid position demand and time-varying force demands with CIMV, the responses in (a) position and (b) to (e) forces for α in N/s 3×10^5, 1.5×10^5, 3×10^4 and 3×10^3.

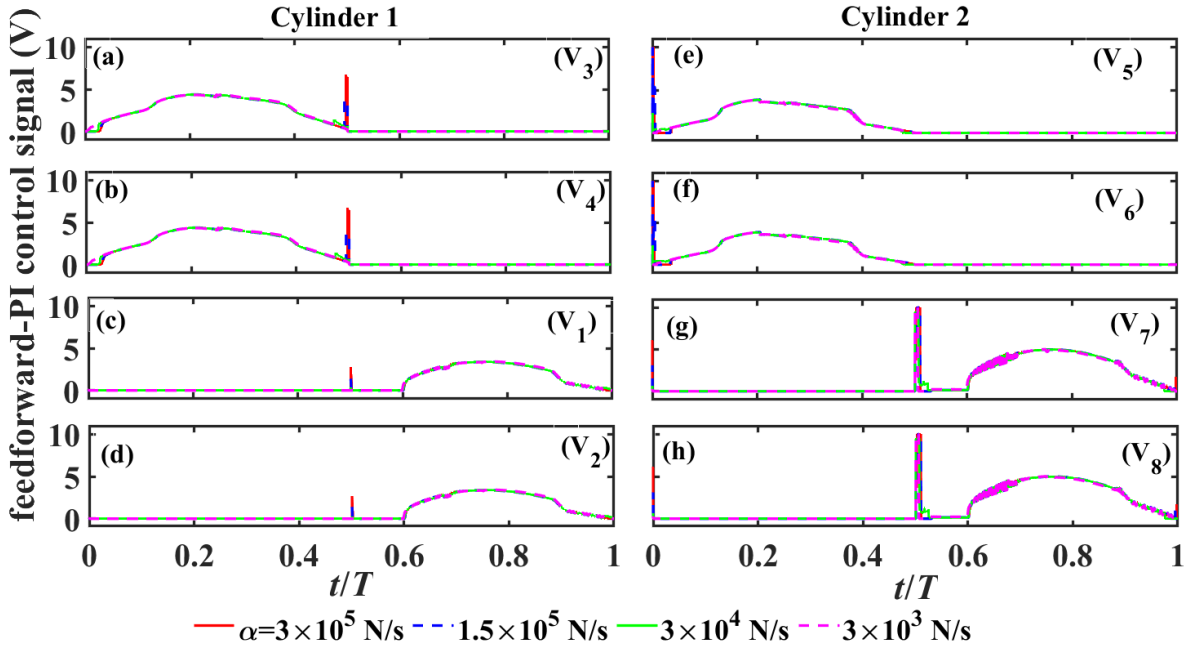

Fig. 4.23 For a sinusoid position demand and time-varying force demands with CIMV, the control voltages for α in N/s equal to (a) 3×10^5, (b) 1.5×10^5, (c) 3×10^4 and (d) 3×10^3.

Fig. 4.23(a) – (h) show V3, V4, V5 and V6 to be active for positive half cycle and V1, V2, V7 and V8 for negative half cycle. As the maximum force is constant for all the demands, there is not much change in the voltage variations with the rate of demanded force variation (apart from the initial spike) – for the range of values explored.

Figures 4.24(a) – (d) describe the chamber pressures for both cap end and rod end of two cylinders for positive half cycle and negative half cycle with different time-varying force demands. The pressure curves mimic the pattern of the force demand in the sense, there are 2 gradients in each half cycle and an intermediate plateau for the constant force demand region. As the maximum force is constant for all the demands, there is not much difference in the pressure patterns.

Fig. 4.25(a) indicates that the IAE_x is almost insensitive to the value of the rate of force change, which is consistent with the tracking performances revealed in Fig. 4.22(a). But it is obvious from Fig. 4.25(b) that the force error (IAE_F) is falling with the fall of slope of the linearly varying force demand. Fig. 4.25(c) indicates the integral square control effort (ISCE) for 1 – 8 metering valves. There is no major change occurred in ISCE for valves V1, V2, V3, and V4. But it is observed that ISCE falls with decrease in the slope of the varying load demands. Power saved from fig 4.25(d) is quite similar in all the cases of demands.

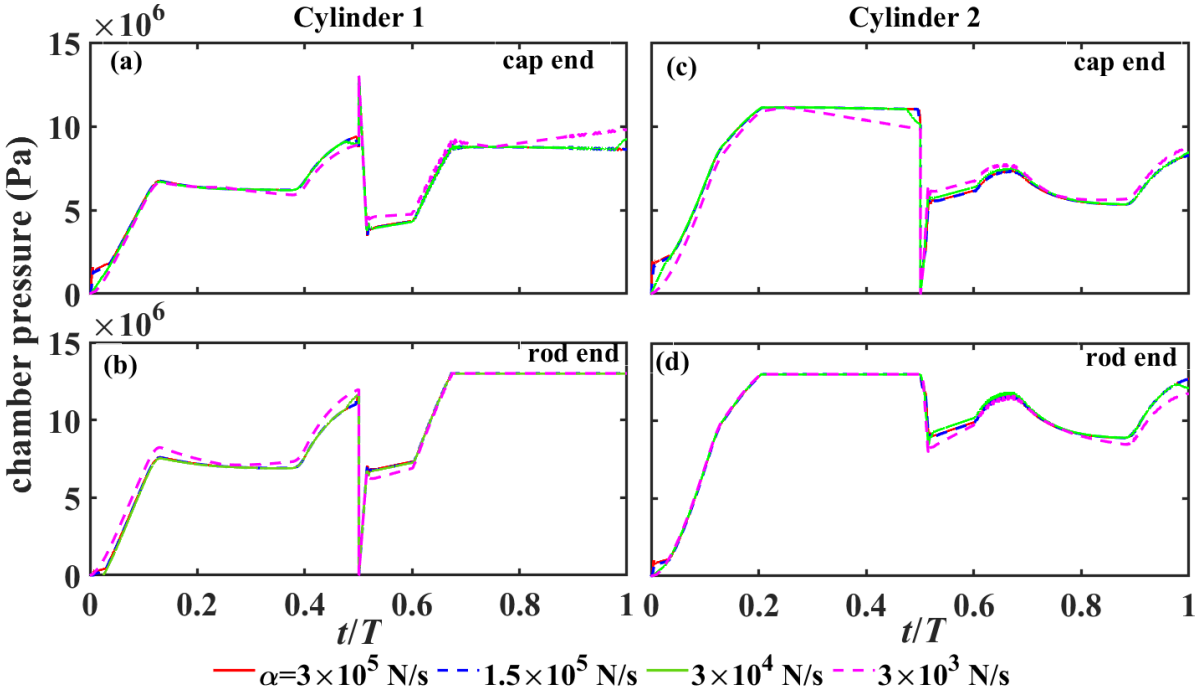

Fig. 4.24: Comparison of cylinder chamber pressures at cap and rod ends of Cylinders 1 and 2 for α in N/s equal to (a) 3×10^5, (b) 1.5×10^5, (c) 3×10^4 and (d) 3×10^3.

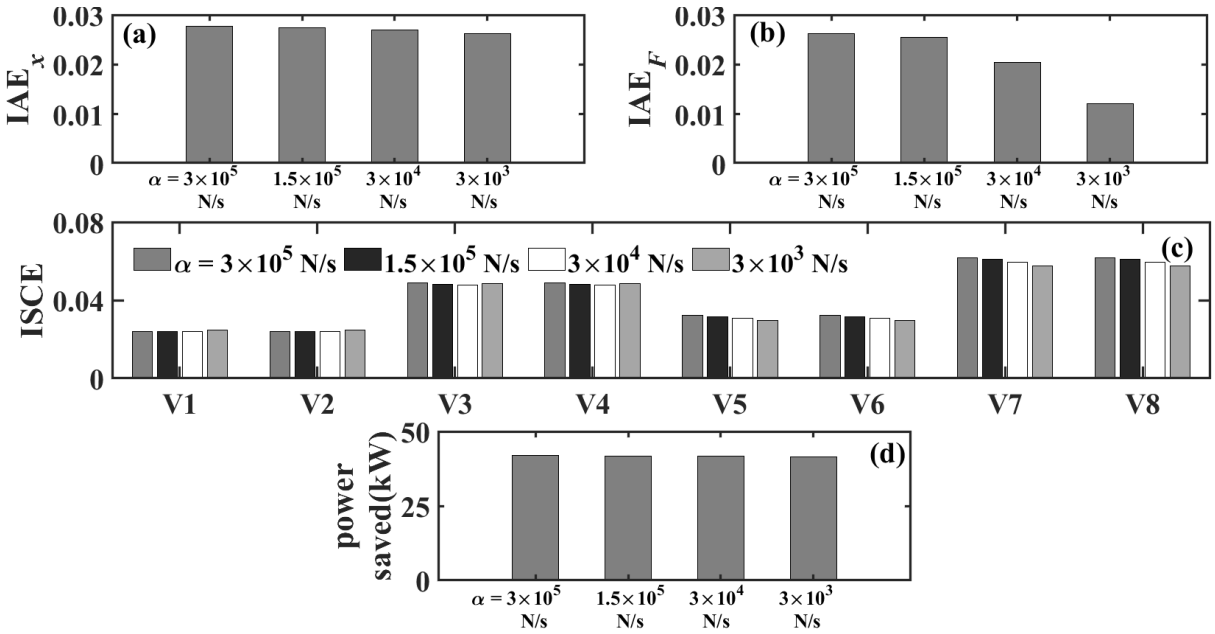

Fig. 4.25: Comparison of cylinder (a) IAE$_x$, (b) IAE$_F$, (c) ISCE and (d) power saved – for a CIMV for a sinusoid position demand and linearly time-varying force demand at the rates of (b) 3×10^5 N/s, (c) 1.5×10^5 N/s, (d) 3×10^4 N/s and (e) 3×10^3 N/s.

In the first half cycle, as the demanded force is positive. During this time as the rod-end of motion cylinder is connected to pump line having a reduced area A_r, the opening of the metering valves should be more. Hence the higher ISCE for V3 and V4 of in Fig. 4.25(c) compared to V5-V6, where the pump line is connected to the cap end with higher area A_c. However, for the second half cycle, the ISCE for V7-V8 is higher than V1-V2 as the in the case of the former, the pump line is connected to the rod-end and for the latter it is connected to the cap-end.

Fig. 4.25(d) indicates that the overall power saved is more or less constant.

4.7 Performance Comparison for Sinusoidal Position Demand and Sinusoidal Force Demands at Different Phase Differences with the Demanded Velocity

For this case the position demand is given by the same sinusoid expression as per eq. (4.2a) with the demand amplitude a_x = 0.1m, the time period T = 2s, the phase $\phi_x = 1.5\pi$ and the bias x_0 = 0.1m. The demanded velocity and force are then expressed as

$$\dot{x}_d(t) = (2\pi a_x/T)\sin\{(2\pi t/T) + \phi_x + \pi/2\} \tag{4.5}$$

$$F_d(t) = a_F \sin\{(2\pi t/T) + \phi_F\} \quad (4.6)$$

where a_F =amplitude, T = time period, and ϕ_F= phase for force demand.

Phase difference between demanded velocity and demanded force can then be expressed as

$$\varepsilon = \phi_F - \{\phi_x + \pi/2\} \quad (4.7)$$

Figures 4.26(a) – (d) presents the position and force responses for different phase differences ε between demanded velocity and force. For different ε, the position responses are similar to each other. There is a small deviation at the mid-point as the demanded velocity changes from positive to negative at that point and within a short time it catches up with the position demand. Hence, it is evident that motion tracking is good in all the cases. It is found from Figs. 4.26(b) – (d), that as the phase difference ε increases, the force error also increases and the time duration of error also increases. It is seen from 4.26(d), when the ε is maximum i.e., π radians, in this case the force error is maximum and that error even lasts for a larger duration.

Fig. 4.27(a) – (h) represents the FFPI control voltage for different metering valves for ε = 0, π/2, π radians. It is found in these figures that control voltages tend to rise in all the valves of cylinder 1 as the ε rises from 0 to π. But in cylinder 2, the control voltages tend to fall with the rise of ε. Some oscillations also observed in valves 7 and 8.

Fig. 4.28(a) – (d) represents the chamber pressures at cap and rod end of the two cylinders.

Figure 4.29(a) presents the integral absolute error for position. This error is quite similar when ε = 0 and π and higher when $\varepsilon = \pi/2$ radians. From Fig. 4.29(b), it is evident that force error is least when ε = π/2, and it is maximum at ε = π. If one closely follows Fig. 4.29(c), one can tell that the ISCE for Cylinder 1 valves gradually rises up as the ε rises from 0 to π. But it decreases gradually for cylinder 2 valves. Power saved from Fig. 4.29(d), is almost same in all the cases. Phase change ε has no effect in power saved.

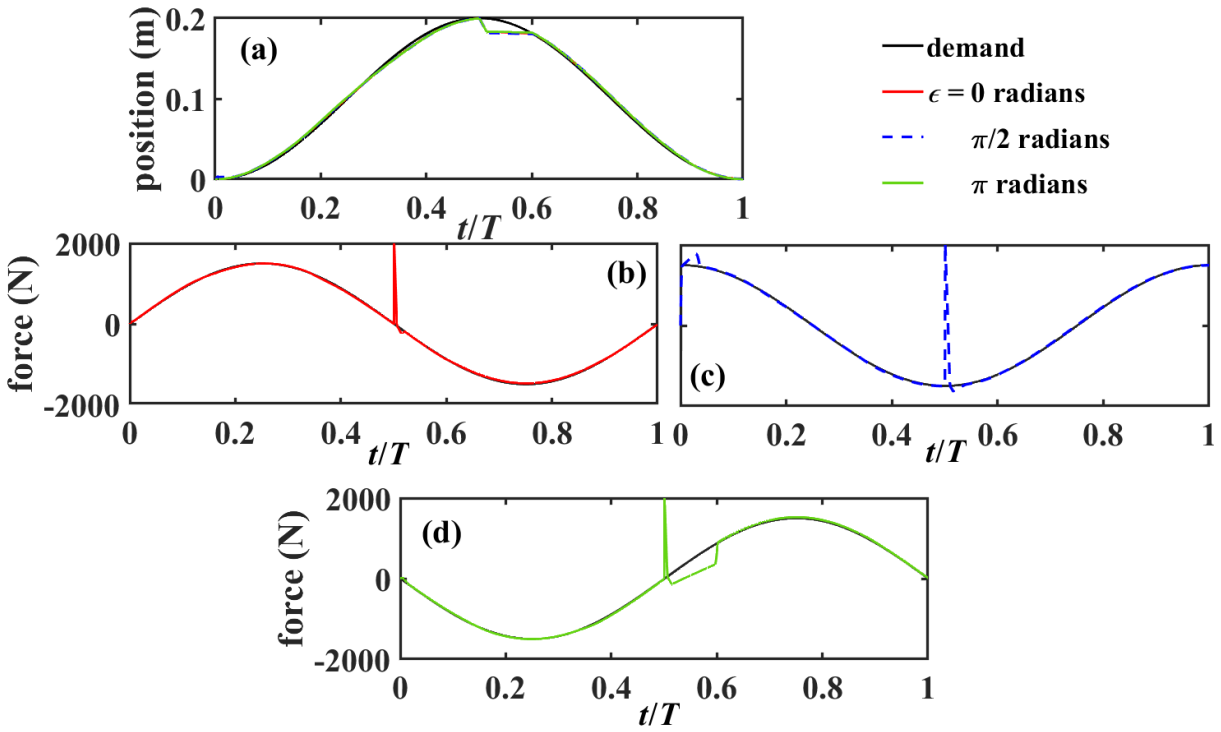

Fig. 4.26: (a) Position response and force responses with CIMV for a sinusoid position demand and sinusoid load demands at phase differences with the demanded velocity of (b) 0 radians, (c) $\pi/2$ radians, and (d) π radians.

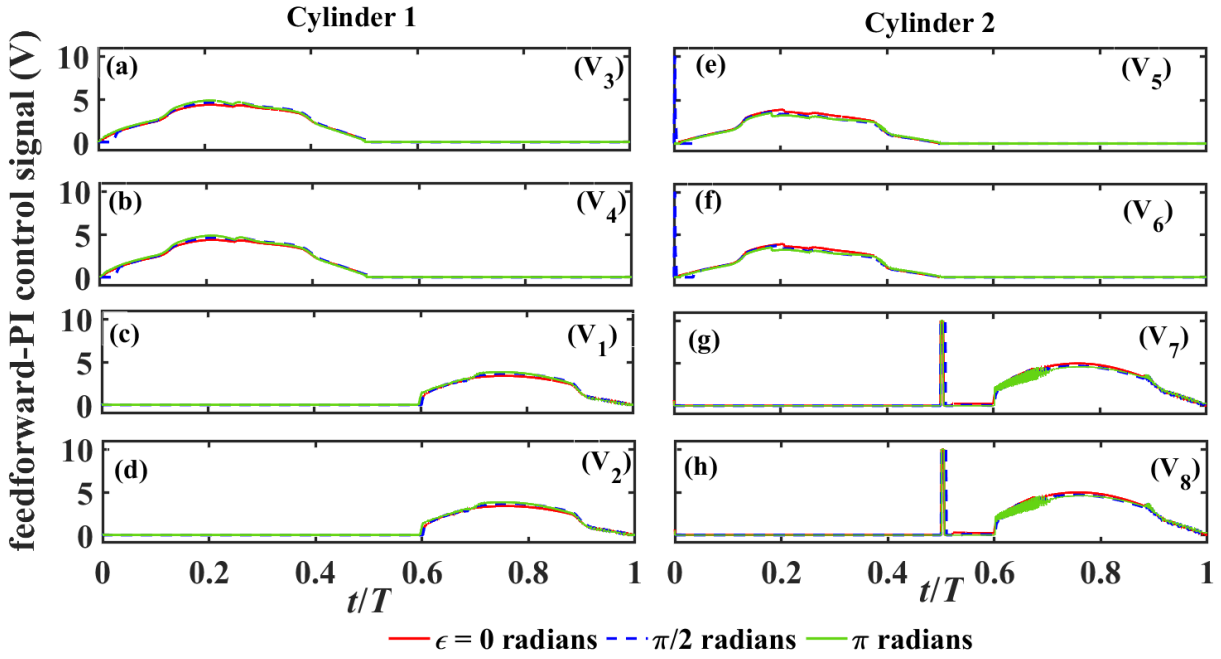

Fig. 4.27: FFPI control voltage for metering valves 1 to 8 – for a CIMV with a sinusoid position demand and sinusoid load demands at phase differences with the demanded velocity of 0 radians, $\pi/2$ radians, and π radians.

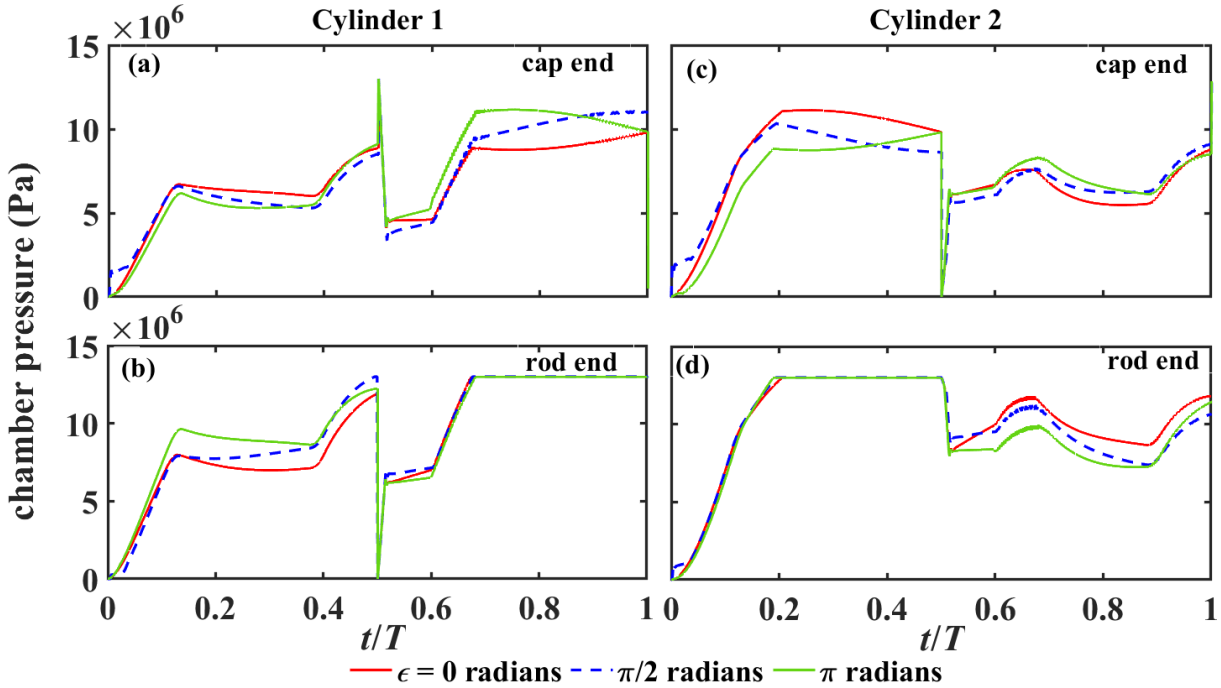

Fig. 4.28: Comparison of cylinder chamber pressures in (a) cap end of Cylinder 1, (b) rod end of Cylinder 1, (c) cap end of Cylinder 2 and (d) rod end of Cylinder 2 – for a CIMV with a sinusoid position demand and sinusoid load demands at phase differences with the demanded velocity of 0 radians, $\pi/2$ radians, and π radians.

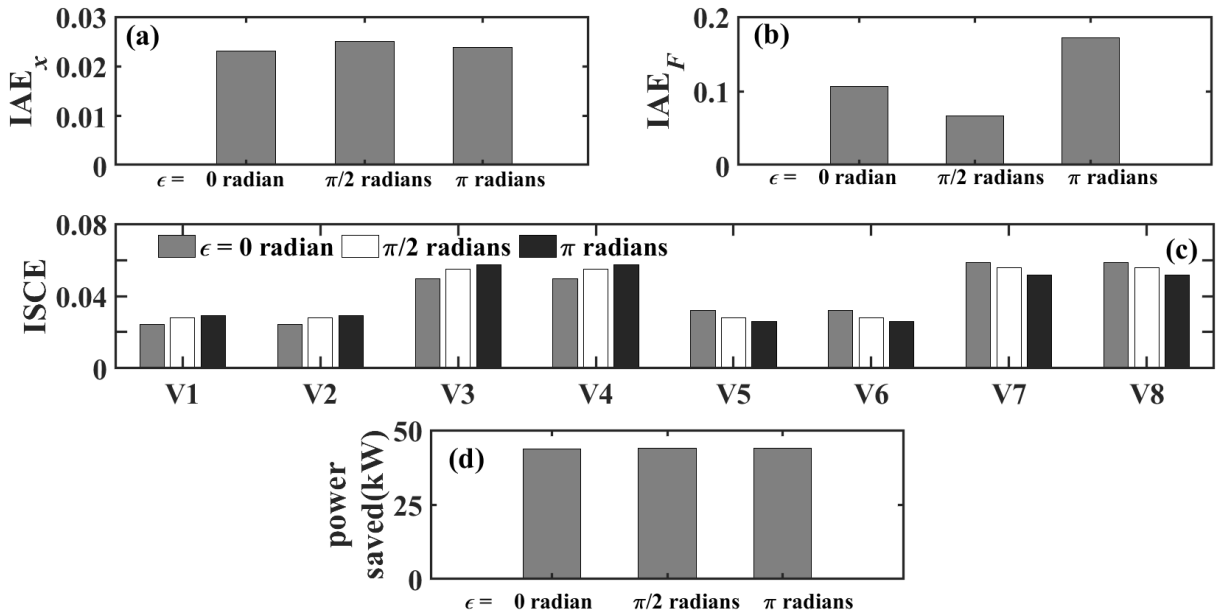

Fig. 4.29: Comparison of cylinder (a) IAE_x, (b) IAE_F, (c) ISCE and (d) power saved – for a CIMV with a sinusoid position demand and sinusoid load demands at phase differences with the demanded velocity of 0 radians, $\pi/2$ radians, and π radians.

4.8 Performance Comparison for Sinusoidal Position Demand at 0.5Hz and Sinusoidal Load Demands at Different Frequencies

Figures 4.30(a) – (e) shows the position and force responses for different frequency ratios (ω_F/ω_x) of force and position demand with a sinusoid position demand of constant frequency (ω_x=0.5). It is found that position responses do not change much with change in the frequency ratio for most of the cycle. However, there is some position error at the beginning, at mid-point and at the end of the cycle time, which increases with the increase in the frequency ratio. This is also manifested in the IAE_x values in Fig. 4.33(a). The force error and time duration of error is more with the rise in frequency ratio. Here, when ω_F/ω_x is 16, the force error is higher. Hence, force tracking is satisfactory for lower frequency ratio. This is again revealed in the IAE_F values in Fig. 4.33(b).

Figures 4.31(a) – (h) represent the FFPI control voltages for all the eight metering valves sinusoid force demands at different frequencies. As expected, it is found that control voltages tend to oscillate more with the rise in frequency ratio ω_F/ω_x. It is seen when ω_F/ω_x is 16, the control voltage oscillates with high frequency than when ω_F/ω_x is 1.

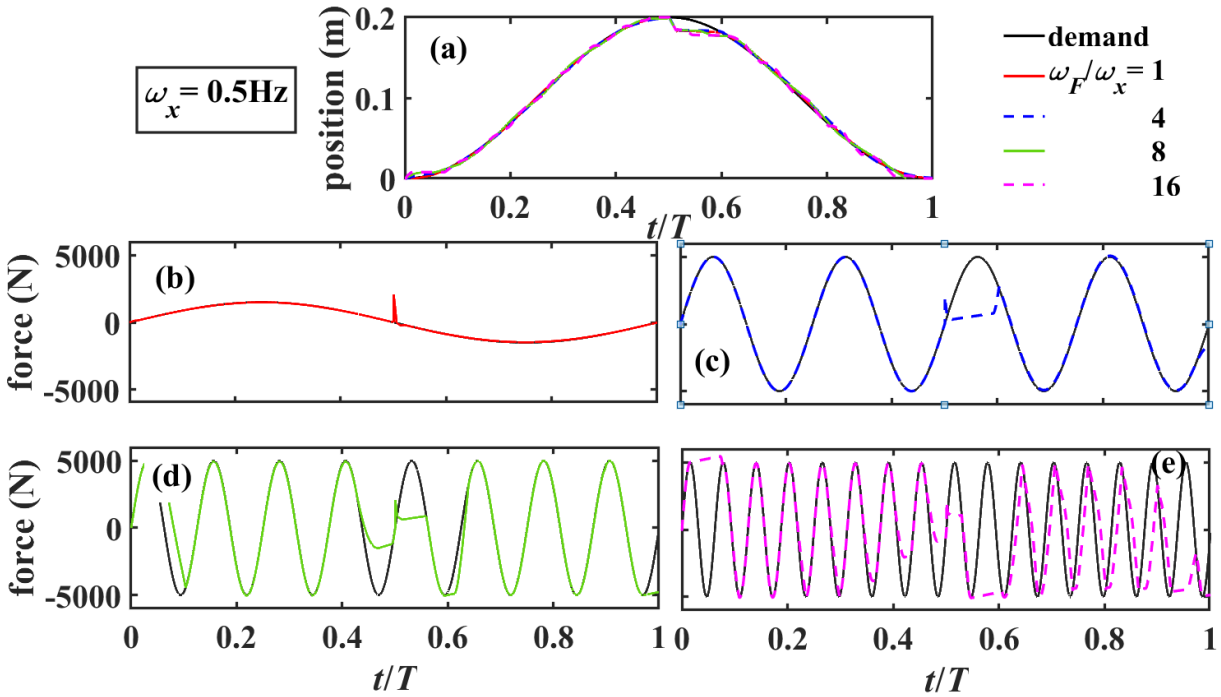

Fig. 4.30: (a) Position response and Force Responses with CIMV for a sinusoid position demand at a frequency of 0.5hz and sinusoid load demands at different frequencies with ω_F/ω_x equal to (b) 1, (c) 4, (d) 8 and (e) 16.

Figures 4.32(a) – (d) represents chamber pressures at the cap and rod ends of both the cylinder for different frequency ratios of force and position demand. As mentioned earlier, higher the frequency ratio, higher are the pressure oscillations.

Figures 4.33(a) and (b) depict integral absolute error for position (**IAE**$_x$) and force (**IAE**$_F$) increases with the rise in frequency ratio. Integral square control effort (**ISCE**) for the valves in cylinder 1 rises with the rise in ω_F/ω_x. This is also valid for cylinder 2 valves except for the case when $\omega_F/\omega_x = 1$, as shown in Fig. 4.33(c). Power saved shown in Fig. 4.33(d) is almost equal for all the cases.

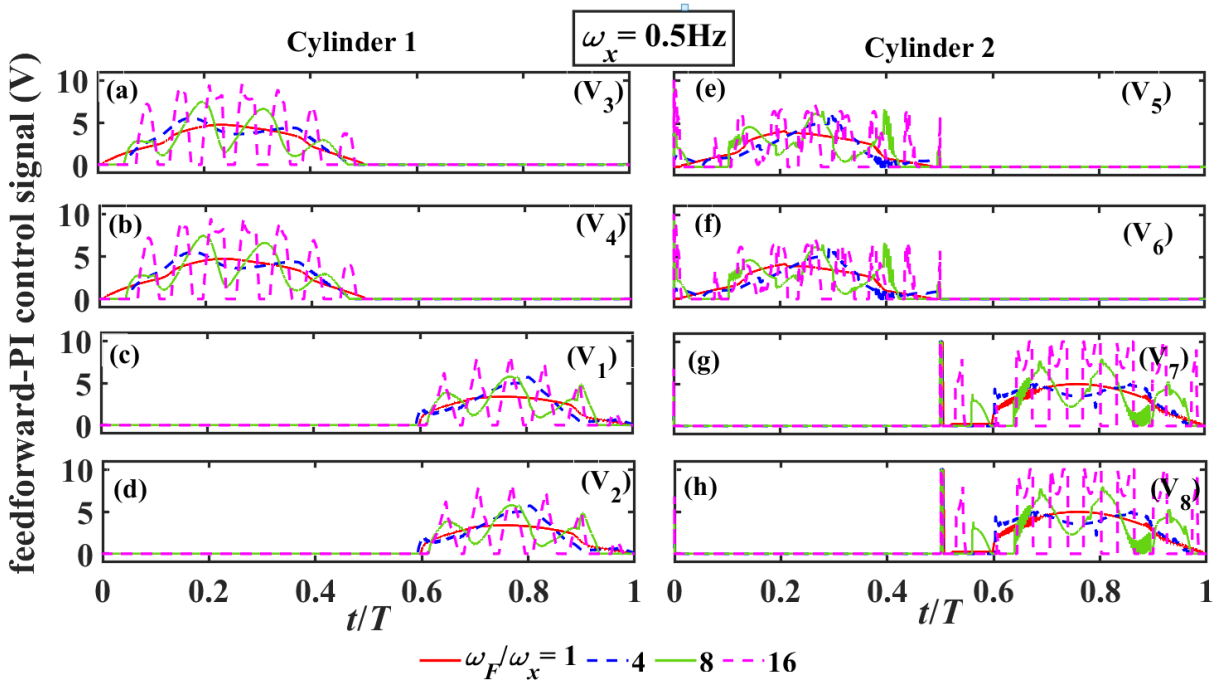

Fig. 4.31: FFPI control voltage for metering valves 1 to 8 – for a CIMV with a sinusoid position demand at a frequency of 0.5Hz and sinusoid load demands at different frequencies with ω_F/ω_x equal to 1, 4, 8 and 16.

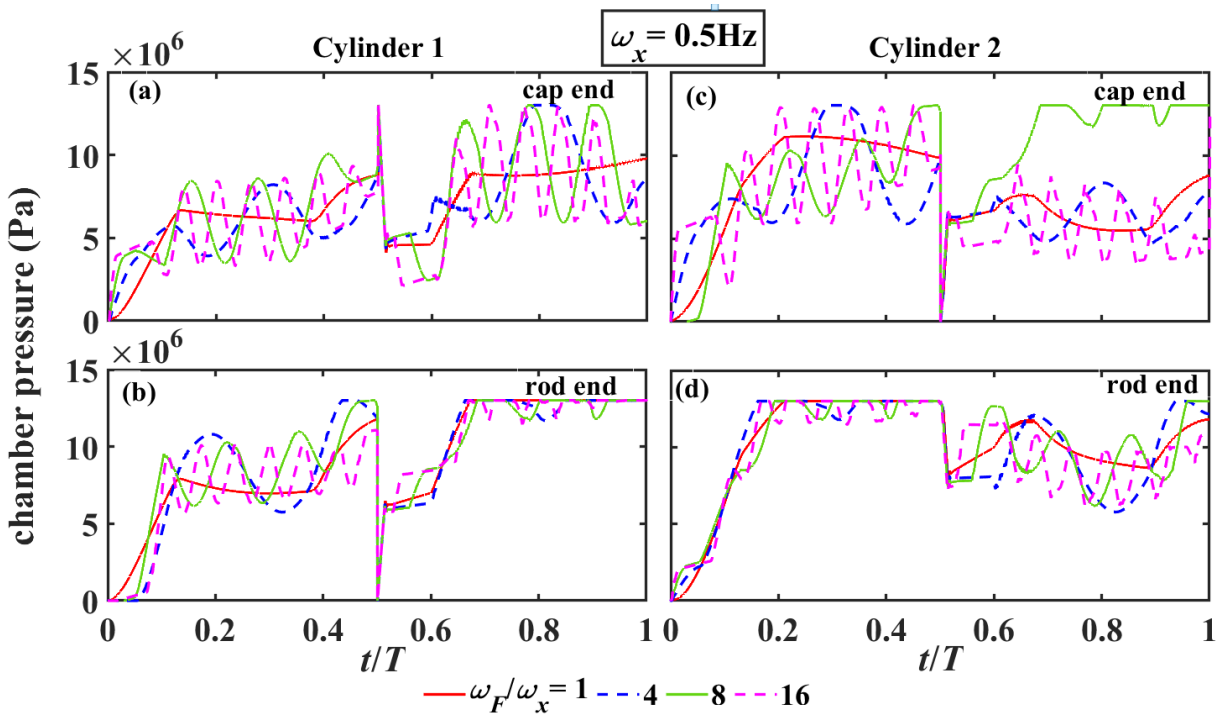

Fig. 4.32: Comparison of cylinder chamber pressures in (a) cap end of Cylinder 1, (b) rod end of Cylinder 1, (c) cap end of Cylinder 2 and (d) rod end of Cylinder 2 – for a CIMV with a sinusoid position demand at a frequency of 0.5Hz and sinusoid load demands at different frequencies with ω_F/ω_x equal to 1, 4, 8 and 16.

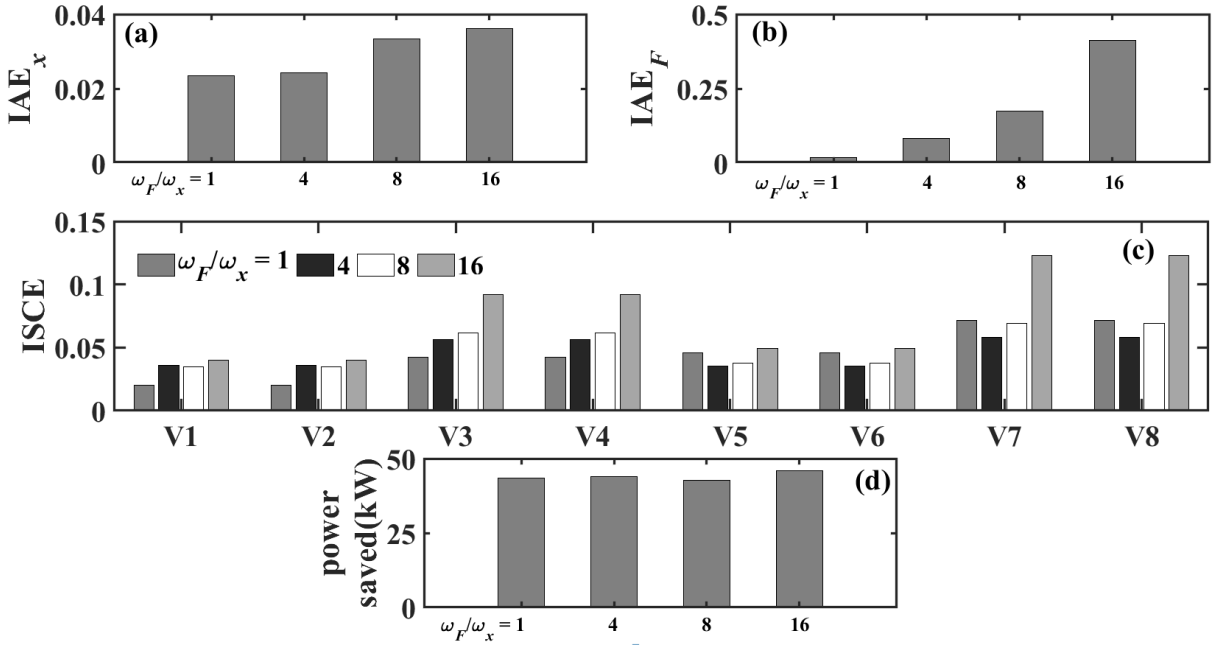

Fig. 4.33: Comparison of cylinder (a) IAE_x, (b) IAE_F, (c) ISCE and (d) power saved – for a CIMV with a sinusoid position demand at a frequency of 0.5Hz and sinusoid load demands at different frequencies with ω_F/ω_x equal to 1, 4, 8 and 16.

4.9 Performance Comparison for Sinusoid Load Demands at 0.5Hz and Sinusoidal Position Demand at Different Frequencies

Figures 4.34(a) – (e) represents the position and force response for combined sinusoidal load demand with constant frequency (0.5 Hz) and position demand at different frequencies. The position and force tracking are well for low frequency ratio (ω_x/ω_F). As this ratio increases position error as well as force error increases. Even these errors last longer as the ratio increases. Hence, satisfactory results found in lower frequency ratio. At a value of the frequency ratio 2.0, the position tracking fails miserably, as is seen in Fig. 4.34(a). As is seen in Figures 4.35(a) – (h), the control voltages for this case also reaches the saturation value of 10V. These indicate that for the case of ω_x/ω_F = 2.0, the demanded speed of motion exceeds the bandwidth of the system.

Figures 4.35(a) – (h) gives the FFPI control voltages of eight metering valves for different frequencies of position demand and constant frequency (0.5Hz) of force demand. It seems like higher the frequency, higher the control voltage for all the cases – as should be the case as higher frequency implies greater speed of the piston requiring higher flows from the metering valves which demand their greater openings.

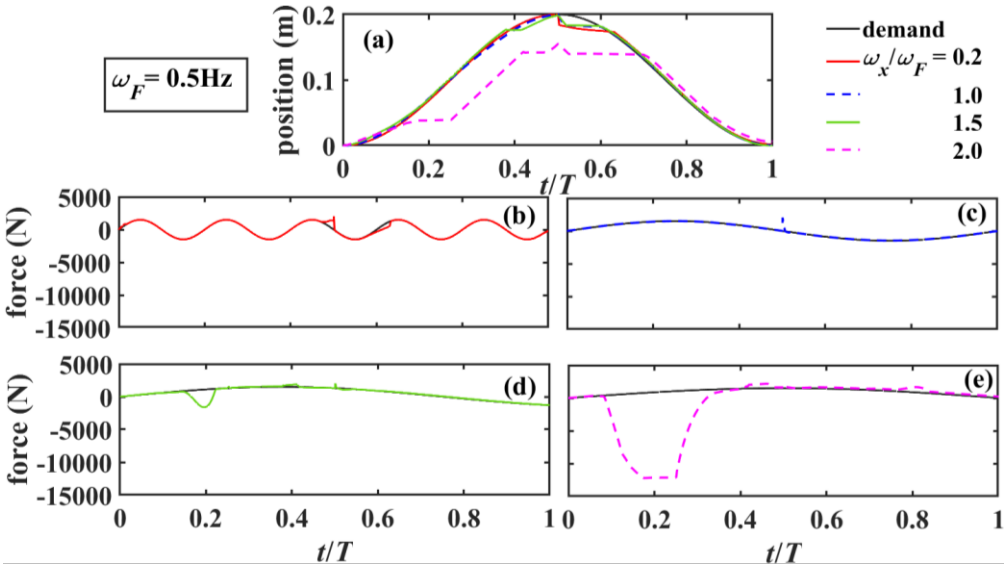

Fig. 4.34: (a) Position response and Force Responses with CIMV for a sinusoid force demand at a frequency of 0.5Hz and sinusoid position demands at different frequencies with ω_x/ω_F equal to (b) 0.2, (c) 1.0, (d) 1.5 and (e) 2.0.

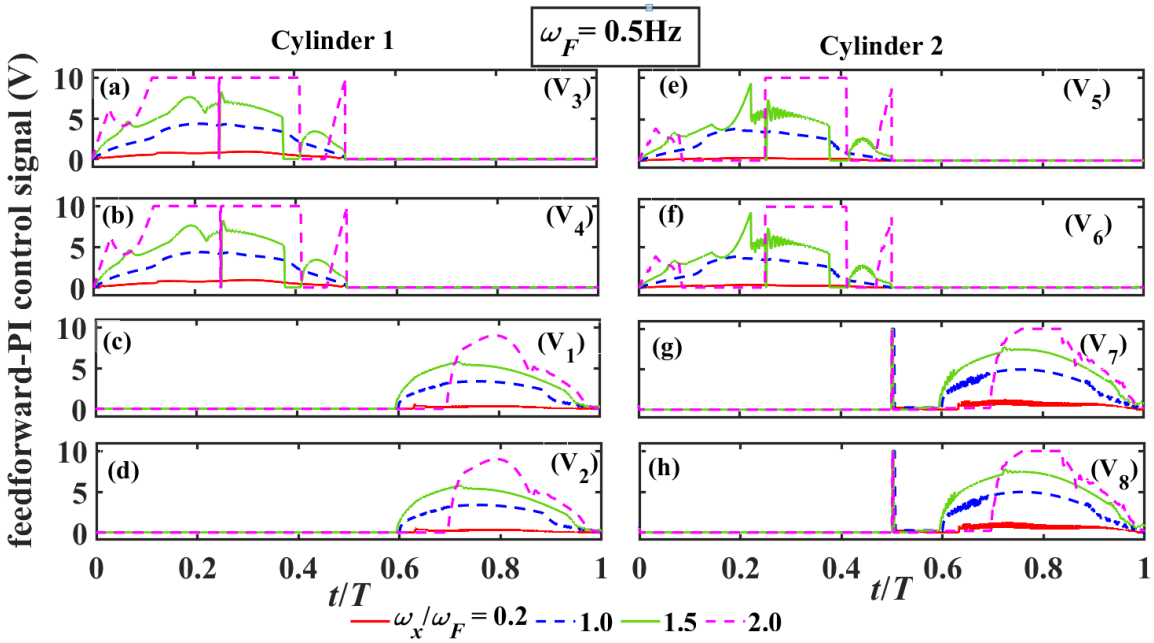

Fig. 4.35: FFPI control voltage for metering valves 1 to 8 – for a CIMV with a sinusoid force demand at a frequency of 0.5Hz and sinusoid position demands at different frequencies with ω_x/ω_F equal to 0.2, 1.0, 1.5 and 2.0.

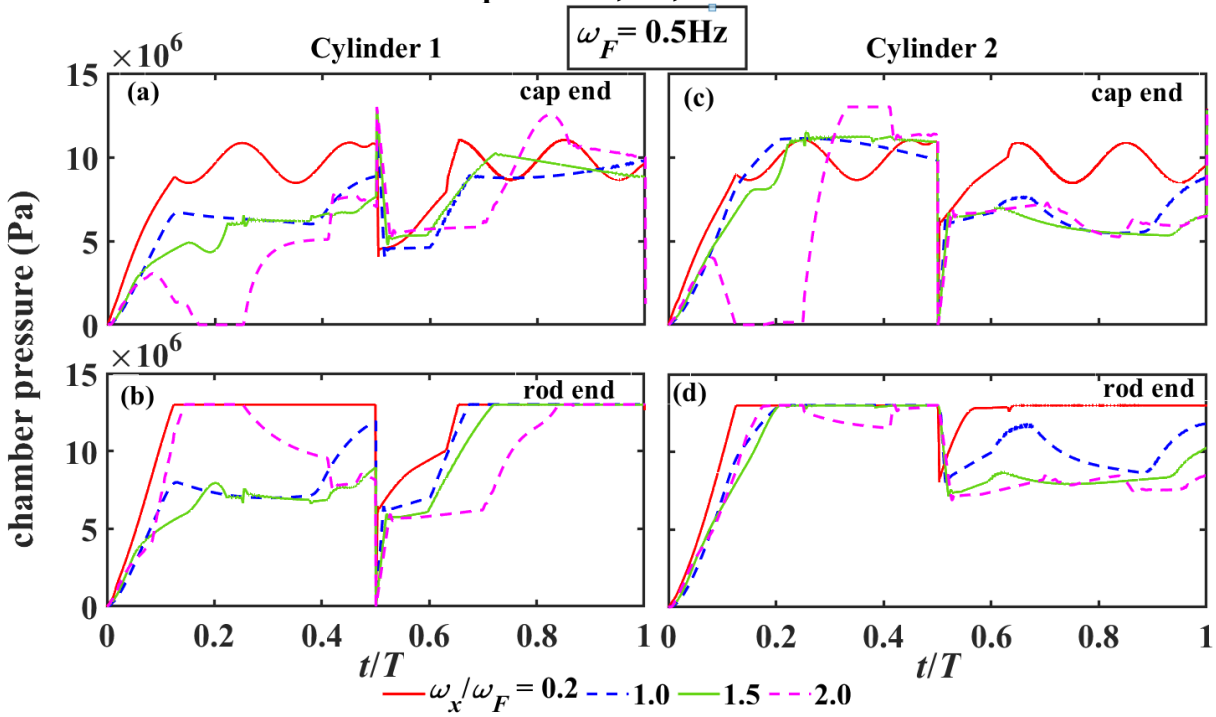

Fig. 4.36: Comparison of cylinder chamber pressures in (a) cap end of Cylinder 1, (b) rod end of Cylinder 1, (c) cap end of Cylinder 2 and (d) rod end of Cylinder 2 – for a CIMV with a sinusoid force demand at a frequency of 0.5Hz and sinusoid position demands at different frequencies with ω_x/ω_F equal to 0.2, 1.0, 1.5 and 2.0.

Chamber pressures for both cap end and rod end for the two cylinders for different frequencies of sinusoid position demand and constant frequency of force demand are described in Figs. 4.36(a) – (d). When ω_x/ω_F = 0.2, at rod-ends pressure saturations occur, but at cap-ends oscillations occurred in both cylinders for most of the time of a cycle.

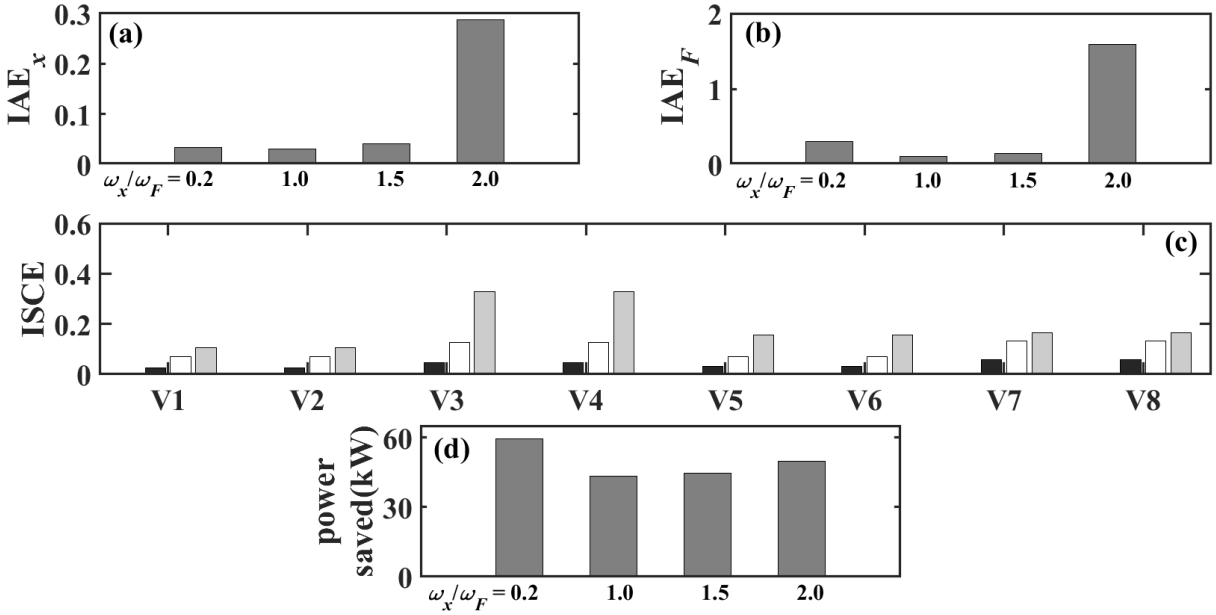

Fig. 4.37: Comparison of cylinder (a) IAE$_x$, (b) IAE$_F$, (c) ISCE and (d) power saved – for a CIMV with a sinusoid force demand at a frequency of 0.5Hz and sinusoid position demands at different frequencies with ω_x/ω_F equal to 0.2, 1.0, 1.5 and 2.0.

It is evident from Fig. 4.37(a) integral absolute error for position (IAE$_x$) increases with increasing frequency of position demand. It is highest when frequency of position demand ω_x = 1 Hz. Even integral absolute error for force (IAE$_F$) also higher in this case shown in Fig. 4.37(b). One can relate this from the response plot of position and force shown in Figs. 4.34(a) – (e). If one look into Fig. 4.37(c) closely, one can see that integral square control effect (ISCE) getting bigger with increasing ω_x for each valve of both the cylinders.

From Fig. 4.37(d), it can be said that power saved is maximum at ω_x = 0.1 Hz and minimum at 0.5 Hz.

4.10 Summary

A simulation study in MATLAB-SIMULINK has been carried out and results of the closed loop simulations performed for sinusoidal position and force tracking demand has been compared for both the

CIMV and IMV configurations. Several force demands, like sinusoid, fixed, linearly time-varying, spring load, spring-damper load – have been explored for sinusoid and fixed position demands. It has been found out that for a fixed gain FFPI controller, CIMV exhibits better performance than IMV –on count of tracking error, control effort, power savings and exit loss. However, there is scope for further investigating by using different PI gains for the IMV configurations.

For constant load tracking, a degradation of performance with increase in the load has been found both for position and force tracking. For a spring load, it has been found out that the for very low spring stiffness, there is appreciable force tracking error, which drops for a higher value of the stiffness. Further increase of the stiffness of the spring shows marginal degradation of the force tracking performance. An increase in the damping coefficient in the damper for a combined spring-damper loading improves the force tracking performance. For a linearly time varying load demand, the tracking improves as the slope of the variation of the force becomes smaller. Performance degradation is observed for larger phase difference between force and velocity demands. Also, higher frequency of force or position demands affects the performance significantly. Very poor position tracking performance is observed for motion demands at a speed higher than the system bandwidth.

In all the cases, it has been observed that as the demanded piston velocity changes sign at half the cycle time, the position response shows a sudden drop and then follows a track with lesser slope than that of the demand for some duration till it catches up with the demand again. This effect is manifested as spikes – first positive which is soon followed by a negative one – in the force responses. This has been attributed to the nature of the control structure; for positive and negative $\dot{x}_d$, all the active metering valve combinations intending to move the cylinders in the positive and negative x direction respectively. But during the reversal, if the position error is still positive, to minimize this error, it is essential for the piston to carry on moving in the positive x direction – which it is unable to do due to switching of the valve combinations. Hence this sudden drop occurs and it regains effective tracking once the demand falls below the actual position that is the position error becomes negative. Alternative control structures should be explored to overcome this shortcoming.

CHAPTER 5

CONCLUSIONS AND FUTURE SCOPE OF WORK

5.1 Conclusions

Electrohydraulic systems have become increasingly important in various industries such as construction machinery, aerospace, and heavy-duty manipulators due to their high power-to-weight ratio. The growing demand for electrohydraulic systems in robotics and high-tech manufacturing has further increased the need for developing high-performance systems. However, there are two main the challenges associated with electrohydraulic systems. Firstly, achieving high control accuracy in the presence of nonlinearities and uncertainties such as flow leakages, complex flow properties, and nonlinear friction force is difficult. Secondly, the energy efficiency of the system is also a major concern due to limited energy sources, unwanted system heating, and cost reduction. Although many researchers have focused on either high control accuracy or high energy efficiency, achieving both simultaneously remains a challenge in electrohydraulic systems. This thesis focuses on combined electrohydraulic actuation system (EHAS) and electrohydraulic force system (EHFS) for both tracking accuracy as well as efficiency. Most common application of simultaneous EHAS and EHFS is an Electrohydraulic load simulator (EHLS) which is a crucial device in hardware-in-loop (HIL) experiments, and is widely used in aerospace engineering.

In this proposed EHLS consisting of two co-axial hydraulic cylinders, two configurations are studied – one is CIMV, where all the eight metering valves are proportional valves excited by continuously varying voltage; another is IMV, where return path proportional valves are operated as simple ON-OFF valves excited by fixed control voltages. The objective of the study to see if any improvement in energy efficiency occurs vis-à-vis tracking accuracy of force and motion.

A Feedforward-PI Feedback control structure has been proposed in the thesis for suitable force and motion tracking of the EHLS. In earlier studies, feedforward controllers have been designed for individual force or motion tracking problems. In the present work a composite motion-force feedforward controller has been proposed which is based on both the force as well as motion demands. To handle the nonlinearities in the mathematical models of the hydraulic system due to friction, compressibility, leakage flows in the valves and the cylinders, orifice like flow at the metered ports and the difficulty in model inversion due to the asymmetry in the cylinder configurations, the order-separated technique of Sarkar et. al., 2023, has been used to develop the composite motion-force feedforward controller.

A fixed speed, pressure compensated, swash plate type variable displacement pump has been considered in the study. The static characteristics of the pump has been obtained from an earlier work by Naskar et.

al., 2022. The energy saving on account of variable flow from the pump has been calculated in comparison to when a fixed displacement pump with pressure relief valve is used in the circuit.

The performance studies have been carried out in terms of variations of the position and force responses, control voltages at the metering valves, variations of chamber pressures of the 2 cylinders as well as the Integral Absolute Position Error, the Integral Absolute Force Error, the Integral Square Control Effort in the 8 metering valves, the energy saved compared to a fixed displacement pump – pressure relief valve combination and the exit losses in the metering valves.

Because of the direct coupling of the two hydraulic cylinders, the force response of the loading cylinder is severely affected by the motion of the actuating cylinder. Performance comparison of the 2 configurations – CIMV and IMV is studied is detail at section 4.2. It is observed, for a fixed gain FFPI controller, a better performance is shown in CIMV than IMV – on count of tracking error, control effort, power savings and exit loss.

In this study, as CIMV performs better, CIMV configuration of several combination of position and load demands are considered – fixed, sinusoid, linearly time-varying, spring load, spring-damper load has been explored.

Performance deterioration is observed when the load increases, affecting both position and force tracking in constant load demand and sinusoid position demand scenarios. When dealing with a spring load, low spring stiffness leads to noticeable force tracking errors, which decrease with higher stiffness values. However, further increasing the spring stiffness only marginally impacts force tracking performance. The force tracking performance in a combined spring-damper loading is enhanced by studied for different values of the damping. It has been found that higher damping coefficient values result in superior tracking performances. In the case of linearly time varying load demands, better tracking is achieved with smaller slopes of force variation. Performance degradation occurs with larger phase differences between force and velocity demands. Additionally, higher frequencies of force or position demands have a significant impact on performance. Motion demands at speeds exceeding the system bandwidth result in very poor position tracking performance. In this study, dead-band of the metering valves and transmission losses are not considered.

5.2 Future Scopes of Work

Designing a composite force-motion feedforward controller coupled with feedback PI-controllers for the 2 cylinders is quite a challenging task on account of the complexity of the mathematical models of the coupled systems with multiple valves. The present work acts a pointer to several areas for future study that can be and should be pursued to upgrade the electrohydraulic load simulator.

5.2.1 The Controller

If one looks at the control performance of the EHLS, it will be found that as the demanded piston velocity changes sign at half the cycle time, the position response shows a sudden drop and then follows a track with lesser slope than that of the demand for some duration till it catches up with the demand again. This effect is manifested as spikes – first positive which is soon followed by a negative one – in the force response. This is attributed to the nature of the control structure. For positive $\dot{x}_d$, the metering valve combinations which are activated are V3 – V4 for Cyl1 and V5 – V6 for Cy2 – all intending to move the cylinders in the positive x – direction. Since the demanded piston velocity changes sign at half the cycle time, the active valve combination also changes to V1 – V2 for Cyl1 and V7 – V8 for Cyl2 – all now intending to move the cylinders in the negative x – direction. But during this reversal, if the position error is still positive, to minimize this error, it is essential for the piston to carry on moving in the positive x – direction – which it is unable to do due to switching of the valve combinations. Hence this sudden drop occurs and it regains effective tracking once the demand falls below the actual position i.e.; the position error becomes negative.

Suitable modification of the control logic should be pursued in future to overcome this difficulty leading to the discontinuity in the response with sign reversal of the position response.

Furthermore, the overall power required for the IMV configuration has been found to be higher than its CIMV counterpart. As discussed earlier, this may be attributed to the poorer tracking performances of the IMV due to loss of continuous control in the return path metering valves. However, the present study has been carried with identical PI gains for the feedback controllers for both the IMV and CIMV. Further exploration needs to be carried out with different PI gains for the IMV than the CIMV to see if it can improve its tacking performances and reduce the power requirement.

5.2.2 The Valves

A possibility that probably will have to be explored is using 3×3 PVs instead of 2×2 PVs as shown in Fig. 5.1 below. With this the control algorithm needs to be re-tuned to check if smoother responses are obtained. This also reduces the number of metering valves from 8 to 4.

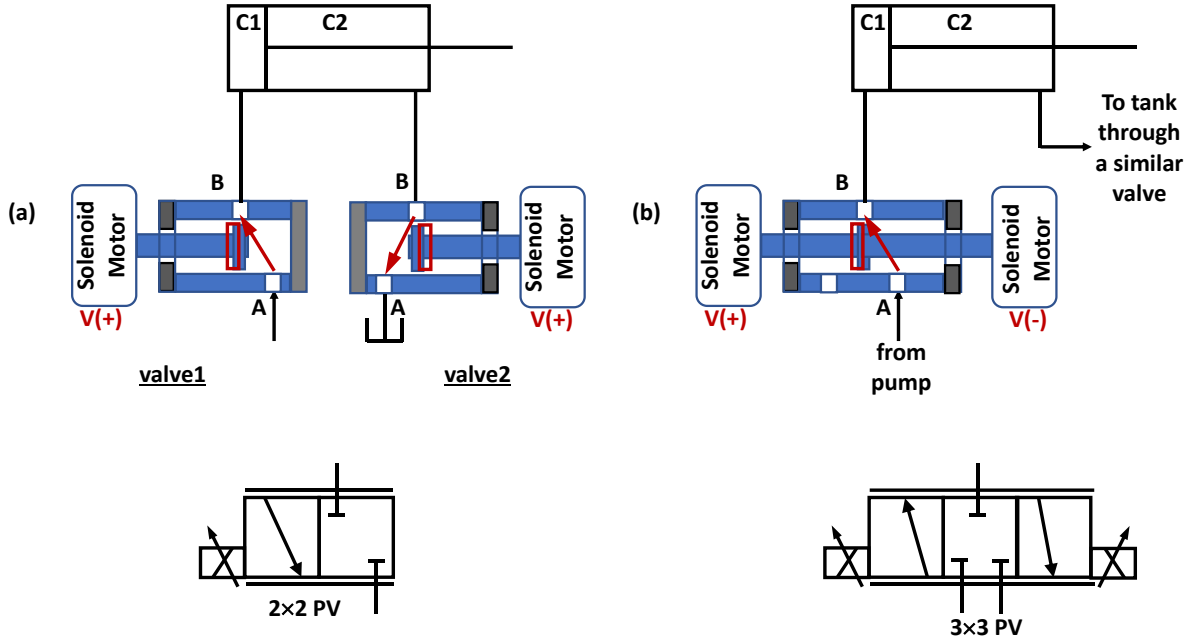

Fig.5.1: Comparison of (a) 2×2 PVs and (b) 3×3 PVs – in flow metering of hydraulic cylinders

While for the case of 2×2 PVs in Fig. 5.1(a), each cylinder requires a pair of valves for motion in a particular direction and a separate pair for motion reversal, for the case of 3×3 PVs, a single pair of valves can cater to both forward and reverse motion. Hence the number of valves required for the second case is half that of the first case. This should be explored in future studies. However, such a configuration will allow only for CIMV operation and not IMV operation.

5.2.3 The EHLS Configuration

Another area to be explored in the future is designing the controllers for an EHLS where the cylinders are parallel to each other and connected by a common linkage as shown In Fig. 5.2 below. This contrasts with the coaxial configuration of the 2 cylinders as taken up in the present study.

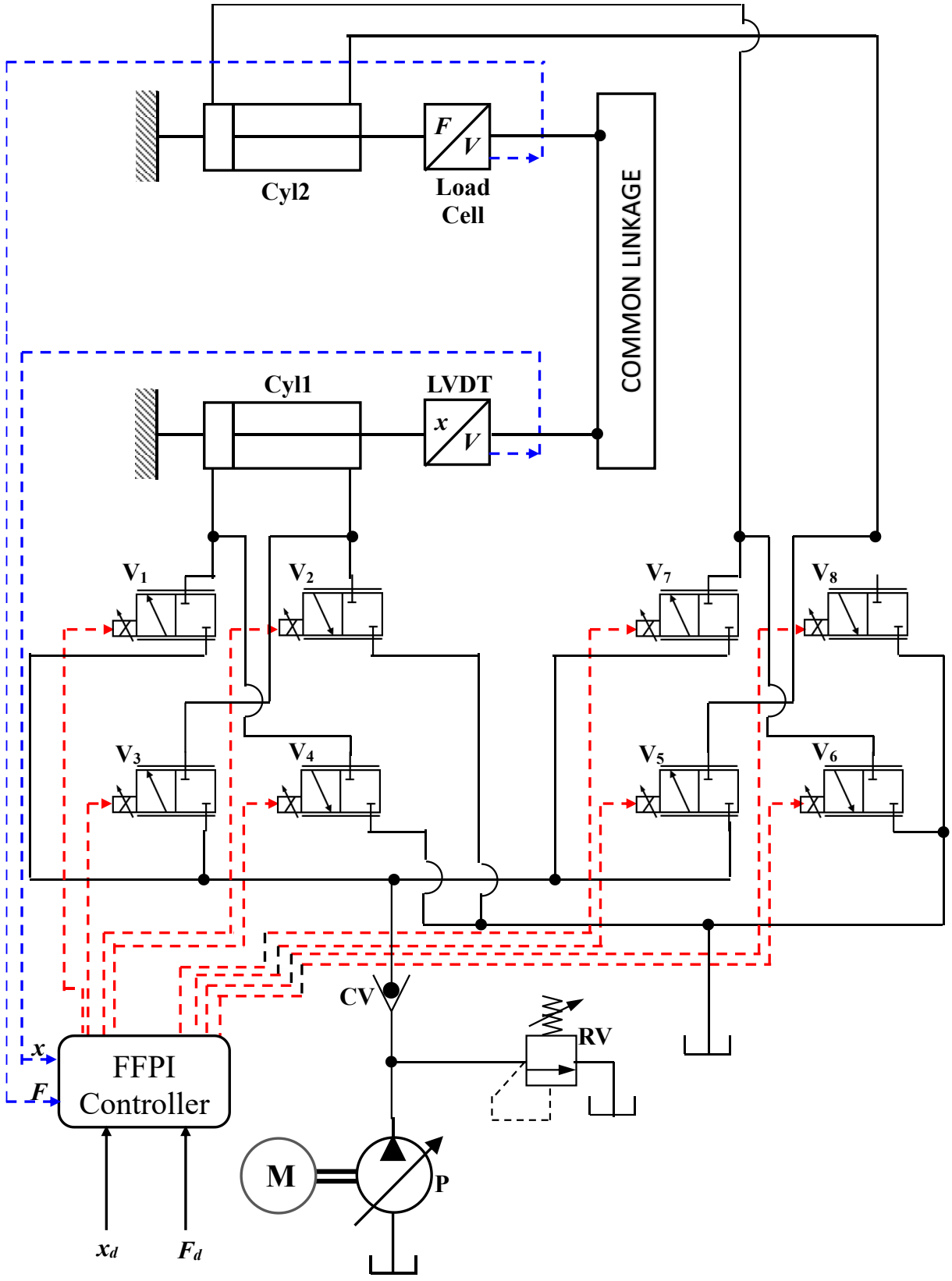

Fig.5.2: Schematic of Electrohydraulic Loading System, EHLS with parallel cylinders

5.2.4 Real-time Experiments

The entire work carried out in the present thesis is based on simulation studies. Such a work is only the preamble to experimental investigations. Hence, experimental realization of the configurations discussed should be carried out in future. This calls for procuring assembling the cylinders, valves, data acquisition and control systems, sensors, hydraulic power pack. The present work will prove to be useful in identifying the specifications of the components while designing the real-time system. Furthermore, it will remain a valuable asset for offline tuning of the controllers.

REFERENCES

Alleyne, A. G., Liu, R. (2000) *Systematic Control of a Class of Nonlinear Systems with Application to Electrohydraulic Cylinder Pressure Control*. IEEE Transactions on Control Systems Technology **8**(4), pp. 623-634.

Asokan, T., Singaperumal, M. (1997) *Control of interaction impedance using an electrohydraulic servosystem: an application to robotic deburring*. Journal of Materials Processing Technology **65**(1-3), pp. 172-178. https://doi.org/10.1016/S0924-0136(96)02258

Bongain, S. , Jamett M. (2018) *Electrohydraulic active suspension fuzzy-neural based control system*. IEEE Latin America Transactions **16**(9), pp. 2454-2459.

Cheng, L., ZHU, Z-C., SHEN, G., WANG, S., LI, X., TANG, Y. (2020) *Real-Time Force Tracking Control of an Electro-Hydraulic System Using a Novel Robust Adaptive Sliding Mode Controller*. IEEE Access **8**(), pp. 13315-13328. https://doi.org/10.1109/ACCESS.2019.2895595

Chengwen, W., Zongxia, J., Shuai, W., Yaoxing, S. (2013) *An experimental study of the dual-loop control of electro-hydraulic load simulator (EHLS)*. Chinese Journal of Aeronautics, **26**(6), pp. 1586-1595. https://doi.org/10.1016/j.cja.2013.10.002.

Cho, S. H., Räcklebe, S., Helduser, S. (2009) *Position tracking control of a clamp-cylinder for energy-saving injection moulding machines with electric-hydrostatic drives*. Proceedings of the Institution of Mechanical Engineers, Part I: Journal of Systems and Control Engineering **223**(4), pp. 479-491. https://doi.org/10.1243/09596518JSCE681

Choi, K., Seo, J., Nam, Y., Kim, K. U. (2015) *Energy-saving in excavators with application of independent metering valve*. Journal of Mechanical Science and Technology **29**(1), pp. 387–395. https://doi.org/10.1007/s12206-014-1245-5

Cochoy, O., Hanke, S., Carl, U. B. (2007) *Concepts for position and load control for hybrid actuation in primary flight controls*. Aerospace Science and Technology **11**(2-3), pp. 194–201. https://doi.org/10.1016/j.ast.2006.09.004

Daachi, B., Benallegue A. (2003) *A stable neural adaptive force controller for a hydraulic actuator*. Proceedings of the Institution of Mechanical Engineers, Part I: Journal of Systems and Control Engineering **217**(4), pp. 303-310. https://doi.org/10.1177/095965180321700406

Dai, K., Zhu, Z., Shen, G., Tang, Y., Li, X., Wang, W., Wang, Q. (2022) *Adaptive force tracking control of electrohydraulic systems with low load using the modified LuGre friction model*. Control Engineering Practice **125**, August, p 105213:1-17. https://doi.org/10.1016/j.conengprac.2022.105213

Dasmahapatra, S., Saha,R., Mookherjee, S., Sanyal, D. (2018) *Designing an Input-Linearized Adaptive Sliding Mode Coupled Nonlinear Integral Controller*. IEEE/ASME Transactions on Mechatronics **23**(6), pp. 2888-2895. https://doi.org/10.1109/TMECH.2018.2870911

Feng, H., Qiao, W., Yin, C., Yu, H., Cao, D. (2019) *Identification and Compensation of Non-Linear Friction for an Electro-Hydraulic System*. Mechanism and Machine Theory **141**, November, pp. 1–13. https://doi.org/10.1016/j.mechmachtheory.2019.07.004

Gain, S., Sanyal, D., Acharyya, S. K., Das, S. K., 2022 *Friction stir welding of AISI-316L steel pipes: Mechanical and metallurgical characterization of the joint*. Proceedings of the Institution of Mechanical Engineers, Part E: Journal of Process Mechanical Engineering, April, Online. https://doi.org/10.1177/09544089221096104.

Han, W., Xiong, L., Yu, Z. (2020) *Interconnected pressure estimation and double closed-loop cascade control for an integrated electrohydraulic brake system*. IEEE/ASME Transactions on Mechatronics **25**(5), https://doi.org/10.1109/TMECH.2020.2978534

Horn, J., Bamberger, J., Michau, P, Pind, S. (2003) *Flatness-based clutch control for automated manual transmissions*. Control Engineering Practice **11**(12), pp. 1353–1359. https://doi.org/10.1016/S0967-0661(03)00099-6

Huang, J., Song, Z., Wu, J., Guo, H., Qiu, C., Tan, Q. (2023) *Parameter Adaptive Sliding Mode Force Control for Aerospace Electro-Hydraulic Load Simulator*. Aerospace **10**(2), pp. 160(1)-160(22). https://doi.org/10.3390/aerospace10020160

Isermann, R., Schaffnit, J., Sinsel, S. (1999) *Hardware-in-the-loop simulation for the design and testing of engine-control systems*. Control Engineering Practice **7**(5), pp. 643-653. https://doi.org/10.1016/S0967-0661(98)00205-6

Jacazio, G., Balossini, G. (2007) *Real-time loading actuator control for an advanced aerospace test rig*. Proceedings of the Institution of Mechanical Engineers, Part I: Journal of Systems and Control Engineering **221**(2), pp. 199-210. https://doi.org/10.1243/09596518JSCE269

Jerouane, M., Sepheri, N., Lamnabhi-Lagarrigue, F. (2004) *Dynamic analysis of variable structure force control of hydraulic actuators via the reaching law approach*. International Journal of Control. **77**(14), pp. 1260–1268. http://dx.doi.org/10.1080/00207170412331305579

Jing, C., Xu, H., Jiang, J. (2019) *Flatness-based adaptive nonlinear control for torque tracking of electro-hydraulic friction load simulator with uncertainties*. Proceedings of the Institution of Mechanical Engineers, Part I: Journal of Systems and Control Engineering **233**(8), pp. 1009-1016. https://doi.org/10.1177/0959651818813230

Jing, C., Xu, H., Jiang, J. (2020) *Practical torque tracking control of electro-hydraulic load simulator using singular perturbation theory*. ISA Transactions **102**, July, pp. 304–313. https://doi.org/10.1016/j.isatra.2020.02.035

Kang, S., Yan, H., Dong, L., Li, C. (2018) *Finite-time adaptive sliding mode force control for electrohydraulic load simulator based on improved GMS friction model*. Mechanical Systems and Signal Processing **102** (2018) pp. 117–138. https://doi.org/10.1016/j.ymssp.2017.09.009

Karpenko , M., Sepehri, N. (2010) *Electrohydraulic force control design of a hardware-in-the-loop load emulator using a nonlinear QFT technique*. Control Engineering Practice **20**(6), pp. 598-609. https://doi.org/10.1016/j.conengprac.2012.02.004

Kemmetmuller, W. , Fuchshumer, F. , Kugi A. (2010) *Nonlinear pressure control of self-supplied variable displacement axial piston pumps*. Control Engineering Practice **18**(1), pp. 84-93. https://doi.org/ https://doi.org/10.1016/j.conengprac.2009.09.006

Komsta, J., van Oijen, N., Antoszkiewicz P. (2013) *Integral sliding mode compensator for load pressure control of die-cushion cylinder drive*. Control Engineering Practice **21**(5), pp. 708-718. https://doi.org/10.1016/j.conengprac.2011.12.006

LeQuoc, S., Xiong, Y. F., Cheng, R. M. H., Zhang, H. Q. (1994) *Design of Electrohydraulic Force Loading System*. SAE Transactions **103**, pp. 297–305. http://www.jstor.org/stable/44473347

Li, L., Huang, H., Liu, Z., Li, X., Mathew, J. T., Zhao, F. (2016) *An energy-saving method to solve the mismatch between installed and demanded power in hydraulic press*. Journal of Cleaner Production **139**, December, pp. 636-645. https://doi.org/10.1016/j.jclepro.2016.08.063

Li, J. -Y., Shao, J. -P., Han, G. -H., Wang, Z. -W., Wu, B. (2009) *Study of the Electro-hydraulic Load Simulator Based on Flow-Press Servo Valve and Flow Servo Valve Parallel Control*. Proceedings of the International Conference on Intelligent Human-Machine Systems and Cybernetics, Hangzhou, China, pp. 70-74, https://doi.org/10.1109/IHMSC.2009.143

Luo, C., Yao, J., Chen, F., Li, L., Xu, Q. (2017) *Adaptive repetitive control of hydraulic load simulator with RISE feedback*. IEEE Access **5**, October, pp. 23901-23911. https://doi.org/10.1109/ACCESS.2017.2762665

Mondal, N., Saha, R., Mookherjee, S., Sanyal, D. (2019) *A novel method to design pressure compensator for variable displacement axial piston pump*. Proceedings of the Institution of Mechanical Engineers, Part E: Journal of Process Mechanical Engineering **233**(2), pp. 314-344. https://doi.org/10.1177/0954408918783409

Nakkarat, P., Kuntanapreeda, S. (2009) *Observer-based backstepping force control of an electrohydraulic actuator*. Control Engineering Practice **17**(8), pp. 895–902. https://doi.org/10.1016/j.conengprac.2009.02.011

Nam, Y., Hong, S.K. (2002) *Force control system design for aerodynamic load simulator*. Control Engineering Practice **10**(5), pp. 549-558. https://doi.org/10.1016/S0967-0661(02)00004-7

Naskar, N., Adhikary, A., Das, S., Paul, S., Nag, S. (2022) *Motion control study in energy-saving electrohydraulic system for RCGA-based identification of valve-cylinder parameters*. Proceedings of the 67th International Congress of Indian Society of Theoretical and Applied Mechanics (ISTAM), I.I.T. Mandi, Mandi, **PA0225**, 14-16th December, pp. 1-8.
chrome-extension://efaidnbmnnnibpcajpcglclefindmkaj/https://istam.iitkgp.ac.in/resources/2022/proceedings/Full_paper/PA0225.pdf

Naskar, N., Paul, S. (2022) *Force tracking in an electrohydraulic system with variable-displacement pump by a novel feedforward controller with PI feedback*. Proceedings of the 67th International Congress of Indian Society of Theoretical and Applied Mechanics (ISTAM), I.I.T. Mandi, Mandi, **PA0228**, 14-16th December, pp. 1-8.
chrome-extension://efaidnbmnnnibpcajpcglclefindmkaj/https://istam.iitkgp.ac.in/resources/2022/

proceedings/Full_paper/PA0225.pdf

Park, C-G., Yoo, S., Ahn, H., Kim, J., Shin, D. (2020) *A coupled hydraulic and mechanical system simulation for hydraulic excavators*. Proceedings of the Institution of Mechanical Engineers, Part I: Journal of Systems and Control Engineering **234**(4), pp. 527-549. https://doi.org/10.1177/0959651819861612

Park, S-H., Lee, J-M., Kim, J-S. (2009) *Robust control of the pressure in a control-cylinder with direct drive valve for the variable displacement axial piston pump*. Proceedings of the Institution of Mechanical Engineers, Part I: Journal of Systems and Control Engineering **223**(4), pp. 455-465. https://doi.org/10.1243/09596518JSCE677

Plummer, A. R. (2007) *Robust electrohydraulic force control*. Proceedings of the Institution of Mechanical Engineers, Part I: Journal of Systems and Control Engineering **221**(4), pp. 717-731. https://doi.org/10.1177/0959651819861612

O'Brien, J. F., Carruthers, D. J. (2013) *Nonlinear dynamic compensation for large-feedback control of a servomechanism with multiple nonlinearities*. Control Engineering Practice **21**(11), pp. 1531-1541. https://doi.org/10.1016/j.conengprac.2013.06.005

Sarkar, A., Maji, K., Chaudhuri, S., Saha, R., Mookherjee, S., Sanyal, D. (2023) *Actuation of an electrohydraulic manipulator with a novel feedforward compensation scheme and PID feedback in servo-proportional valves.* Control Engineering Practice, **135**(2023), pp.105490, ISSN 0967-0661. https://doi.org/10.1016/j.conengprac.2023.105490.

Sarkar, B. K., Das, J., Saha, R., Mookherjee, S., Sanyal, D. (2013) *Approaching Servoclass Tracking Performance by a Proportional Valve-Controlled System*. IEEE/ASME Transaction on Mechatronics **18**(4), pp. 1425–30. https://doi.org/10.1109/TMECH.2013.2253116

Sarkar, B. K., Mandal, P., Saha, R., Mookherjee, S., Sanyal, D. (2013) *GA-optimized feedforward-PID tracking control for a rugged electrohydraulic system design*. ISA Transactions **52**(6), pp. 853-861. https://doi.org/10.1016/j.isatra.2013.07.008

Sekhavat, P, Sepheri, N., Wu, Q. (2006) *Impact stabilizing controller for hydraulic actuators with friction: Theory and experiments*. Control Engineering Practice 14(12) pp. 1423–1433. https://doi.org/10.1016/j.conengprac.2005.10.007

Truong, D. Q., Ahn K., K. (2009) *Self-tuning quantitative feedback theory for parallel force/position control of electro-hydrostatic actuators*. Proceedings of the Institution of Mechanical Engineers, Part I: Journal of Systems and Control Engineering **223**(4), pp. 537-556. https://doi.org/10.1243/09596518JSCE700

Truong, D. Q., Ahn K., K. (2011). *Parallel control for electro-hydraulic load simulator using online self tuning fuzzy PID technique*. Asian Journal of Control. **13**(4), pp. 522 - 541. https://doi.org/10.1002/asjc.348

Xiao, L., Lu, B., Yu, B., Ye, Z. (2015) *Cascaded sliding mode force control for a single-rod electrohydraulic actuator*. Neurocomputing **156**, May, pp. 117-120. http://dx.doi.org/10.1016/j.neucom.2014.12.078

Xiong, L., Wei, H., Yu, Z. (2020) *Adaptive sliding mode pressure control for an electro-hydraulic brake system via desired-state and integral-antiwindup compensation*. Mechatronics **68**, June, p.102359:1-13. https://doi.org/10.1016/j.conengprac.2022.105213

Xu, G., Lu, N., Lv, G. (2019) *High-gain observer-based sliding mode force control for the single-rod electrohydraulic servo actuator*. IEEE Access **7**, Novemer, pp. 161849-161857. https://doi.org/10.1109/ACCESS.2019.2951696

Yan, H., Sun, J., Zuo, H. (2021) *Anomaly detection based on multivariate data for the aircraft hydraulic system*. Proceedings of the Institution of Mechanical Engineers, Part I: Journal of Systems and Control Engineering **235**(5), pp. 593-605. https://doi.org/10.1177/0959651820954577

Yan, X., Chen, B. (2021) *Analysis of a novel energy-efficient system with a bidirectional supercharger for forging hydraulic press*. Journal of Cleaner Production **286**, March, p.125520:1-11. https://doi.org/10.1016/j.jclepro.2020.125520

Yang, G., Yao, J. (2022) *Multilayer neuroadaptive force control of electro-hydraulic load simulators with uncertainty rejection*. Applied Soft Computing **130**, pp. 109672. https://doi.org/10.1016/j.asoc.2022.109672

Yuan, Y., Zhang, J., Li, Y., Li C. (2018) *A novel regenerative electrohydraulic brake system: development and hardware-in-loop tests*. IEEE Transactions on Vehicular Technology **67**(12), pp. 11440-11452. https://doi.org/10.1109/TVT.2018.2872030

Yu, B., Zhu, Q., Yao, J., Zhang, J., Huang, Z., Jin, Z., Wang., X. (2020) Design, mathematical modeling and force control for electro-hydraulic servo system with pump-valve compound drive. IEEE Access **8**, July, pp. 171988-172005. https://doi.org/10.1109/ACCESS.2020.3012091

Zhang, Y., Alleyne, A. G., Zheng, D. (2005) *A hybrid control strategy for active vibration isolation with electrohydraulic actuators*. Control Engineering Practice **13**(3), pp. 279–289. https://doi.org/10.1016/j.conengprac.2004.03.009

Bosch Rexroth AG: 4/4-way servo solenoid directional control valves, directly operated, with electrical position feedback and on-board electronics (OBE) -Type 4WRPEH6. Datasheet (2010).